Nanoscale and ultrafast *in situ* techniques to probe plasmon photocatalysis **②** ⊘

Claire C. Carlin (a); Alan X. Dai (b); Alexander Al-Zubeidi (b); Emma M. Simmerman (c); Hyuncheol Oh (c); Niklas Gross (c); Stephen A. Lee (c); Stephan Link (c); Christy F. Landes (c); Felipe H. da Jornada (c); Jennifer A. Dionne (c)



Chem. Phys. Rev. 4, 041309 (2023) https://doi.org/10.1063/5.0163354





CrossMark



The Journal of Chemical Physics

Special Topic: Algorithms and Software for Open Quantum System Dynamics

Submit Today





Nanoscale and ultrafast *in situ* techniques to probe plasmon photocatalysis •

Cite as: Chem. Phys. Rev. **4**, 041309 (2023); doi: 10.1063/5.0163354 Submitted: 16 June 2023 · Accepted: 24 October 2023 · Published Online: 1 December 2023







AFFILIATIONS

- ¹Department of Applied Physics, Stanford University, Stanford, California 94305, USA
- ²Center for Adopting Flaws as Features, Rice University, Houston, Texas 77005, USA
- Department of Chemical Engineering, Stanford University, Stanford, California 94305, USA
- Department of Materials Science and Engineering, Stanford University, Stanford, California 94305, USA
- Department of Chemistry, Rice University, Houston, Texas 77005, USA
- ⁶Department of Chemical and Biomolecular Engineering, Rice University, Houston, Texas 77005, USA
- 7 Department of Electrical and Computer Engineering, Rice University, Houston, Texas 77005, USA
- ⁸Stanford PULSE Institute, SLAC National Accelerator Laboratory, Menlo Park, California 94025, USA
- Stanford Institute for Materials and Energy Sciences, SLAC National Accelerator Laboratory, Menlo Park, California 94025, USA
- Department of Radiology, Stanford University, Stanford, California 94305, USA

ABSTRACT

Plasmonic photocatalysis uses the light-induced resonant oscillation of free electrons in a metal nanoparticle to concentrate optical energy for driving chemical reactions. By altering the joint electronic structure of the catalyst and reactants, plasmonic catalysis enables reaction pathways with improved selectivity, activity, and catalyst stability. However, designing an optimal catalyst still requires a fundamental understanding of the underlying plasmonic mechanisms at the spatial scales of single particles, at the temporal scales of electron transfer, and in conditions analogous to those under which real reactions will operate. Thus, in this review, we provide an overview of several of the available and developing nanoscale and ultrafast experimental approaches, emphasizing those that can be performed *in situ*. Specifically, we discuss high spatial resolution optical, tip-based, and electron microscopy techniques; high temporal resolution optical and x-ray techniques; and emerging ultrafast optical, x-ray, tip-based, and electron microscopy techniques that simultaneously achieve high spatial and temporal resolution. *Ab initio* and classical continuum theoretical models play an essential role in guiding and interpreting experimental exploration, and thus, these are also reviewed and several notable theoretical insights are discussed.

Published under an exclusive license by AIP Publishing. https://doi.org/10.1063/5.0163354

V. HIGH SPATIAL RESOLUTION TECHNIQUES	8
A. Optical microscopy	8
1. Single-particle scattering spectroscopy	9
2. Photoluminescence microscopy	9
3. Vibrational spectroscopy	10
4. Fluorescence microscopy	11
5. In situ optical microscopy	11
B. Scanning probe microscopy	11
	11
2. Atomic force microscopy	13
	A. Optical microscopy

^{a)}Author to whom correspondence should be addressed: jdionne@stanford.edu

3. In situ SPM	14	KPFM	Kelvin probe force microscopy
4. Electrochemical scanning probe microscopy	14	LDA	Local density approximation
C. Scanning probe optical microscopy	14	LSPR	Localized surface plasmon resonance
1. IR atomic force microscopy	14	LUMO	Lowest unoccupied molecular orbital
2. Scanning near-field optical microscopy	15	MBPT	Many-body perturbation theory
3. Tip-enhanced Raman spectroscopy	15	MOF	Metal-organic framework
D. Electron microscopy	15	NIR	Near-infrared
1. Scanning electron microscopy	16	PES	Potential energy surface
2. Transmission electron microscopy	17	PIICT	Plasmon-induced interfacial charge transfer
VI. HIGH TEMPORAL RESOLUTION TECHNIQUES	20	PIRET	Plasmon-induced resonant energy transfer
A. Ultrafast transient absorption spectroscopy	20	PL	Photoluminescence
B. Ultrafast x-ray probes	21	SEM	Scanning electron microscopy
1. X-ray absorption	21	SERS	Surface-enhanced Raman spectroscopy
2. X-ray scattering	22	SMJ	Single-molecule junction
3. In situ x-ray methods	22	SNOM	Scanning near-field optical microscopy
VII. HIGH SPATIOTEMPORAL RESOLUTION		SPM	Scanning probe microscopy
TECHNIQUES	23	SPV	Surface photovoltage
A. Ultrafast optical microscopy	23	STEM	Scanning transmission electron microscopy
1. Transient absorption microscopy	24	STM	Scanning tunneling microscopy
2. Ultrafast Raman microscopy	24	STS	Scanning tunneling spectroscopy
B. Ultrafast x-ray microscopy	24	TA	Transient absorption
C. Ultrafast STM	25	TDDFT	Time-dependent density functional theory
D. Ultrafast electron microscopy	25	TEM	Transmission electron microscopy
1. Ultrafast SEM	25	TERS	Tip-enhanced Raman spectroscopy
2. Dynamic TEM	26	TIR	Total internal reflection
3. Ultrafast TEM	26	TRXAS	Time-resolved x-ray absorption spectroscopy
VIII. COMPUTATIONAL METHODS	27	UEM	Ultrafast transmission electron microscopy
A. Theoretical approaches	27	UHV	Ultrahigh vacuum
B. Illustrative theoretical results	28	UV	Ultraviolet
1. Bulk, surfaces, and thin films	28	UV-Vis	Ultraviolet-visible
2. Large nanoparticles	29	XANES	X-ray absorption near-edge structure
3. Small nanoparticles	29	XAS	X-ray absorption spectroscopy
IX. CONCLUSIONS AND OUTLOOK	30	XC	Exchange-correlation
A. Challenges	30	XFEL	X-ray free-electron laser
B. Opportunities	31	XRD	X-ray diffraction
C. Outlook	31	XRM	X-ray microscopy

NOMENCLATURE

AFM	Atomic force microscopy
CARS	Coherent anti-Stokes Raman scattering
CPD	Contact potential difference
CT	Charge transfer
CW	Continuous wave
DFT	Density functional theory
DOS	Density of states
DTEM	Dynamic transmission electron microscopy
e-h	Electron-hole
EDX/EDS	Energy dispersive x-ray spectroscopy
EELS	Electron energy loss spectroscopy
ETEM	Environmental transmission electron microscopy
EXAFS	Extended x-ray absorption fine structure
FTIR	Fourier-transform infrared
FWHM	Full width at half maximum
GGA	Generalized gradient approximation
IETS	Inelastic electron tunneling spectroscopy
IR	Infrared

I. INTRODUCTION

Eliminating the use of fossil fuels is one of the most pressing challenges of our time. Ever since the Industrial Revolution, advances in energy production, chemical manufacturing, and infrastructure have had a dramatic impact on our quality of life. ^{1,2} However, these processes have made us dependent on fossil fuels and we now produce enormous amounts of climate-changing greenhouse gases. ^{3,4} The detrimental impacts of carbon emissions, together with the fact that fossil fuels are finite and unevenly distributed around the world, require us to find alternatives to fossil fuels.

To reach a green future and meet global climate targets, the chemical industry must be decarbonized. This task is challenging due to the variety of emission sources, including fuel consumption for reactor heating and by-products from manufacturing processes. Promising advances in renewable energy, including solar and hydropower, pave the path to sustainable energy use in the chemical industry. However, to eliminate emissions from on-site fuel consumption and by-products, industrial processes have to be fundamentally changed. New reaction pathways that do not rely on high reactor temperatures, do not produce carbon emissions as

by-products, and/or do not utilize fossil feedstocks have to be developed and implemented.

Inspired by natural processes such as photosynthesis, researchers have become interested in using light to drive chemical reactions. ^{11–14} By directly harvesting sunlight or using light from energy-efficient renewably powered light-emitting diodes (LEDs), energy can be supplied to catalysts to induce chemical reactions. ¹⁵ Furthermore, driving chemical reactions using light rather than heat allows access to transition states that are not thermally attainable, enabling new reaction pathways. ^{16–28} However, many light-driven catalytic processes are currently limited by low catalyst turnover and low quantum efficiencies. ^{29,30} Advances in nanoscience, both experimental and theoretical, offer an ever-increasing ability to manipulate light–matter interactions and design new, higher efficiency photocatalysts. ^{31–33}

Plasmonic photocatalysis takes advantage of the light-induced resonant collective oscillation of free electrons in a metal nanoparticle, known as a localized surface plasmon resonance (LSPR). LSPRs concentrate optical energy to sub-particle scales, which can induce and control chemical reactions. 34,35 Changing the composition and structure of a metal nanoparticle alters the LSPR, thereby allowing the excitation wavelength to be aligned to a particular spectrum, such as the solar spectrum, or tuned to selectively induce specific chemical reactions.^{36–39} Numerous applications of plasmonic catalysis have been proposed and demonstrated, including solar hydrogen and fuel production,^{30,40–47} ammonia synthesis, 48,49 and various organic reactions. $^{50-53}$ To fully harness the potential of these systems and translate lab-scale proofs-of-concept into industrial processes, an improved theoretical and experimental understanding of excited-state potential energy surfaces (PESs) and excited-state electronic and optical properties is needed.

In this review, we examine methods for elucidating the underlying mechanisms of plasmonic photocatalysis. We focus on methods that enable the characterization at the spatial and temporal scales relevant to charge transfer and chemical reactions, with particular emphasis on those which can be performed in situ.⁵⁴ We begin with a review of the relevant mechanisms in plasmon-induced heterogeneous catalysis, followed by a brief discussion of the available materials in plasmon catalysis. A detailed discussion of high spatial resolution methods (optical, scanning probe, and electron microscopies) is followed by a discussion of high temporal resolution methods (ultrafast transient absorption spectroscopies). We then examine ongoing efforts to combine high spatial and temporal resolution methods (ultrafast optical, x-ray, scanning tunneling, and electron microscopies). Many of these methods are made especially powerful by correlation to theoretical models, used to calculate potential energy surfaces and electronic and optical properties; thus, these will be reviewed as well. We conclude with a brief discussion of the needed developments in characterization methods in order to further address the open questions in the field and the authors' outlook on the future of the field.

II. BACKGROUND

A. Heterogeneous catalysis

Heterogeneous catalysis, in which the catalyst is in a different phase than the reactants and products, is the predominant method of facilitating chemical reactions.⁵⁵ In order to maximize the surface area available for chemical reactions, catalysts often take the form of nanoparticles⁵⁶ supported on a porous material to improve the diffusion of

reactants and products and to facilitate separation.⁵⁷ The basic steps of a reaction are as follows: (1) diffusion of the reactants to the catalyst surface, (2) adsorption of the reactants to the surface, (3) chemical reaction on the catalyst surface, (4) desorption of products, and (5) diffusion of the products away from the catalyst. While diffusion is essential and can limit the activity of a catalyst, in this review we will focus on the interaction between the reactants, intermediates, products, and the catalyst (steps 2-4). These interactions determine the activity, selectivity, and stability of the catalyst. The adsorption of a molecule to the catalyst surface is determined by its interaction with the electronic states of the catalyst and is described by a ground- or excited-state PES.⁵⁸ The PES indicates potential reaction pathways, intermediates, and energy barriers. Faceting, size, shape, and composition all alter the surface electronic structure of the catalyst and thus the PES. Computational techniques, especially ab initio methods, are powerful tools for predicting PESs and the evolution of chemical reactions in time. 17,22

To overcome the ground-state activation barrier, catalytic reactions often still require high temperatures and pressures. 61,62 As an alternative to energetically demanding thermal reaction conditions, photocatalysis uses light to access excited-state energy landscapes. 63 These include not only reduced energy barriers leading to increased reaction rates 20 but also new pathways enabling higher selectivity and improved catalyst stability $^{16-19}$ or entirely new products inaccessible in thermal equilibrium. $^{21-28}$

B. Mechanisms of plasmon-induced chemistry

Plasmon excitation can be used to drive chemical reactions using light. When the free electrons in a metal nanostructure coherently couple to the oscillating electric field of incident photons, a plasmon oscillation is induced. The plasmon resonance results in an increased optical absorption cross section and electric near-field enhancement of more than an order of magnitude around the particle. 64 The plasmon begins to decay within 10 fs, either scattering light into the far-field (larger particles, $>50\,\mathrm{nm}$) or forming electron—hole (e—h) pairs (small particles). 34,63 There are several microscopic mechanisms by which the plasmon can interact with adsorbates:

- 1. *Indirect charge transfer (CT) [Fig. 1(a)]*: Also referred to as plasmon-induced hot-electron transfer. A plasmon decays to form a non-thermal distribution of e-h pairs, including a small population of high-energy (hot) carriers. Electron-electron scattering produces near-zero momentum intraband (s to s) e-h pairs. Electron-phonon, electron-defect, or electron-surface scattering transfers finite momentum from the LSPR, producing high-energy intraband e-h pairs. In contrast, interband (d to s) transitions can proceed directly with no momentum transfer from the LSPR. Plasmonic enhancement of reactions may occur if hot carriers produced in the nanoparticle can travel to the surface and transfer to unoccupied states of a molecular adsorbate or adjacent semiconductor. 65-68 Hot carriers must be extracted quickly for hot-carrier-driven catalysis before their rapid decay. 34,69
- 2. Plasmon-induced interfacial charge transfer (PIICT) [Fig. 1(b)]: The plasmon decay resonantly excites an electron from the metal into the lowest unoccupied molecular orbital (LUMO) of the

adsorbate, or into the conduction band of a semiconductor. ^{70,71} Electronic states in the adsorbate couple to the coherent LSPR oscillation and provide an additional decay pathway for the plasmon. ^{31,72} This approach avoids the challenges associated with the internal relaxation of electrons and holes. ^{70,73}

- 3. Plasmon-induced resonant energy transfer (PIRET) [Fig. 1(c)]: The electric field of the plasmon and the transition dipole in the adjacent material couple, forming an exciton in the coupled material (adsorbate or semiconductor). Energy transfer efficiencies of up to 50% have been reported, and no direct electrical contact between the nanoparticle (donor) and acceptor is necessary. Both PIICT and PIRET manifest themselves through broadening of the resonance linewidth as an additional plasmon decay pathway and are often referred to as chemical interface damping. 74,78
- Photothermal heating [Fig. 1(d)]: Collisions of excited electrons with phonons increase the temperature of the nanoparticle, leading to thermal catalysis.^{79,80}
- 5. Nanoantenna effects [Fig. 1(e)]: The plasmon-induced electric field can enhance existing optical processes such as interfacial charge transfer and interband transitions.^{70,81} The plasmonic nanoparticle can act as an antenna to enhance the performance of nearby photocatalysts through near-field confinement and far-field scattering.^{82,83} A forced plasmon in a non-plasmonic nanoparticle is induced when a plasmonic nanoparticle is close by,

generating an antenna–reactor structure where catalytically active transition metals can be used as reactor sites. ^{17,84}

All of these methods change the energy landscape on which the catalyst and reactants/products interact, and thus alter chemical processes. Transfer of an electron to an adsorbate can lead to desorption induced by electronic transitions, introducing new reaction pathways that are not accessible through thermal catalysis. Charge and energy transfer from plasmonic metal nanoparticles onto transition metals or semiconductors allow non-plasmonic materials with high catalytic activity to take advantage of the strong light–matter interactions of plasmonic nanoparticles. 30,77,86

The challenge to distinguish between these mechanisms and clarify the role of light in a reaction cannot be overstated. While all of the above mechanisms have been reported to drive catalysis, it is often not clear which pathway dominates for which system. ^{31,65,66,70,74,79,80} However, to optimize an existing catalyst system, the exact mechanism has to be known. For example, indirect CT across a metal–semiconductor interface is most efficient when the hot carrier energy is highest, ^{67,87} while PIRET depends on the spectral overlap between the plasmonic nanoparticle and the acceptor. ⁷⁴

To form a complete picture of a catalytic mechanism, a broad toolset of *in situ* methods is required. The spatial and temporal regimes of these processes vary by orders of magnitude. The small length scales at which reactions happen and the small size of catalytically active

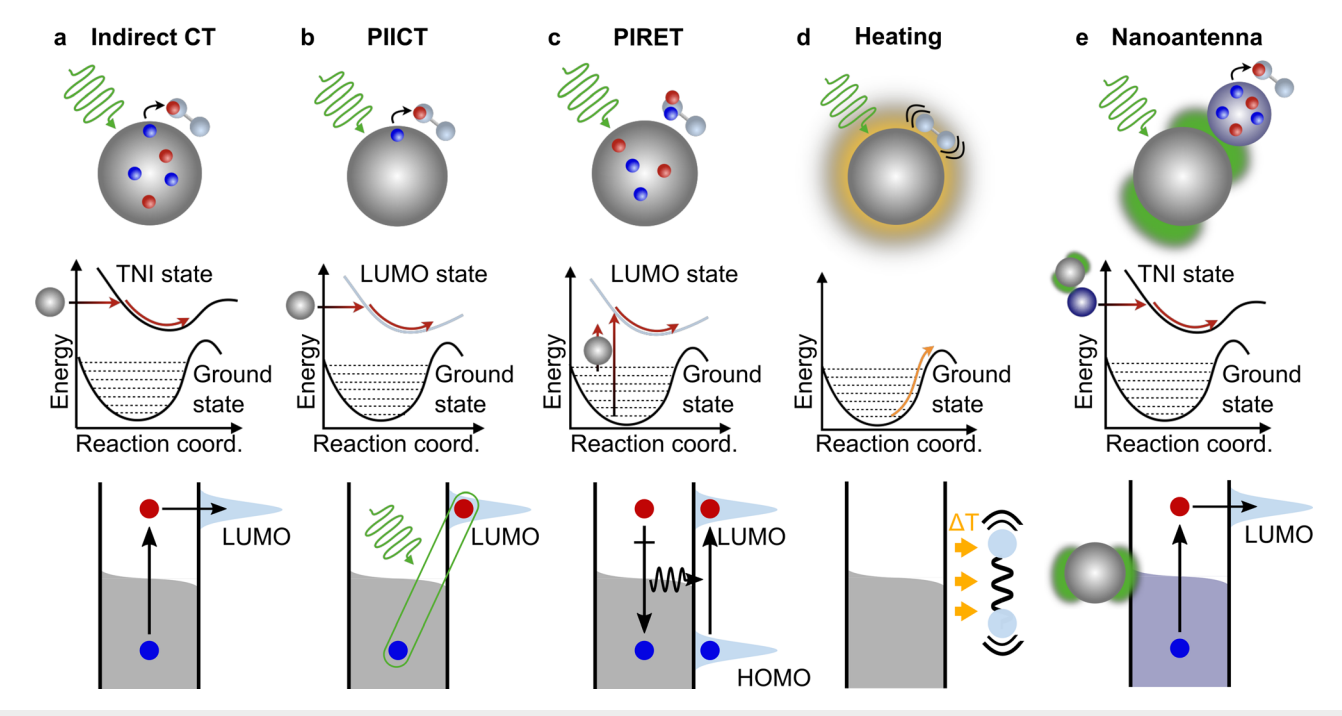


FIG. 1. Mechanisms of plasmon-induced catalysis. The top row is a schematic representation of the reaction, the middle row is a PES schematic, and the bottom row is an electron energy distribution and transfer schematic. (a) Indirect charge transfer (CT): hot carriers from non-radiative plasmon decay are injected into adsorbed molecules, forming transient negative ions (TNIs). (b) Plasmon-induced interfacial charge transfer (PIICT): plasmon decay results in the transfer of electrons between the nanoparticle and adsorbates. (c) Plasmon-induced resonant energy transfer (PIRET): resonant coupling of the plasmon and adsorbates results in electron excitation in the adsorbate. PIICT and PIRET both cause accelerated plasmon dephasing and are often referred to as chemical interface damping. (d) Heating: plasmon decay results in heating of the nanoparticle and adsorbate, leading to photothermal catalysis. (e) Nanoantenna: the nanoparticle acts as an antenna, enhancing light—matter interactions in a nearby reactor.

sites—often just single atoms—requires spatial resolution down to the nanometer and angstrom scale. ^{17,88} Plasmon dephasing occurs in several femtoseconds, hot electron thermalization by electron–electron scattering in hundreds of femtoseconds, and electron–phonon scattering in several picoseconds. ^{89,90} Observing charge transfer requires techniques with pico- to femtosecond temporal resolution; otherwise, only quasi-steady-state observations can be made. ^{35,91,92} Finally, these techniques need to be combined and correlated to gain a complete picture of catalysis.

III. PLASMONIC CATALYST MATERIALS

We briefly discuss catalyst nanoparticles that support a plasmon resonance and material aspects that specifically influence its plasmonic behavior. We refer the reader to other resources for the fundamentals of material choice and design in heterogeneous catalysis. ^{56–58}

A. Metal nanoparticles

Metal nanoparticles smaller than the corresponding wavelength of light both support LSPRs (if they have suitable electronic structure) and have a large surface area-to-volume ratio, making them suitable for plasmonic catalysis. 94-96 The canonical plasmonic metals (copper, silver, and gold) have visible LSPRs due to their full d-bands lying below the Fermi level⁸⁵ and are readily synthesized into nanoparticles. 97-99 Due to a higher likelihood of populating the hybridized adsorbate anti-bonding modes, these metals typically have a weaker affinity for binding. 100 Nevertheless, there are numerous demonstrations of plasmon-driven reactions catalyzed on these plasmonic pure metals. For example, both electrons and holes generated by plasmon decay were used to drive the oxidative coupling of benzylamine on gold (Au) nanoparticles through indirect CT [Fig. 1(a)], as depicted in Fig. 2(a).⁵³ A benzylamine radical cation was generated by hot hole-induced oxidation of the amine group, followed by hydrogen abstraction through O₂ radicals originating from the interaction of hot electrons with atmospheric oxygen. The benzylamine radical was further converted into benzaldehyde and reacts with another benzylamine to form the imine.

Nanoparticles made of other metals, such as more earth-abundant aluminum and magnesium, can support LSPRs as well, but they often require particular morphologies such as shapes with a large aspect ratio to tune the LSPRs into the visible. ^{64,101–103} For example, Trinh *et al.* have photocatalyzed Suzuki coupling over hexagonal palladium nanoplates; ¹⁰⁴ Zhou *et al.* have photocatalyzed hydrogen dissociation over faceted aluminum nanocrystals; ¹⁰⁵ and Lomonosov *et al.* have photocatalyzed acetylene hydrogenation over hexagonal magnesium nanoplates and rods decorated with palladium. ¹⁰⁶

The electric-field enhancement induced by the LSPR depends on the shape of the nanoparticle, with stronger enhancement occurring at sharper tips when excited on resonance. On Combining multiple plasmonic nanoparticles leads to emergent behavior, for instance in the case of nanoparticle dimers, in which the small gap between two nanoparticles leads to significant E-field enhancement. More complex arrangements have been nanofabricated for even higher enhancements.

B. Multimetallic nanostructures

Combining multiple metals in one nanoparticle system has enabled researchers to take advantage of synergistic effects to create improved catalysts. 108,109 Plasmonic materials such as gold and silver can be combined to fine-tune the absorption spectrum of the catalyst and to modify catalytically relevant electronic properties such as the Fermi energy and the interband transition threshold. 110 Catalytically desirable metals that otherwise do not support the desired plasmon can also be combined with a plasmonic metal to drive photochemical reactions by absorption and electric field enhancement through the plasmonic metal.⁸⁴ Thus, multimetallic systems can achieve synergistic optical and catalytic properties, which are not readily available in single-metal systems. Multimetallic nanoparticle systems have three main spatial configurations: antenna-reactor, core-shell, and alloy. 10 In an antenna-reactor system, the metals are formed as distinct particles either in direct contact or separated by a small gap. The plasmonic metal acts as the "antenna," strongly absorbing incident light and transferring energy to the coupled "reactor" metal particle that catalyzes the reaction on its surface. ¹¹1,112 In a core-shell system, the metals are still in distinct volumes, but one completely or partially envelops the other. Core-shell particles have substantial direct interfaces, affecting both metals' electronic states. 113 Typically, the plasmonic metal is the light-absorbing core, while the active metal is the outer shell, which is accessible by reactant molecules. 114 Finally, in alloyed systems, the metals are mixed to varying degrees in the same particle, forming a material with new properties. 115-117 As the fraction of nonplasmonic to plasmonic metal increases, the plasmon resonance will generally be damped. However, the optical and electronic properties of the particle are not a simple linear combination of the component metals, even in a homogeneous alloy. 118 In the extreme case of single-atom alloys, an isolated atom of one metal sits atop a more extended lattice of the other [Fig. 2(b)]. 17 The Halas group was able to demonstrate a new reaction pathway for methane reforming where PIICT triggered the desorption of carbon-containing intermediates from the catalyst surface, preventing catalyst poisoning from coking, a common issue when this reaction is performed thermally. The parameter space extends even further by incorporating more than two metals for more precise control over the desired plasmonic and catalytic properties of the components. This extension is demonstrated in Figs. 2(c)-2(e), where various antenna-reactor configurations composed of three metals have been fabricated and the catalytic properties are shown to vary depending on the precise configuration. 93 The orientation of the reactor relative to the incident illumination determines whether a forced plasmon is excited in the reactor. $H_2 + D_2 \rightarrow 2HD$ and $NH_3 + D_2 \rightarrow$ NH₂D + HD were investigated and synergistic effects were found depending on the orientation and the reaction, demonstrating a photocatalytically driven process with spatial and chemical control. For more detail on bimetallic nanostructures for plasmonic catalysis, we refer to another review by Sytwu et al. 10

C. Heterostructures

The design of heterostructures allows non-plasmonic catalyst materials with tunable optoelectronic properties, such as semiconductors, organic molecules, and metal-organic frameworks (MOFs), to take advantage of the strong and tunable light–matter interactions enabled by plasmonic nanoparticles. ¹¹⁹ The plasmonic domain concentrates light on the nanoparticle surface, creating a large absorption cross section and redistributing the energy or charge to the catalytically active material. ^{107,120–124} This approach allows superior tunability of reaction selectivity and activity as the electronic structure of the

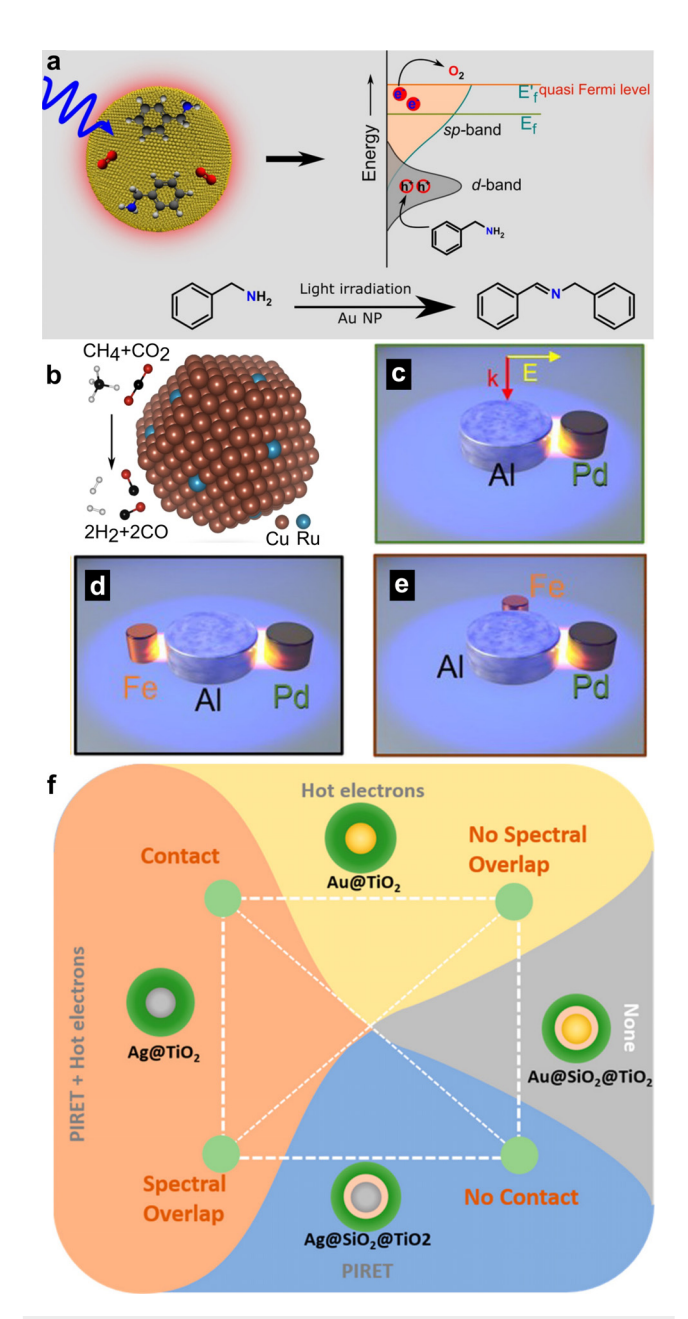


FIG. 2. Examples of materials commonly used for plasmonic catalysis. (a) Pure gold nanoparticle (Au NP) catalyst for the oxidative coupling of benzylamine to an imine. (b) Copper (Cu) nanoparticle with single ruthenium (Ru) atom dopants for dry reforming of methane, showing high selectivity and stability. (c)–(e) Heterodimers and heterotrimers consisting of an aluminum (Al) antenna and (c) palladium (Pd), (d) iron (Fe) and palladium at 180, and (e) iron and palladium at 90. (f) Diagram showing the properties that affect plasmon-induced charge and energy transfer. Electrical contact and spectral overlap between the nanoparticle and co-catalyst enabled charge and energy transfer, respectively. (a) Adapted with permission from Swaminathan et al., Angew. Chem., Int. Ed. Engl. 60, 12532–12538 (2021). Copyright 2021 Wiley-VCH GmbH. (b) Adapted with permission from Zhou et al., Nat. Energy 5, 61–70 (2020). Copyright 2020 Springer Nature Limited. (c)–(e) Adapted with permission from Yuan et al., ACS Nano 16, 17365–17375 (2022). Copyright 2022 American Chemical Society. (f) Reprinted with permission from Cushing et al., J. Phys. Chem. C 119, 16239–16244 (2015). Copyright 2015 American Chemical Society.

catalyst material can be tuned by controlling the materials, doping, and physical structure of the semiconductor or polymer. Depending on the energy-level alignment, interface, and spectral overlap, charge and energy transfer between the plasmonic nanoparticle and the reactor material may be possible.

Metal–semiconductor heterostructures combine catalytic materials such as ${\rm TiO_2}$, ${\rm Cu_2O}$, ${\rm ZnO}$, and CdSe with plasmonic antennas to generate value-added chemicals through photocatalytic small-molecule activations. $^{28,125-141}$ To help elucidate the underlying mechanisms in such structures, Cushing *et al.* showed that in Ag@TiO2 core–shell nanoparticles both energy and charge can be transferred from the plasmonic antenna to the semiconductor due to excellent electrical contact and spectral overlap [Fig. 2(f)]. When an interstitial layer of insulating silica was added between the silver and TiO2, charge could no longer be transferred, but energy transfer was still possible through dipole–dipole coupling between the plasmonic nanoparticle and TiO2. In contrast, the plasmon resonance of gold does not spectrally overlap with TiO2, and only charge transfer was possible for Au@TiO2. After adding an insulating layer of silica, TiO2 could no longer be sensitized by the gold plasmon.

Plasmonic metal-organic heterostructures have been developed using 2D/3D carbon materials, 142-144 graphitic carbon nitride (g-^{45–150} and MOFs for CO₂ hydrogenation, water splitting, and dye decomposition. 151-158 These hybrid materials provide vast synergistic impacts toward various small molecular activations, delivering high electrical conductivity, controllable porosity, and ease of incorporating catalytically active functional groups. Furthermore, various governing factors, such as nanoparticle size and metal co-catalysts, have been investigated for high photocatalytic performance. Cheng et al. presented a combination of gold clusters and nanoparticles on g-C₃N₄ to achieve efficient plasmonic hot electron injection in photocatalytic H₂ generation. ¹⁵⁹ The high H₂ generation rate was attributed to the synergetic effect of a reduced Schottky barrier between gold and g-C₃N₄ by strong sp² hybridization and the prolonged lifetime of hot electrons. While not discussed in detail here, metal oxides and metal nitrides can independently support plasmon resonances and be used as stable and relatively cheap plasmonic photocatalysts. 150,160 2D transition metal carbides, nitrides, and carbonitrides, classified as MXenes, have also been recently explored as photocatalysts for water treatment and ${\rm CO_2}$ reduction. $^{161-163}$ MXenes may also support a plasmon resonance, which has been used to boost their photocatalytic

The lifetime of charge carriers in plasmonic heterostructures can be increased by introducing heterojunction interfaces, ¹²², ¹³⁶, ¹⁶⁶ oxygen vacancies, ¹²⁶ and defect sites in catalytic active domains. In addition, these catalysts can be highly nanostructured and often contain complex geometries, multiple components in various configurations, and spatially discrete optically and chemically active sites. ¹⁰⁷, ¹²¹, ¹³⁰

IV. CHARACTERIZATION METHODS OVERVIEW

As discussed in Sec. II B, there is a need to ascertain the mechanisms underlying plasmonic photocatalysts. Ensemble-scale methods demonstrate the improved activity and selectivity of plasmonic photocatalysts and contribute mechanistic insights. Optical characterization methods, such as ultraviolet-visible (UV-Vis) extinction, photoluminescence (PL), and dark-field spectroscopies, can be performed *in situ*. ^{167,168} Tools from analytical chemistry such as gas chromatography and mass spectroscopy are used to analyze reaction products. ¹⁶⁹

TABLE I. Overview of methods discussed in this review. The table is not meant to be all-inclusive, but rather to highlight the elements that will be covered in the text. Submethods are italicized, with general information that applies to all submethods provided with the main method.

Method	Origin of signal	Information derived	Practical considerations	
Optical microscopy	Scattering, transmission, emission, or absorption of light by particles or reactants	Optical properties of materials	 Easy <i>in situ</i> implementation Noninvasive Often inexpensive Often combined with other techniques Requires super-resolution techniques to overcome diffraction limit 	
Single-particle scatter- ing spectroscopy	Inelastic light scattering by particle	 Particle size and shape¹⁷⁴ Refractive index of surrounding medium^{174,175} Plasmon decay time^{71,78} 	• Particle size and shape are determined indirectly	
PL microscopy	Light emission from hot carrier decay	 Particle size and shape¹⁷⁶ Charge transfer¹⁷⁷ 	 Particle size and shape are determined indirectly 	
Vibrational spectroscopy	IR absorption and inelastic (Raman) scattering	 Chemical identification of molecules on nanoparticle surface¹⁷⁸ Molecular orientation¹⁷⁹ Molecular temperature¹⁸⁰ 	• Strong water background (IR)	
Fluorescence microscopy	Fluorescence	 Transformations of fluorescent molecules¹⁸¹ Location of fluorescent molecules on or close to nanoparticles¹⁸² 	Molecule of interest must be fluorescent	
Scanning probe microscopy STM	Interaction of chemical or physical processes with a scanning tip Tunneling current	 Topography and/or electronic information Surface density of states¹⁸³ 	Sample must be relatively flatSerial scanningSample must be conductive	
		 Reaction time ¹⁸⁴ Vibrational signatures 	Atomic resolution	
AFM	Short-range forces	 Particle size and shape ^{185,186} Charge transfer and redistribution (KPFM) ¹⁸⁷⁻¹⁹³ 	• Easy in situ implementation	
Electrochemical SPM	Interfacial charge transfer or solu- tion conductivity	• Electrochemical reaction kinetics ¹⁹⁴	 Liquid only Easy in situ implementation Sometimes difficult to determine the source of current 	
Optical SPM	Light- and/or tip-matter interactions	• Local optical properties of materials	• Serial scanning	
AFM-IR	IR absorption	 Near-field vibrational signatures¹⁹⁵ 		
SNOM	Transmitted or reflected near-field light	Near- and far-field optical scattering, transmission, and absorption spectra Vibrational signatures 197	Complex instrumentation compared to other optical methods Strong water harborism of IR.	
TERS	Inelastic scattering of light with molecules	 Vibrational signatures¹⁹⁷ Chemical identification of molecules close to TERS tip¹⁹⁸ 	 Strong water background in IR SERS electric field enhancement from tip (not substrate) 	
Electron microscopy	Scattering or transmission of electrons	Particle size and morphologyElemental identification (EDS)	 Difficult <i>in situ</i> implementation Difficult to control for e-beam effects	
SEM	Back and secondary scattering of	• Surface morphology ¹⁷³	• Serial scanning	

TABLE I. (Continued.)

Method	Origin of signal	Information derived	Practical considerations
	electrons	• Grain orientation	Charging on non-conductive samples Cannot be performed in liquid
TEM	Transmission and diffraction of electrons	 Lattice structure Optical properties (EELS)²⁰⁰⁻²¹¹ Electronic and bonding structure and energy transfer (EELS)^{212,213} 3D structure (tomography)²¹⁴ Electric and magnetic fields (holography, ²¹⁵ 4D-STEM)²¹⁶⁻²¹⁸ Vibrational signatures (EELS)²¹⁹⁻²³⁰ 	 Atomic resolution Serial scanning (STEM) Sample must be thin
Ultrafast TA spectroscopy	Absorption of light pulses	 Carrier and phonon lifetimes^{231,232} Temporal evolution of carriers²³³ Carrier-phonon coupling constants²³⁴ Changes in absorption cross section²³⁵ 	• Process must be reversible
Ultrafast x-ray probes	Absorption, scattering, or emission of x rays due to a light pulse	• Atomic structure	Requires XFELs for pulsed x raysMeasurements in reciprocal space
Ultrafast x-ray absorption	X rays absorbed by core-electron transitions due to a light pulse	 Elemental identification²³⁶ Electronic and oxidation states (XANES)²³⁷⁻²³⁹ Arrangements and properties of neighboring atoms (EXAFS)²³⁷⁻²³⁹ 	• May require high vacuum (soft x rays)
Ultrafast x-ray scattering	X rays scattered by electron density due to a light pulse	 Lattice structure^{240–242} Longer-range order^{243,244} 	• Highly penetrating (hard x rays)

Wavelength- and power-dependent measurements can be used together to calculate apparent activation barriers.²⁰ The difference in reaction rates when a reactant is exchanged with one of its isotopes is regarded as one of the more conclusive ensemble methods to distinguish between thermal and electron-mediated reactions as the effect of changing isotopes will be much more pronounced in the case of an electron-mediated reaction. 124,170 Several relatively simple experimental methods for distinguishing between photothermal and photochemical effects have been proposed,80 and other standard characterization methods from the surface science and heterogeneous catalysis communities provide valuable insights. 15,171 While ensemble methods have contributed substantially to our mechanistic understanding of plasmonic photocatalysis, they alone are not sufficient. The chemical and optical properties of nanoparticles strongly depend on local, atomicscale structure. To identify how atomic structure, crystallinity, and active site reconstruction impact plasmon excitation and catalytic activity, sub-particle resolved techniques are required. 111,172,173 Ultrafast methods must be also incorporated, in order to distinguish between the various plasmon decay processes and methods of electron

transfer on their relevant timescales. Studying catalysts *in situ* often requires specialized equipment that is both robust to reaction conditions and accessible to stimuli and detection methods (e.g., light, electrons, and x rays). Below, we review several state-of-the-art methods for high spatial resolution and real-space imaging of plasmonic catalysts, before discussing ultrafast methods, and finally the prospects for combining the two. The individual nanoscale and ultrafast characterization methods discussed and their suggested use are summarized in Table I, while the methods combining both limits of resolution are more nascent and found discussed in the text only.

V. HIGH SPATIAL RESOLUTION TECHNIQUES A. Optical microscopy

Optical microscopy is a noninvasive and relatively low-cost method for characterizing nanoscale materials by detecting light scattering, emission, or absorption from nanoparticles, surrounding molecules, or semiconductors. Changes to the plasmon resonance, observable in single-particle scattering and photoluminescence (PL), give information about catalytic reactions and plasmon or hot-carrier

lifetimes. 176,245 Meanwhile, techniques that detect molecules, such as surface-enhanced Raman spectroscopy (SERS) and fluorescence microscopy, give information about chemical reactions occurring on a nanoparticle and, in some cases, even resolve reactive sites on nanoparticles. 181,246,247 One of the primary challenges in using optical microscopy for plasmonic catalysis is that these methods will generally be limited by the diffraction of light, which practically limits the spatial resolution to about 200 nm. 174 Emitters or scatterers smaller than the diffraction limit can still be detected but will appear as diffractionlimited point spread functions. 174 Given that nanoparticles of interest are often on the order of 10 nm, this limits the applicability of diffraction-limited optical methods. However, when the sample is dilute enough that the point spread functions of single emitters do not overlap, the position of the emitter can be superlocalized by fitting the emission and finding the center, overcoming the diffraction limit of light.²⁴⁸ The noninvasive nature, relative ease of in situ implementations, and ability to be combined with tip-based techniques (Sec. VB) make optical microscopy a promising method for studying photocatalysts. Several of the most relevant methods in the area of plasmonic photocatalysis are discussed below. A more detailed review of nanoscale optical imaging was written by Wilson et al.2

1. Single-particle scattering spectroscopy

In single-particle scattering spectroscopy methods, nanoparticles are excited with light, and the light scattered by the nanoparticles is collected. Different illumination geometries are used to avoid collecting the overpowering excitation light, the most common of which is darkfield microscopy. Normal incidence and high-angle dark-field methods use far-field light to excite the nanoparticles and collect only light scattered in geometric directions different from the incident light.² Dark-field methods based on near-field excitation, most notably total internal reflection (TIR) geometries, excite with near-field light and collect only the far-field scattered light.²⁵²⁻²⁵⁴ The far-field scattered light is collected by an objective and spectrally resolved for individual nanoparticles. 174 Near-field excitation typically results in higher signalto-noise, but sample geometries and the ability for refractive index matching are limited. 174,255 Spectra are often collected by sending light to a spectrograph, ²⁵⁶ although other techniques such as interferometry and ratiometric imaging have been employed.^{257–259} The scattering intensity of nanoparticles scales with the square of the volume, making detection increasingly difficult for smaller particles.²⁶⁰ Dark-field techniques typically cannot measure particles smaller than 30 nm; however, nanoparticles as small as 2 nm have been measured using interferometric scattering microscopy.^{260,261} A detailed review of excitation and detection methods for single-particle scattering spectroscopy was written by Al-Zubeidi, McCarthy et al. 1

While the shape of nanoparticles smaller than the diffraction limit of light cannot be seen directly in optical microscopy, the plasmon spectrum depends on the size, shape, material, and chemical environment of the particle. 262-264 Reactions that change the nanoparticle, such as etching, growth, or deposition of another material, can be monitored through spectral changes, providing insight into the reactivity of nanoparticles. 265-272 By optically tracking decreases in scattering intensity during the hot-hole-assisted dissolution of gold nanorods, Al-Zubeidi *et al.* were able to determine that holes from interband transitions are more reactive toward oxidation compared to holes in the sp-band due to the generation of highly energetic holes in the

d-band.²⁷³ For anisotropic nanoparticles like nanorods or nanocubes, changes in the peak position of the scattering spectrum allow further insight into shape changes, thus giving information about reactive sites on nanoparticles.^{274–276} Since nanoparticle size and shape uniquely determine the spectrum, it has recently been possible to predict nanoparticle sizes from dark-field spectra within 10% error in width and length with the help of simulated spectra and machine learning.^{277,278} The ability to gain information about particle size and morphology using light makes single-particle scattering spectroscopy a relatively noninvasive technique. Although light can cause damage to some catalyst materials and interfere with chemical reactions, the conditions are typically less invasive than those used in electron microscopy. Single-particle spectroscopy, especially in combination with simulations, is therefore a powerful technique for structure–function correlation.

Single-particle scattering spectroscopy can also be used to quantify plasmon decay pathways. The linewidth of the plasmon resonance [full width at half maximum (FWHM)] of a single nanoparticle is inversely proportional to the plasmon damping time. Processes that add additional plasmon decay pathways, such as PIICT and PIRET, lead to additional linewidth broadening. 71,72,279 Unlike ensemble UV-Vis spectroscopy where the linewidth is dominated by the distribution in particle size, the linewidth in single-particle spectroscopy can be used to calculate plasmon dephasing times and thus charge and energy transfer efficiencies.⁷² By comparing the linewidth of individual particles before and after deposition of the energy-accepting polymer poly-nickel(II)-tetra(amino)-phthalocyanine, work by Collins et al. found that up to 50% of the plasmon's energy could be transferred onto the polymer [Figs. 3(a)–3(c)]. The PIRET efficiency (η_{RET}) was calculated from the homogeneous plasmon linewidth and followed the spectral overlap between the nanostructure resonance energy (E_{res}) and the polymer absorption spectrum. Even though plasmon decay happens on the order of femtoseconds, ⁶⁹ single-particle spectra can be used to determine plasmon decay times and provide valuable insight into reaction mechanisms.

2. Photoluminescence microscopy

The photoluminescence (PL) of nanoparticles provides information on nanoparticle shape and hot carrier lifetime. 176,280,281 Radiative recombination of hot carriers leads to the emission of photons. The plasmon resonance acts as an antenna through the Purcell effect, increasing the emission brightness and enabling diffraction-limited single-particle PL measurements.²⁸¹ The Purcell effect and, thus, the PL spectrum resemble the plasmon spectrum and can be used to report on chemical reactions similar to dark-field spectroscopy. 1 PL microscopy has also been recently established as a viable technique for in situ monitoring electrochemical charging of nanoparticles, by observing plasmon shifts resulting from charge density tuning and changes in absorption cross section.²⁸² However, unlike scattering, PL is Stokes or anti-Stokes-shifted relative to the excitation, allowing spectral filtering of the emitted light to reduce the background.²⁸¹ PL microscopy setups, therefore, do not require particles to be illuminated in a dark-field geometry and epi-illumination is common.²⁸¹ The excitation light is spectrally removed using longpass, shortpass, or notch filters.²⁸¹ Only one excitation wavelength is needed to collect an entire PL spectrum.

The PL quantum yield gives information about hot carrier recombination. Lee *et al.* used decreases in PL intensity to study charge transfer from gold nanorods to TiO₂, ITO, and SiO₂. ¹⁷⁷ Compared to the insulator SiO₂, which cannot accept charge, PL quantum yields on TiO₂ and ITO were lower and depended on the plasmon energy due to the charge transfer of hot electrons from gold into the semiconductor, reducing the number of hot electrons in gold that could radiatively recombine.

3. Vibrational spectroscopy

Vibrational spectroscopy can be used to detect molecules, therefore allowing the direct monitoring of chemical transformations. Infrared (IR) and Fourier-transform infrared spectroscopy (FTIR) measure the absorption of light by the vibrational modes of molecules. Raman spectroscopy measures the inelastic scattering of light from the molecules. ²⁸³

The detection of reactant and product molecules at a single and sub-particle level is possible through Raman scattering. ^{246,284–290} The Raman signal is increased by the nanoparticle's electric field enhancement by 5–10 orders of magnitude, enabling surface-sensitive nano-localized detection of molecules. ^{246,291} Raman microscopy setups function similarly to PL microscopy; the substrate is illuminated and Stokes or anti-Stokes Raman scattering is collected using an objective and spectrally filtered. ⁸⁸ This technique is particularly useful for studying plasmon-driven chemical processes, as the signal from only the

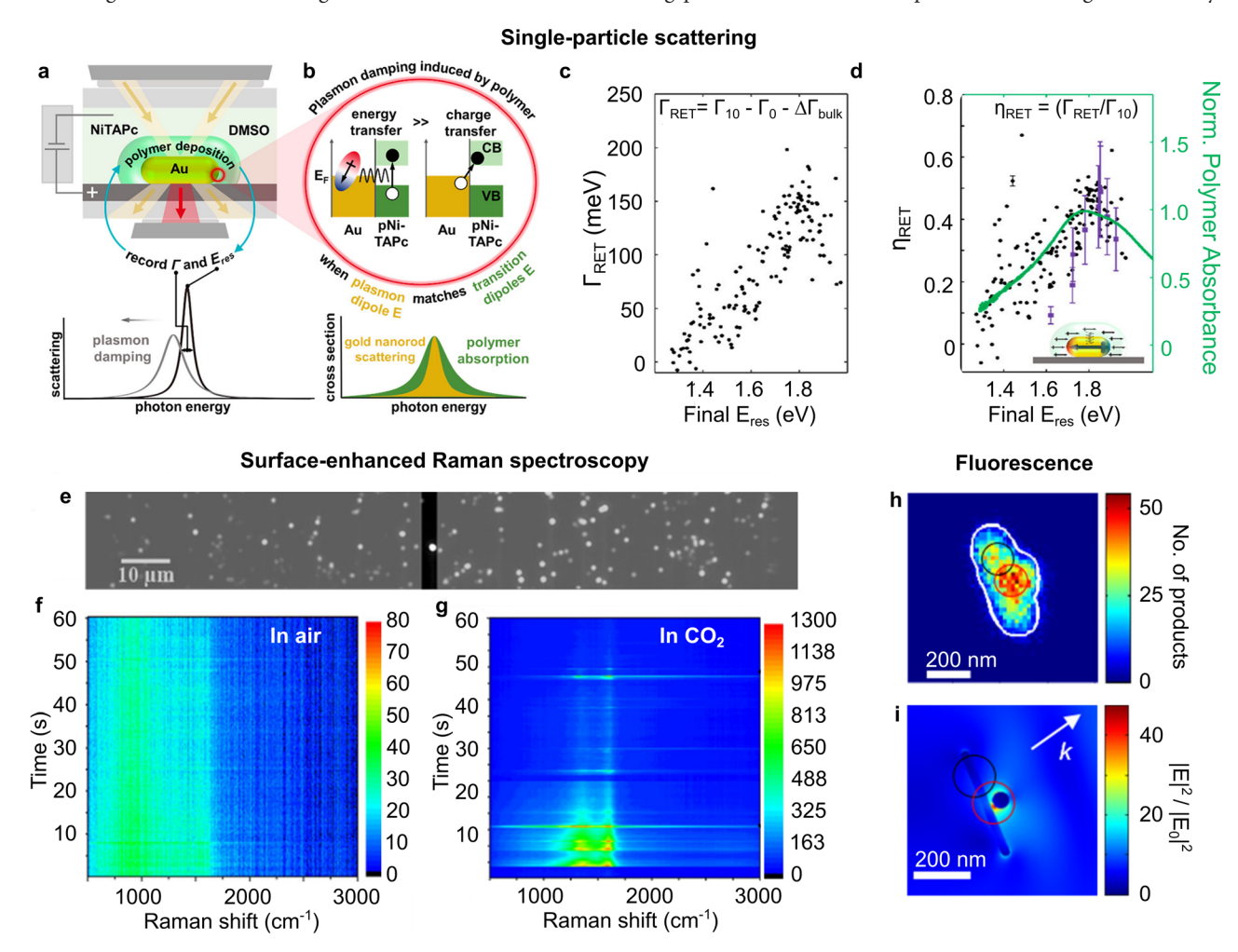


FIG. 3. Optical methods. Noninvasive optical microscopy can track photocatalysis on single nanoparticles. (a) Nanoparticles were illuminated in an *in situ* spectroelectrochemical cell, and light scattered from individual nanoparticles was collected by an objective and sent to a spectrograph. (b) Plasmon broadening due to energy transfer onto a spectrally overlapping polymer. (c) Linewidth broadening of single-particle spectra due to PIRET (Γ_{RET}) as a function of the resonance energy of the hybrid structure. (d) PIRET efficiency follows the polymer spectrum. (e) Dark-field image of silver nanoparticles used for CO_2 reduction. (f) and (g) Waterfall plot of SERS spectra acquired in air and during plasmon-induced CO_2 reduction of single nanoparticles, respectively. (h) Super-resolved map of fluorescent events on a nanorod–nanosphere aggregate. The nanosphere was at the center-right of the nanorod where the highest number of fluorescent events was observed. (i) Simulated electric field enhancement at 532 nm for the structure used in (h). The electric field hot-spot was located in the same location where the highest number of products was observed. (a)–(d) Adapted with permission from Collins *et al.*, ACS Nano 12, 8330–8340 (2018). Copyright 2020 American Chemical Society. (e)–(g) Adapted with permission from Kumari *et al.*, ACS Nano 12, 8330–8340 (2018). ACS Nano 12, 83570–5579 (2018). Copyright 2018 American Chemical Society.

molecules that are located in electric field hot-spots, and thus those which are susceptible to plasmon-driven processes, will be enhanced.²⁹² By choosing a chemical reaction where the reactants, intermediates, and products are Raman active, chemical transformations can be monitored using SERS. 88,178,293,294 Kumari et al. used SERS to elucidate the mechanism of CO₂ reduction on plasmonic silver nanoparticles [Figs. 3(e)-3(g)]. SERS spectra were measured in air and under CO2. In air, no change in SERS spectra was observed, while under CO₂, time-resolved photocatalytic activity was observed. The band near 1600 cm⁻¹ corresponds to CO. Kumari et al. correlated in situ SERS with single-particle dark-field and PL to monitor the surface restructuring of nanoparticles during photocatalysis. 88 By simultaneously monitoring and correlating the structure and catalytic hydrogenation of CO₂, the authors concluded the catalytic activity of silver nanodisks is affected by the transient formation of silver clusters on the nanoparticle surface. The high number of Raman active molecules allows this technique to be broadly applicable to many reactions.2 making Raman spectroscopy one of the only methods that can directly monitor the reactions of industrially relevant chemicals. While product quantification in ensemble photocatalysis using mass spectrometry can prove that a catalyst produces products, SERS offers the opportunity to conduct mechanistic studies on individual nanoparticles. However, this abundance of Raman signals can also make data collected using this technique difficult to interpret, and quantification is difficult due to the complex nature of SERS enhancement. 297 Raman spectroscopy can also be used to determine the temperature of molecules using the relative intensity of the Stokes and anti-Stokes signals (see Sec. VII A 2).

4. Fluorescence microscopy

Fluorescence microscopy enables the visualization of reactive sites on nanoparticles. Fluorescent molecules can be detected in a microscopy setup by illuminating the field of view and collecting the spectrally shifted fluorescence of individual molecules.^{298–300} A commonly employed technique is total internal reflection (TIR) fluorescence microscopy, where near-field light from TIR at the substrate interface is used to excite the molecules.³⁰⁰ The resulting evanescent field only extends ~100 nm away from the surface, exciting only dyes close to the surface to minimize imaging the background. Alternatively, farfield light, e.g., from epi-illumination or a light sheet, can be used to also excite dyes away from the surface. 301 Similar to Raman scattering, the fluorescence of molecules is enhanced by the electric field enhancement of plasmonic nanoparticles, generating bright signals that allow the detection of single molecules. 302,303 Superlocalization of these molecules has been used to detect reactive sites on nanoparticles with \sim 30 nm localization precision. However, coupling of plasmon modes from nanoparticles with single-molecule fluorescence can also result in the mislocalization of the emitter.2

Zou *et al.* used this technique to map the reductive deoxygenation of resazurin to the fluorescent molecule resorufin on gold–silver nanoparticle dimers. ¹⁸¹ By correlating sites with high fluorescence intensity, and hence high reaction rates, with scanning electron microscopy (SEM) and finite-difference time-domain electric field simulations, the authors found excellent agreement between electric field intensity and reactive hot-spots [Figs. 3(h) and 3(i)]. While limited to fluorescent molecules, this technique is powerful for superlocalizing reaction hot-spots due to low background and high localization precision.

5. In situ optical microscopy

A substantial benefit of optical methods is that they are easy to perform in situ since photocatalysts are inherently designed to operate under illumination. While many of these methods were initially developed for dry and static samples, all techniques mentioned here have been performed in liquid cells and time-resolved. For measurements in liquid, illumination and/or collection of light through a liquid medium become necessary. When samples are built into cells for measurements in liquid or gas, additional interfaces are introduced into the illumination and detection geometry, lowering the signal and introducing background from scattering. 174 These issues are mitigated by using liquid immersion objectives directly in the sample liquid. 310 Additionally, the effect of the refractive index of the medium has to be considered, as a setup that is designed to achieve TIR at a glass-air interface (critical angle 41°) may no longer achieve TIR at a glass-water interface (critical angle 61°), requiring modifications in the setup. ¹⁷⁴ When optical microscopy is used to monitor reactions in real time, the temporal resolution is limited by the intensity of the signal or the frame rate of the detector, although millisecond and sub-millisecond temporal resolutions are achievable with optical microscopy. 311,312 Due to their experimental similarities, different optical techniques can be performed using the same setup with only minor modifications, making it possible to collect complementary data, such as nanoparticle spectra and SERS signals from molecules from the same sample, potentially even simultaneously. Optical microscopy can also be combined with other techniques, especially tip-based techniques.

B. Scanning probe microscopy

While there is a suite of methods within optical microscopy that provide insight into optical, electronic, and chemical properties with relative ease, they rarely achieve the nanometer-scale resolution required to identify active sites on a catalyst and distinguish between local effects. Scanning probe microscopy (SPM) can exceed the spatial resolution achieved by optical microscopy, directly imaging molecular transformations such as dissociation. Various forms of SPM, discussed below, have been used to determine the density of states (DOS) near a surface, map charge separation, calculate hot carrier populations, detect molecular vibrations, and perform spectroscopy to provide mechanistic insight into plasmon-driven chemical transformations. In SPM, a probe is rastered across a surface to form an image. The probe is often atomically sharp, with material, shape, and electronic density of states at the tip all potentially affecting the resolution, depending on the interaction mechanism being investigated. However, it is often performed on a smooth surface with an LSPR excited in the tip. Hot carrier transfer rates are highly sensitive to the band structure and geometry of the plasmonic element (see also Sec. VIII), 314,315 so extending the insight inferred here to industrially relevant systems is an outstanding challenge.

1. Scanning tunneling microscopy

Scanning tunneling microscopy (STM) achieves spatial resolution on the order of 1 Å in the lateral direction and sub-angstrom in the vertical direction. The resolution is determined by both the tip diameter and the electronic properties of the tip and sample. In STM, a conductive tip is precisely scanned over a conductive surface with a piezoelectric transducer, producing a map related to the topography

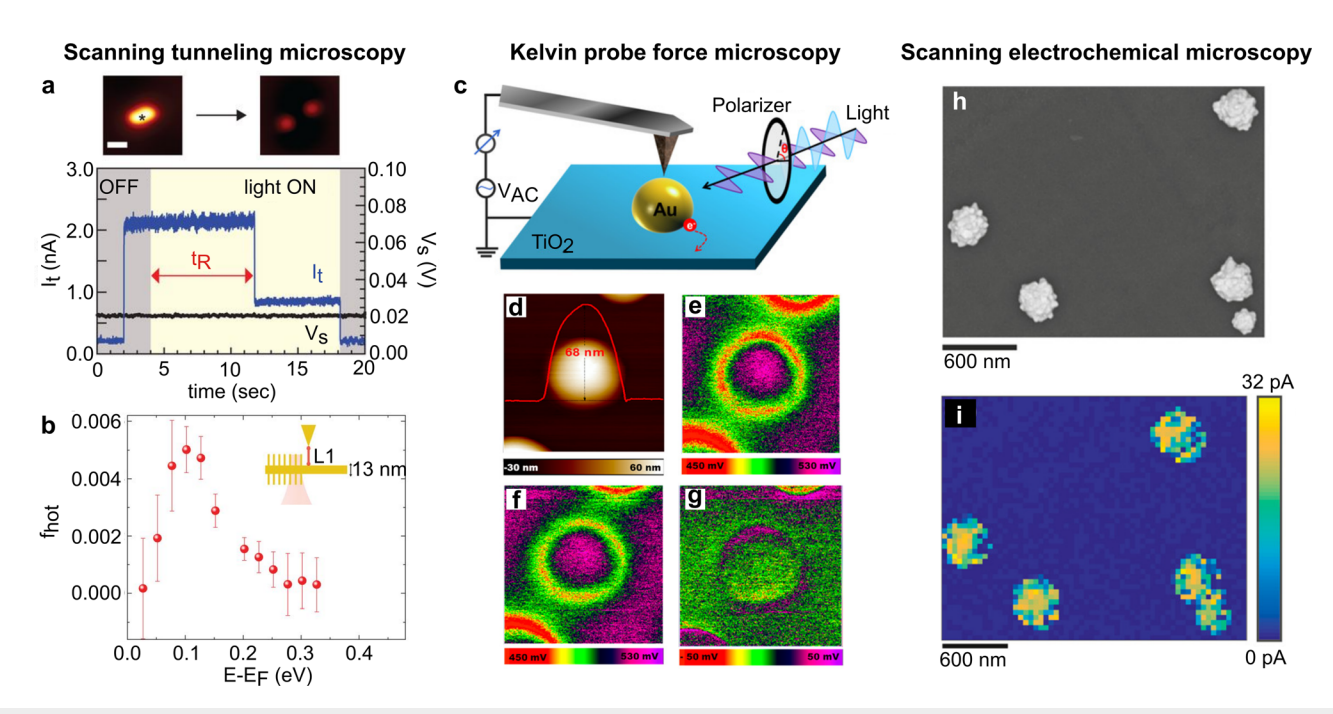


FIG. 4. Scanning probe methods. (a) STM image showing dissociation of dimethyl disulfide on Ag(111) surface (scale bar = 0.5 nm) from excitation of an LSPR under a silver tip. The time required for the molecule to dissociate (t_R) is read from the current trace (I_t) with gap resistance V_s . (b) Hot-electron distribution for a single-molecule junction (SMJ) on a gold film as a function of energy relative to the Fermi energy. (c) Schematic for KPFM. (d) AFM topography of a gold nanoparticle on TiO₂ from a different study performed under humid ambient conditions, showing KPFM maps (e) in the dark (f) under illumination and (g) the SPV map from subtracting (e) from (f). (h) SEM and (i) electrochemical current map (hydrazine oxidation) of poly-crystalline gold nanoparticles. (a) Adapted with permission from Kazuma *et al.*, Science 369, 521–526 (2018). To Copyright 2018 American Association for the Advancement of Science. (b) Adapted with permission from Reddy *et al.*, Science 369, 423–426 (2020). Copyright 2018 American Association for the Advancement of Science. (c) Adapted with permission from Gao *et al.*, Angew. Chem., Int. Ed. Engl. 59, 18218–18223 (2020). Copyright 2020 Wiley-VCH GmbH. (d)–(g) Adapted with permission from Wang *et al.*, J. Am. Chem. Soc. 139, 11771–11778 (2017). Opyright 2017 American Chemical Society. (h) and (i) Adapted with permission from Bentley *et al.*, J. Am. Chem. Soc. 139, 16813–16821 (2017). Page Copyright 2017 American Chemical Society.

and electronic structure of the surface.¹⁸³ The ideal tip is mechanically robust, with a flat density of states at the tip to ease deconvolution with the local density of states of the sample.³¹⁸ When the tip is brought sufficiently close to the surface, the electronic wavefunctions of the tip and sample overlap, and electrons are able to tunnel through the gap, which can be facilitated by an applied voltage. STM can operate in a constant-current mode, where the map corresponds to the height of the tip necessary to maintain this current.³¹⁹ If the surface is sufficiently flat, the tip can also be held at a constant height over the surface and the change in current is mapped.³²⁰ The constant-current mode provides higher resolution because of the reduced tip-sample distance, but the tip has an increased chance of being damaged, while thermal drift is an issue in constant-height mode.

Typical STM tips such as tungsten and platinum–iridium are not plasmonic. To study a plasmonic process on a smooth surface (i.e., one without plasmonic nanoparticles), a sharp plasmonic tip (e.g., silver, gold) is brought close to the surface and optically excited at the resonance frequency, producing a plasmon resonance in the junction.³²¹ This method has been applied to investigate the optical and electronic properties of plasmon resonances.^{322,323} Kazuma *et al.* observed the catalytic dissociation of a dimethyl disulfide molecule mediated by the optical excitation of a plasmon in the gap between a silver STM tip and metal (silver or copper) surface at cryogenic temperatures under ultrahigh vacuum (UHV).³¹³ The time required for the reaction was

read directly from the current trace, and the rotation and dissociation of the molecule were directly imaged [Fig. 4(a)]. The authors concluded PIRET explained the energy transfer.³²⁴ Kazuma *et al.* have also examined the dissociation of molecular oxygen on an Ag(110) surface, which chemisorbs more strongly than dimethyl disulfide, concluding plasmon-induced hot-electron transfer was the primary transfer mechanism. ¹⁸⁴ Böckmann *et al.* investigated the tautomerization of porphycene on a Cu surface with a gold tip.³²⁵ By varying the distance between the tip and surface, as well as the wavelength of the excitation laser, it was theorized that the enhancement in tautomerization observed when the laser was on resonance with the LSPR was dominated by plasmon-induced hot-electron transfer, although they did not rule out contributions from other mechanisms. Pensa and Albrecht used *in situ* STM to study the substrate-induced restructuring of catalytically active 1–3 nm gold nanoparticles at an atomic level.³²⁶

Scanning tunneling spectroscopy (STS), an extension of STM, is performed by measuring the current as a function of bias voltage (i.e., differential conductance), tip height, or time. Differential conductance measurements lend additional insight into the electronic structure of metals by inducing tunneling to unoccupied (occupied) states above (below) the Fermi level by applying a positive (negative) bias. ¹⁸³ An action spectrum is produced by measuring the reaction yield as a function of applied bias, which can help elucidate mechanisms as exemplified below. ³²⁷ In inelastic electron tunneling spectroscopy (IETS), the

second-derivative spectrum is measured. 183 IETS provides vibrational information, useful for identifying chemical species. 183,328 In their study of dimethyl disulfide, Kazuma et al. recorded an action spectrum to help elucidate the dissociation mechanism.³¹³ In their investigation of the dissociation of molecular oxygen, action spectroscopy led Kazuma et al. to conclude that the adsorbate states below the Fermi energy contributed more to the dissociation reaction than the states above the Fermi energy. 184 Combining these insights with the density functional theory (DFT) (see Sec. VIII B 1), they concluded that the plasmon-induced dissociation and inelastic tunneling-induced dissociation were both driven by hot hole transfer to the antibonding orbitals, creating a transient positive ion state. Studies of inelastic electron transfer resulting from the injection of tunneling electrons have been compared to hot carrier transfer as both produce a broad distribution of electrons and the reaction should proceed by the same pathway regardless of the source of excitation. 324 STS was used by Reddy et al. to directly quantify steady-state hot carrier energy distributions for a single-molecule junction (SMJ) on a gold film using the measured tunneling current as a function of applied bias and transmission function for the SMJ [Fig. 4(b)] (see also Sec. VIII B 1). 316 Wieghold et al. used single-molecule optical absorption STM to show that plasmon excitation in a gold thin film resulted in a change in the occupation of electronic states in Pt clusters on the surface of the film. Both STM and STS have been performed in non-conductive liquids, which do not contribute to the electronic states near the Fermi level of the examined sample and therefore do not generate any tunneling currents.3

2. Atomic force microscopy

Atomic force microscopy (AFM) was developed to overcome one of the primary limitations of STM: it requires a conductive sample. Instead of relying on tunneling currents, AFM makes use of Pauli repulsion, electrostatic interactions, short-range chemical forces, and van der Waals forces to determine the topography of a sample. 183 These interactions enable imaging at larger tip-sample distances compared to STM.³³³ Extensions of AFM can monitor total electron density and interfacial charge separation, although only in the steady state. By combining AFM with IR spectroscopy, chemical characterization becomes possible, which may serve to increase the applicability of AFM methods to photocatalysis in the future. In contact mode, a tip on the end of a cantilever is scanned across the sample. A laser reflects off the back of the cantilever, and the motion of the laser spot on a photodiode corresponds to changes in topology. AFM can also be performed in tapping mode, where the cantilever oscillates as it scans the sample and the frequency or amplitude of the oscillations is recorded.³³⁴ This approach preserves the sample and tip by minimizing lateral friction as the tip is scanned and can provide a greater variety of spectroscopic information. While AFM with a standard silicon or silicon nitride tip cannot discriminate between different materials or chemical species, functionalization of the tip is used to measure the adsorption properties of molecules.31

Kazuma et al. used AFM to determine morphological changes in pyramidal silver nanorods on a TiO₂ surface. ¹⁸⁵ They mapped the surface before and after illumination in an inert gas atmosphere at 0 and 50% humidity and tapping-mode AFM images revealed the dissolution and redeposition of silver ions resulting from the plasmon-induced charge separation at the interface. Tanabe and Tatsuma performed similar work with silver nanospheres on TiO₂ where, when combined

with optical spectroscopy, selective excitation of the modes resulted in color changes in the scattering spectrum. 186 While these studies focus on observing morphological changes, coating standard AFM tips with a plasmonic metal can excite resonances near the sample.³³⁵ Giugni et al. demonstrated the efficient generation of hot carriers at a gold tip from which a surface plasmon polariton was launched, resulting in plasmon-induced charge transfer to a GaAs substrate. 336 Lee et al. used photoconductive AFM with a metallic tip to spatially resolve the photocurrent generated at the interface between a gold nanoprism and TiO₂ surface, demonstrating the photocurrent distribution aligns with that of the plasmonic electric field determined by simulations.³³⁷ Galarreta et al. mapped the near-field enhancement of silver or gold nanotriangle arrays with AFM using a photopolymer, which migrates based on electric field intensity, thus allowing topography to be used as a proxy for field distribution.³³⁸ AFM can be performed in situ, as demonstrated by the monitoring of the surface structure of a zeolite material in various liquid environments.³³

The resolution of AFM depends on the size and shape of the tip. In general, the complex relationship between the forces, which contribute to the signal in AFM, makes it harder to obtain high spatial-resolution images compared to STM, where the current-distance relationship is more straightforward. The ability of standard AFM methods to directly monitor electric fields or chemical properties in plasmonic catalysts is somewhat limited. However, numerous extensions of AFM provide a huge range of additional information relevant to plasmonic catalysis. These methods include AFM-based infrared spectroscopy (AFM-IR), also known as photothermal-induced resonance 195,338 (Sec. V C 1) and Kelvin probe force microscopy (KPFM).

a. KPFM. When different materials are in electrical contact and their Fermi levels are able to equilibrate, charging at the surface occurs. 341 This charging results in a change in the contact potential difference (CPD). By measuring the CPD in the dark vs under illumination, the surface photovoltage (SPV) is determined. In KPFM, the CPD is determined by measuring the external bias voltage needed to minimize the electrostatic force between an AFM tip and the sample. KPFM correlates electronic properties (i.e., charge transfer and redistribution) and structure with lateral spatial resolution on the order of 10 nm. 341 This method has been used by Kazuma and Tatsuma to study Au/TiO2 interfacial charge separation, showing that electrons were transferred from gold nanoplates to the conduction band of TiO₂ when excited resonantly. 187 Gao et al. used KPFM to show that the charge density at an Au/TiO2 interface was greatest when the electric field vector of the illuminating laser was oriented perpendicular to the interface [experiment schematic shown in Fig. 4(c)]. In another study, Wang et al. used selective photodeposition to map the spatial distribution of reaction sites in the Au/TiO2 system and KPFM to determine the hole distribution. 189 The KPFM measurements were carried out in ambient conditions and 50% humidity, resulting in a water layer on the sample surface to mimic the conditions for water oxidation. The surface potential was found to be higher at the Au/TiO₂ interface due to hole accumulation [Figs. 4(d)-4(g)].

Other systems studied include plasmon-induced charge separation between silver nanoparticles and organic semiconductor nanowires¹⁹¹ and between noble metals and the semiconductor NMTO (Na_{0.9}Mg_{0.45}Ti_{3.55}O₈).¹⁹² As described in greater detail by Chen *et al.*, CPD changes could also arise from photothermal heating or

photo-induced changes in the atmosphere, which will not be readily apparent in the SPV signal. The authors developed frequency-modulated spatially resolved SPV spectroscopy to overcome this limitation, applying the method to reveal anisotropic photogenerated hole transfer on differing crystal facets of the (non-plasmonic) photocatalyst BiVO₄. The tip must be calibrated in order to know the work function, and contamination can ruin this calibration. KPFM also suffers from slow acquisition times, which generally limits its application to determining steady-state charge accumulation. Modulated methods help to deconvolve slow processes that are hard to isolate in KPFM measurements. The authors developed frequency-modulated methods help to deconvolve slow processes that are hard to isolate in KPFM measurements.

3. In situ SPM

SPM can be performed in gaseous or liquid environments; however, these environments introduce new challenges. In STM, instabilities from the ambient gas can affect tunneling currents in the junction, and water films formed at the air-sample interface can complicate results, but instrumentation development has made observations in reactive gases possible. 342,343 In liquid environments, the chemical composition is more readily controllable, improving the uniformity at the junction. 183,343 However, when STM is performed in polar liquids such as water, the flow of the liquid can produce currents substantial enough to obscure the tunneling current, although coating the tip with an insulator helps minimize this effect.³⁴⁴ Achieving realistic temperatures is also a challenge, with low temperatures stabilizing the system and reducing the thermal spread of electrons (an energy resolution of $10 \,\mu\text{eV}$ has been achieved with a dilution fridge³⁴⁵). Appropriate microscope stage design and feedback mechanisms have been developed to overcome thermal drift, enabling operating temperatures as high as 850 K. 346 Ultimately, in situ experiments are typically limited by the characteristics of the tip, which can lack sufficient chemical and thermal stability to endure in situ experiments, 342 although this can be minimized by limiting the tip-sample interaction time when fast dynamics are being investigated. 347 The tip can also perturb surfaces and adsorbates, compromising the results. As a consequence of these limitations, STM in particular is often performed in ultrahigh vacuum at low temperatures on smooth surfaces, while AFM is typically performed under ambient conditions. Frenken and co-workers have developed in situ systems for monitoring reactions at high temperatures (600 K) and pressures (several bar) for both AFM and STM, including a coupled mass spectrometer to monitor the reaction products. 348,349 Using this system, Groot and co-workers observed the restructuring of the Pt(110) and Pt(111) surface during CO oxidation and NO reduction, and MoS2 hydrodesulfurization over MoS2 nanoislands.3

The ability to achieve atomic resolution is often difficult, with the precise structure at the tip determining the resolution. Methods to sharpen and functionalize the tip within the apparatus are often needed and cannot necessarily be performed in a reactive environment. STM tip sharpening is done by applying a high voltage to the tip ($\sim 10 \, \text{V}$), while the tip is about 1 nm from the sample to produce field emission. For AFM, a sharp tip can be prepared by picking up a small cluster of atoms on the tip by touching it to the sample. However, the near-field properties of a plasmonic tip that has been prepared *in situ* cannot necessarily be determined, thus limiting quantitative conclusions. 325

4. Electrochemical scanning probe microscopy

Electrochemistry is a powerful in situ technique to drive and monitor catalytic reactions by directly observing and manipulating charge transfer events. 353,354 Scanning electrochemical probe microscopies enable monitoring reactions electrochemically at a singleparticle and sub-particle level. 355,356 Three main techniques have been developed; scanning electrochemical microscopy, scanning ion conductance microscopy, and scanning electrochemical cell microscopy. In scanning electrochemical microscopy, the local concentration of redox species is measured using an ultramicroelectrode positioned in solution close to the sample. 357-360 In scanning ion conductance microscopy, the changes in local ionic conductivity due to chemical reactions are monitored using a nanopipette with an opening on the order of tens of nanometers to tens of micrometers. 361,362 In scanning electrochemical cell microscopy, a tip filled with electrolyte and a protruding nanosized droplet is brought close enough to a sample to create an electrochemical cell the size of the droplet. 194,355 In all three setups, the tips can be scanned to obtain spatial maps of the electrochemical activity of nanoparticle-decorated substrates or held stationary to locally study electrochemical reactions over time. Scanning electrochemical cell microscopy was employed by Bentley et al. to study sub-particle-resolved variations in the catalytic activity of gold nanoparticles with 30 nm spatial resolution [Figs. 4(h) and 4(i)]. 194 Scanning probe techniques can be correlated with electron microscopy or dark-field spectroscopy to determine structure-function relationships in electrochemical catalysis.³⁶³ While single-entity electrochemistry is powerful in quantitatively monitoring how much charge is passed by a catalyst, reaction products are not directly observed, as they are for example in SERS. Therefore, rigorous control experiments have to be performed to ensure the observed current comes from the desired reaction. Additionally, corrections for Ohmic potential drop have to be applied to obtain quantitative data. 364 Currents measured in scanning probe microscopy experiments are typically on the order of picoamperes, ^{194,363} corresponding to the transfer of about 10¹⁰ electrons per second, far from the single-molecule sensitivity of fluorescence microscopy. 194,363 However, the ability of electrochemistry to directly monitor charge transfer from an electrode to the reactant promises opportunities for electrochemical scanning probe microscopy to study hot carrier-driven reactions by quantifying changes in reaction rate and onset potential of individual nanoparticles.²

C. Scanning probe optical microscopy

Optical and scanning probe microscopies are complementary techniques. In several of the discussed methods, the tip of the scanning probe was excited optically to establish a plasmon resonance. The optical excitation of the tip can also be used to perform optical spectroscopy. These methods can be used to gain local vibration information and provide near-field maps of surfaces.

1. IR atomic force microscopy

FTIR is a widely used infrared spectroscopic method that detects molecular bonds indicative of the chemical structure of a sample.³⁶⁵ However, FTIR is a traditional optical method insofar as it is limited by the diffraction of light, preventing it from providing nanoscale chemical insights. In AFM-IR, the tip acts as a near-field detector and changes in the tip oscillation amplitude are correlated with thermal

expansions resulting from localized IR absorption at the tip. ¹⁹⁵ AFM-IR has found applications, particularly in the characterization of MOFs. ^{283,366,367} While it is often possible to perform IR spectroscopy under ambient gas conditions, *in situ* IR spectroscopy in liquid environments remains a challenge due to the strong absorption of IR light by water and the impact on cantilever vibrations. ¹⁹⁵ However, methods for liquid environments, which are particularly important for electrocatalysis, have been demonstrated using graphene liquid cells for nano-FTIR ³⁶⁸ and resonantly enhanced AFM-IR with attenuated total reflectance illumination. ^{369,370}

2. Scanning near-field optical microscopy

Scanning near-field optical microscopy (SNOM) images the electric field below the diffraction limit using evanescent waves generated at the surface of an aperture smaller than the wavelength of the light. This method has been used to investigate the optical properties of, for example, dewetted gold plasmonic structures on $\mathrm{TiO_2}^{.371}$ SNOM using an aperture achieves a spatial resolution of around 50 nm, and the introduction of substantial artifacts complicates analysis. However, when operated in an apertureless configuration by confining the light between a sharp metal tip and the sample, spatial resolutions below 20 nm can be achieved.³⁷² Instead of collecting light that has been transmitted or reflected as is standard in SNOM with an aperture, scattered light is collected (thus, the method is also called scattering-SNOM or s-SNOM). Due to poor scaling of transmitted power through the aperture with the wavelength of light, the apertureless method is particularly useful for detecting IR signals.³⁷³ While AFM-IR probes the photothermal expansion of the material, in s-SNOM, the electric field enhances the IR absorption in the tip region, and backscattered IR light is collected, providing a near- and far-field IR fingerprint. 195 SNOM can be performed with a modified AFM apparatus and thus is a complementary technique, although similar information can be acquired with the relatively more straightforward methods discussed in Sec. VA.

Both standard Si or $\mathrm{Si_3N_4}$ AFM tips and plasmonic tips have been used in s-SNOM.³⁷⁴ IR-SNOM using a synchrotron light source was used to correlate reactivity with surface sites of Pt nanoparticles on a Si substrate for oxidation and reduction using N-heterocyclic carbene molecules as indicators.³⁷⁵ The response to liquid and gas phase oxidizing conditions on this system was also studied, by exposure prior to the measurement, which was performed at room temperature in nitrogen.³⁷⁶ SNOM has been used for near-field hyperspectral imaging of plasmonic nanostructures and, given the coherent and pulsed nature of the method, has potential for ultrafast applications.¹⁹⁶ While examples of *in situ* IR-SNOM for catalysis are relatively limited, Karst *et al.* developed a custom cell that allowed exposure of a magnesium film to hydrogen gas from below, while the top is available for measurements.¹⁹⁷ As discussed previously, substantial challenges exist for extending any IR method into liquid systems (Sec. V C 1).

3. Tip-enhanced Raman spectroscopy

The ability to precisely position a sharp tip in tip-enhanced Raman spectroscopy (TERS) allows Raman imaging below 1 nm spatial resolutions by only enhancing the Raman signal in a small area. ^{198,377–382} A tip that supports high electric field enhancement, such as a sharp STM tip, is positioned close to the substrate.

The electric field enhancement from the tip amplifies the Raman signal of molecules similar to SERS. However, because the tip can be positioned with nanometer resolution and because the near-field excitation is not limited by the diffraction limit, this method achieves subnanometer and single-molecule resolution.³⁸¹ TERS can be used in vacuum or in a gaseous or liquid environment, allowing in situ tracking of hot carrier-driven chemical reactions. 383-387 Additionally, the electric field enhancement used to increase the Raman signal is independent of the catalyst, which allows the detection of molecules on substrates that do not support strong electric field enhancement. Huang et al. mapped the hot-hole-driven decarboxylation of 4mercaptobenzoic acid to thiophenol between a silver tip and gold substrate.²⁴⁷ The authors locally generated hot holes in a 6-nm area and then performed a line scan of the reactant and product profiles. The profiles extended more than 20 nm in either direction, leading to the conclusion that holes had traveled up to 20 nm from their generation sites, comparable to the expected 10-40 nm mean free path of hot holes in gold. 69,247,315 Time-resolved TERS with a silver-coated AFM tip was used to monitor hot electron-induced N-N bond formation between p-nitrothiophenol groups on a gold film.³⁸⁸ Kusch et al. equipped an s-SNOM setup with a spectrometer to correlate elastically scattered light and Raman scattering from the same spots.³

D. Electron microscopy

Electron microscopy is a high spatial resolution method that can directly image atomic sites on catalysts; determine oxidation states, elemental compositions, and plasmonic properties through spectroscopy; and provide real-time observation of restructuring in catalytic nanoparticles. A major limitation is the difficulty of observing molecular species, although methods to perform vibrational spectroscopy in an electron microscope are becoming increasingly available and are poised to become increasingly important for the monitoring of chemical reactions in environmental electron microscopy experiments. Compared to optical microscopy (wavelength ~300-1000 nm), the wavelength of an imaging electron is \sim 5 pm, thus providing far superior spatial resolution, although the resolution is practically limited by the difficulty of focusing electrons. In electron microscopy, a beam of electrons incident on a sample will produce transmitted, scattered, or secondary electrons (the result of inelastic interactions between the sample and beam), as well as other signals such as characteristic x

There are two main types of electron microscopy that will be considered here: scanning (SEM) and transmission (TEM) electron microscopy. SEM is primarily a surface-sensitive technique, forming topographical images from secondary electrons emitted by atoms upon interaction with an electron beam. Backscattered electrons give information from hundreds of nanometers within the sample, including compositional information since heavier atoms scatter electrons more strongly.³⁹¹ SEM operates with accelerating voltages between 0.5 and 30 kV, achieving resolution on the order of 1 nm. 392 In TEM, transmitted and forward-scattered electrons are detected, producing a 2D projection of the sample. Accelerating voltages are typically between 80 and 300 kV, although accelerating voltages as low as 30 kV are possible, and spatial resolution below 1 Å is readily achievable. Operation at lower voltages reduces beam-induced knock-on damage, although there is not a threshold voltage at which radiolysis (ionization damage) disappears.³⁹³ While SEM more readily provides 3D and

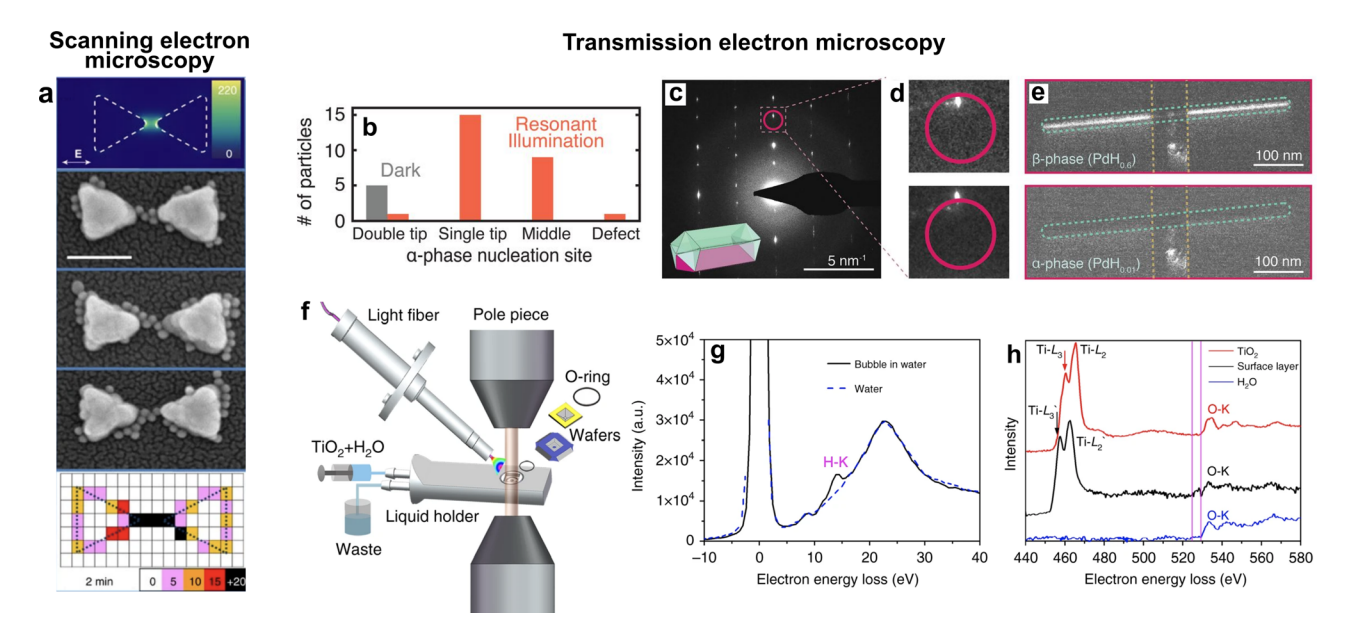


FIG. 5. Electron microscopy. (a) Finite-difference time-domain calculated near-field distribution for a silver bowtie. The surface was coated in 4-NTP. Upon illumination, a six-electron-mediated reduction forms 4-ATP, to which functionalized gold reporter nanoparticles bind, shown in the representative SEM micrographs. The histogram shows the frequency of gold reporters by pixel for 100 silver bowties. Scale bar, 100 nm. (b) Statistics for nucleation site in dehydrogenation of PdH_x nanorods on gold nanobars. (c) The diffraction pattern for a PdH_x nanorod and (d) zoomed-in regions of the diffraction pattern used for the displaced-aperture dark-field images shown in (e). (f) Schematic of homemade liquid flow holder and optical fiber inserted into the pole piece gap of a TEM and resulting (g) low-loss and (h) core-loss EELS spectra indicating the presence of hydrogen nanobubbles and a hydrogenated shell, which is shifted relative to the spectrum of pure anatase TiO₂. (a) Adapted with permission from Cortés *et al.*, Nat. Commun. 8, 14880 (2017).¹⁷³ Copyright 2017 Springer Nature Limited. (b)–(e) Adapted with permission from Sytwu *et al.*, Science 371, 280–283 (2021).¹¹¹ Copyright 2021 American Association for the Advancement of Science. (f)–(h) Adapted with permission from Lu *et al.*, Nat. Commun. 9, 2752 (2018).³⁹⁶ Copyright 2018 Springer Nature Limited.

topographical information than TEM by collecting scattered electrons rather than transmitted ones, the spatial resolution is typically not sufficient for directly imaging catalytic active sites. TEM allows for direct imaging of the atomic-scale structure of catalysts, and numerous methods exist to perform *in situ* experiments.

After a brief discussion of SEM, we will discuss TEM, including some of the relevant operating modes and spectroscopies, as well as the methods that have been developed to enable *in situ* reaction monitoring within TEM. A more detailed discussion of general TEM methods and their relevance to studying solid catalysts are provided in a 2015 review by Su *et al.*³⁹⁴ Methods such as photoemission electron microscopy and low-energy electron microscopy can also be used to observe surface reactions *in situ*, although they are not as widely used as TEM for the investigation of photocatalysts and will not be discussed here.^{395–397}

1. Scanning electron microscopy

While the higher spatial resolution of TEM compared to SEM means it is more often the method of choice for imaging atomic-scale catalytic active sites, such measurements are still possible in the SEM. Cortés *et al.* used SEM to record the position of reporter nanoparticles after various illumination times for mapping the hot carrier-induced transformation of 4-NTP to 4-ATP [Fig. 5(a)] (see also Sec. VIII B 1). A monolayer of 4-NTP was formed on silver bowtie or bar dimers. When illuminated at the plasmon resonance, the silver structures generated hot electrons that locally reduced the terminal

group of the 4-NTP, converting it to 4-ATP primarily at the hot-spot in the dimer gap. Methods such as SERS do not give complete information about the chemical reactivity because only molecules in the electromagnetic hot-spot are detected. Additionally, the system studied here is light-sensitive, and thus, tip-based vibrational methods would affect the reaction. Instead, functionalized 15-nm gold nanoparticles, which can be imaged by SEM, were allowed to interact with the surface and selectively bonded only to the 4-ATP. SEM has also been used in conjunction with electron beam resists to image electron emission from gold nanorods. Hobbs et al. excited the LSPR in lithographically fabricated gold nanorods covered in resist with a femtosecond pulsed laser. 172 The two resists used, poly(methyl methacrylate) (PMMA) and hydrogen silsesquioxane (HSQ), both reacted at the tips of the nanorods, where electron emission caused by high-field enhancements was the greatest. HSQ also reacted at the center of the nanorods, which the authors hypothesized is due to hot electron-induced dissociation of The exposure of the HSQ and PMMA was performed in an ambient environment, but the resists had to be developed before SEM was used to map the exposed areas; thus, this is an ex situ method. SEM has also been used extensively to monitor morphological changes and correlate these observations with methods such as darkfield microscopy (see Sec. IXB for further discussion of correlative methods).2

Environmental SEMs have been used to observe chemical vapor deposition of graphene^{401,402} and vapor–liquid–solid growth of semi-conductor nanowires.^{199,403} Modified sample holders provide sample heating, e.g., to induce *in situ* graphene formation on a carbon layer on

a Ni substrate. ⁴⁰⁴ Barroo *et al.* detected the adsorption and desorption of gaseous NO₂ on platinum by changes in the intensity of secondary electrons over several minutes, arising from modulation of the work function of the platinum. ¹⁹⁹ Electron backscatter diffraction was used to map the grain orientations, which allowed the authors to correlate surface reactivity with grain orientation. While its ability to provide insight into surface dynamics for plasmonic catalysis is limited, environmental SEM has been used to record reaction dynamics, which benefit from multiscale observation and large dynamic pressure ranges (e.g., chemical vapor deposition). ¹⁹⁹

2. Transmission electron microscopy

While there are a large number of imaging modalities in TEM, the general principle is to accelerate electrons down an evacuated column and collect them after they pass through the sample. The electrons are either directly transmitted or elastically or inelastically scattered by the sample. Image contrast is based on both the relative phase and the amplitude of the transmitted beams. TEM can be performed in bright field, where only the direct beam is used for image formation, dark field, where only diffracted electrons are used, and a combination of the two. Scanning transmission electron microscopy (STEM), a variation of TEM in which a focused probe of electrons is scanned across the sample, can achieve higher resolution when probecorrecting electron optics are used and produces images with greater atomic-mass contrast. More details regarding the operating principles of both TEM and STEM are provided in the textbook by Williams and Carter.³⁹⁰ Basic TEM imaging provides insight into the overall nanoparticle structure such as its size, shape, and crystallinity. The crystal structure and faceting are probed directly by electron diffraction. As catalysts are known to restructure under reaction conditions, dramatically altering their behavior, in situ observations of morphology are particularly useful. TEM is generally preferred to STEM for in situ imaging given that TEM acquires snapshots of the entire field of view while STEM requires serial scanning of the sample. While both are limited by the amount of time required to build up enough electron signal for a clear image (and thus, temporal resolution of real-time imaging is determined by the beam brightness and detector sensitivity), the time resolution is typically \sim ms for standard TEMs and \sim s for STEM.

Non-plasmonic catalyst behavior has been observed in near-reaction conditions, lending valuable mechanistic insight into processes such as growth and etching 405-410 and dynamic restructuring and deactivation. A more detailed discussion of such experiments is provided in several reviews. Below, we discuss several examples relevant to plasmonic photocatalysis.

a. Imaging. Direct imaging of plasmonic photocatalysts has allowed for tracking the progress of chemical processes in real time. Using dark-field imaging and contrast changes in STEM 417 and TEM imaging, 418 Dionne and co-workers directly observed the first-order phase transition between hydrogen-rich (alpha) and hydrogen-poor (beta) PdH $_{\rm x}$ nanoparticles. More recently, Dionne and co-workers have coupled PdH $_{\rm x}$ nanoparticles to gold nanoparticles, demonstrating the excitation of an LSPR in the gold nanoparticle altered the dehydrogenation reaction rate and active sites for the catalytic splitting of H $_{\rm 2}$ and subsequent intercalation into the palladium lattice [Figs. 5(b)–5(e)]. 111,112

These experiments reveal the importance of plasmonic hot-spots for locally and selectively initiating chemical transformations. 419 Other plasmon-mediated processes, such as the growth of silver nanotriangular plates, have been monitored *in situ* and in real time. 420

As discussed previously, catalysts can undergo significant restructuring under reaction conditions, with such changes impacting the stability and activity of the catalyst. Weng $et\ al.$ recently investigated the photostability of gold nanoclusters smaller than 1 nm on TiO2. While such clusters are too small to host collective plasmonic properties, they have emergent molecule-like properties, which cause them to interact strongly with light. The authors observed the agglomeration of gold clusters protected by the tripeptide glutathione stabilized on branched poly-ethylenimine-modified TiO2 nanosheets. Gold clusters were found to fuse by both migration and coalescence and Ostwald ripening, with an inert atmosphere being more favorable than an oxidizing environment to stabilize the clusters.

b. Spectroscopy. In the electron microscope, energy dispersive x-ray spectroscopy (EDX or EDS) and electron energy loss spectroscopy (EELS) provide chemical and optical information with the same electron beam and therefore simultaneously with imaging. Spectroscopy relies on inelastic interactions between the electron beam and the sample. Due to the high energy of the electrons (80–300 keV in a TEM), these interactions can occur at virtually all relevant energies. In TEM mode, spectra can be rapidly collected over an ensemble of particles, whereas in STEM mode, serial collection of spectra across each scan point forms a spectral map at the same spatial resolution but reduced temporal resolution. A much more detailed discussion of EDX and EELS and their practical application are provided by Williams and Carter³⁹⁰ and Egerton electron electron microscope, energy dispersive x-ray spectros-

When the electron beam interacts with the sample, it can eject core electrons with an accompanying emission of characteristic x rays. These x rays are detected in EDX, and their energy is indicative of the elemental composition of the sample. Compared to EELS, EDX is preferable for its relative ease of data collection and processing (and can also be performed to an extent in SEM). Quantification methods are well-developed and robust, with software able to automatically determine elemental concentrations from the measured x-ray signal given known coefficients (k- and zeta-factors). These factors can vary for each particular EM system and thus should be measured from a standard for optimal precision. However, EDX should be limited to detecting heavier atoms (e.g., Z > 10), since for lighter atoms, the x-ray signal is less reliable: emission of Auger electrons dominates over x-ray emission, and any emitted x rays are of lower energy, which are more likely to be absorbed by the sample, experience a higher background signal, and are less spectrally separated. 423 For multimetallic nanoparticle catalysts, EDX maps are useful for measuring the relative concentration and spatial distribution of their constituent metals. 42

EELS is a versatile technique that extends beyond elemental analysis alone. Where EDX is valued for its accessibility, EELS can obtain much richer information from the sample. In EELS, the energy of the electron beam is measured after interacting with the sample, with losses in kinetic energy resulting from the electrons inducing an excitation event in the material. Electrons detected in the core-loss region (>50 eV) correspond to excitations of core electrons, giving the same elemental information as EDX but viable for lighter atoms as well. Additionally, the electronic and bonding structure of single atoms can be interrogated from the near-edge fine structure of the EELS core-loss

feature, analogous to x-ray absorption near-edge structure (XANES) in x-ray spectroscopy (Sec. VIB1). Electrons in the low-loss region (<50 eV) result from excitation of transitions at optical and vibrational energies such as plasmon resonances, providing similar information as many other spectroscopic techniques, which probe the same energies but at the nanoscale.

One of the primary uses of TEM in plasmonic photocatalysis is to characterize the plasmonic properties of nanoparticles with EELS. Since the LSPR of plasmonically active materials is directly excited by the electron beam, low-loss STEM-EELS maps are used to determine the location and energies of plasmon modes within and around a plasmonic nanoparticle. Modern TEMs equipped with cold-field emission guns, monochromators, and highly energy-dispersive electron spectrometers can routinely achieve spectral resolutions of <200 meV after signal processing, allowing precise measurement of individual LSPRs in the visible and near-IR (<3 eV). 200,201 Monochromated EELS maps have been used to probe the plasmon resonances in, for example, silver nanodisks and nanotriangles, 202-204 small silver nanoparticles with varying diameters, 205,206 aluminum nanotriangles, 207 and several bimetallic systems. 208-211 EELS has also been used specifically to probe energy transfer in bimetallic plasmonic systems²¹² and between plasmonic metals and semiconductor substrates²¹³ to help elucidate the mechanism of plasmon-driven chemistry. Li et al. used electrodynamics simulations and the extended plasmon hybridization theory alongside EELS data to distinguish between energy transfer arising from PIRET vs indirect charge transfer.²¹

The current state-of-the-art monochromation has brought the pinnacle of EELS energy resolution into the $<\!10\,\text{meV}$ range, first demonstrated in 2014 by Krivanek $et~al.^{219}$ Among widely available commercial TEMs, $<\!50\,\text{meV}$ resolution is now readily achievable, 426 enabling the detection of lower-energy mid-IR plasmons ($<\!400\,\text{meV}$), such as those observed in lengthy gold 427 and copper nanowires, 428 in addition to meaningful measurements of LSPR line widths, which can inform plasmon damping and thus plasmon energy transfer dynamics. 200

These advances in energy resolution have also enabled vibrational spectroscopy with the spatial resolution of the TEM. ²¹⁹ Vibrational spectroscopy (see Sec. V A 3) is used to identify molecular species and characterize material phonons. Vibrational EELS has been used to detect mobile hydrogen in TiH₂, as well as vibrations in biogenic guanine crystals, magnesium oxide nanocubes, and cubic and hexagonal boron nitride; at a grain boundary in SrTiO₃; and in an ionic liquid. ^{219–226} The distinct vibrational modes of carbon isotopes were used to map differently labeled alanine crystals ²²⁷ and determine the diffusion of carbon during self-healing in a cracked graphene flake. ²²⁸ Similar to methods such as SERS, EELS vibrational signatures can be modified by plasmons and the resulting enhancement has been demonstrated in the coupling between plasmonic modes in silver nanowires and phonon modes in h-BN flakes. ^{229,230}

Baldi *et al.* first detected the alpha to beta phase transition in PdH_x nanoparticles using EELS, owing to the bulk plasmon shift between these two hydride states. The plasmon resonance of PdH_x and gold crossed bars determined by EELS was compared to wavelength-dependent nucleation dynamics, demonstrating that unfavorable nucleation of the phase transition is induced when the illumination wavelength overlaps with the resonance. Lu *et al.* examined the formation of a hydrogenated shell on anatase TiO_2 in

water, using imaging to observe the shell and EELS to investigate its chemical composition [Figs. 5(f)-5(h)].

c. Tomography. Electron microscopy tomography elucidates the 3D structure of a nanomaterial from a series of 2D images. Images are acquired, either in STEM or TEM mode, as the sample is tilted. Geometric limitations of the apparatus generally limit tilt angles beyond 79°, leaving a "missing wedge," which is not imaged. The missing wedge together with sample drift, small structural changes over the acquisition time, and additional sources of misalignment make extensive algorithmic realignment and image comparison necessary for accurate reconstruction of the 3D image. However, with the latest advances in electron microscopes and reconstruction algorithms, 3D structures can be obtained of nanoparticles with atomic resolution. Alou et al. used atomic-resolution electron tomography to track the precise 3D arrangement of atoms in bimetallic FePt nanoparticles at different annealing time points, informing their nucleation and growth dynamics.

Tomography is similarly used to map nanoparticle catalysts that undergo complex structural changes during a reaction, such as hollowing or segregation, which are not necessarily discernible from a 2D projection. Han et al. combined electron tomography with environmental TEM (ETEM) to track the change in the structure of a Ni₂Co particle as it oxidized.²¹⁴ The particle was oxidized by heating in an oxygen environment, during which time only projection images could be collected as the particle evolved. To get 3D structural information, the temperature was lowered to quench the reaction and tomography was performed using annular dark-field STEM. STEM-EELS tomography was used to determine chemical structure before and after oxidation. A current limitation to using tomography for systems that cannot easily be quenched is the timescale for data collection (tens of minutes to hours), although fast tomography is an active area of research.⁴³ An additional challenge is the need for specialized environmental or light-coupled holders, which can further limit the tilt range.

d. Detecting adsorbates. A needed step in the field is developing method to identify intermediate species adsorbed to the catalyst surface. While the motion of single atoms on a nanoparticle surface has been recorded in situ, ^{213,433} it is generally not possible to directly observe molecular adsorbates on the surface of a nanoparticle due to their low atomic weights and beam sensitivity. Numerous improvements are making vibrational EELS for detecting adsorbates increasingly possible. ²¹⁹

Raman spectroscopy, as discussed in Sec. V A 3, could also be complementary to vibrational EELS for the identification of chemical species adsorbed to a nanoparticle surface. The direct incorporation of the Raman spectroscopy into electron microscopes has been demonstrated so far for determining sample temperature and structural changes in 2D materials. Using a free-space parabolic mirror on a hollow rod inserted into the objective aperture port on an environmental STEM, Picher *et al.* collected Raman spectra during and after the growth of single-walled carbon nanotubes, although the high temperature of the growth limits the signal. The temperature of the sample can be determined by measuring the shift in Raman peaks, allowing for the quantification of sample heating due to illumination. Allen *et al.* inserted a Raman probe directly into the column, with an additional feedthrough for optical fibers in the sample holder

to investigate laser-induced phenomena. 435 This setup was used to collect Raman spectra before and after pulsed laser ablation of MoS₂ flakes. In both these systems, the Raman signal is limited to probing extended structures and the signal is collected from the entire laser spot size (2 μ m to 15 μ m) and thus cannot be correlated with TEM data from a specific nanoscale section of the sample. Saleh *et al.* have proposed stimulated Raman for TEM, in which a laser is used for the Stokes excitation and plasmonic cathodoluminescence enhances the Raman scattering exclusively from the particle, which has been excited by the electron beam. 436 This approach would allow for nanoscale maps of Raman scattering, rather than a spectrum that is indiscriminately produced by the entire laser spot size.

Another method that has recently been demonstrated for investigating adsorbate properties is off-axis electron holography. Another method is used for detecting electric and magnetic fields on a sample as these fields will produce a phase shift determined by the recorded interference pattern, making it useful for detecting adsorbate-induced changes to electronic structure and chemistry at the catalyst surface. Electron holography has been used to identify the charge state in platinum nanoparticles. Electron holography depends on the coherence of the beam, which will be negatively impacted by the presence of gaseous species inside the microscope, but is nevertheless possible.

Four-dimensional STEM, or 4D-STEM, is an emerging technique that can similarly measure electric fields and thus charge densities and charge transfer. 216-218 Zachman et al. have demonstrated using 4D-STEM to determine the direction of charge transfer between gold nanoparticles and an oxide support, which varied based on chemical treatment and was correlated with CO oxidation catalytic performance. 440 With advancements in electron detectors and data analysis processes enabling 4D-STEM, this technique shows promise for plasmonic photocatalysis by measuring charge transfer in other heterostructure systems, which again can be affected by the presence of adsorbates. In addition, the diffraction patterns acquired in 4D-STEM can be used to map strain across a catalyst, 216 which can be caused by non-uniform adsorbate binding as well as affect adsorbate binding energies.^{217,441} Mapping strain from other nonuniformities in a plasmonic photocatalyst, such as the heterogeneous mixing of metal atoms in a bimetallic nanoparticle, can also be used to characterize spatially resolved photocatalytic behavior.443

e. In situ TEM. To observe photocatalysts under reaction conditions, the reactive species of interest need to be introduced to the catalyst sample, whether in a gas or a liquid environment. However, interactions with gaseous or liquid species will reduce the coherence of the beam; thus, these media are generally confined to a small volume close to the sample to maintain high vacuum throughout most of the column, minimizing electron beam decoherence and preventing contamination of the electron gun.

Gas is introduced to the sample using either a differentially pumped system or a specialized sample holder. A more detailed discussion of both methods is found in the recent review by He *et al.*⁴¹⁶ In order to monitor gaseous products during a reaction for *in operando* studies, a sensitive mass spectrometer (residual gas analyzer) and EELS can both be used, the respective advantages and disadvantages of each have been discussed in detail by Crozier and co-workers. 443,444

In a differentially pumped system, also known as an environmental TEM (ETEM), gas is introduced directly to the column and

confined to a small region around the sample using differential apertures. This method eases sample preparation and allows simultaneous use with a specialized holder (e.g., one which allows illumination of the sample). The maximum pressure when differentially pumping is around 15 Torr, ⁴⁴⁵ substantially lower than the 760 Torr (1 atm) achievable with a specialized holder. Methods to further increase pressure in a differentially pumped system generally come at the cost of resolution due to increased noise. ⁴¹⁶

Early examples of ETEM photocatalyst studies were conducted by Zhang et al. 446 and Hansen and co-workers, 447,448 who flowed water vapor over metal oxide semiconductor photocatalysts under simultaneous illumination and used a combination of imaging and EELS to detect changes in the catalyst structure and oxidation states, respectively. All of the previously mentioned work by Dionne and coworkers studying the phase transitions of PdH_x used ETEM to flow H₂ gas over their Pd nanoparticles, combined with a sample holder equipped with temperature control to adjust the hydrogenation thermodynamics. 111,112,417,418,429 Yang et al. introduced CO gas into their ETEM to monitor plasmonic CO disproportionation by triangular gold nanoprisms supported on TiO2.449 They used STEM-EELS to map the nanoprism LSPRs, measure shifts in those LSPRs with changing CO adsorption, and detect the presence of amorphous-carbon products. As evidence of spatially controlled plasmonic catalysis, they observed that the gold nanoprism tip furthest from the TiO2 both exhibited the highest field enhancement and largest carbon buildup when excited by the electron beam.

If a dedicated ETEM is not accessible, a specialized environmental holder can be used in a standard TEM. This technique is also used to introduce liquid to the sample. A specialized holder can not only achieve higher pressures, but it also inputs a user-defined flow rate, allowing for further tailoring of reaction conditions. While a specialized holder does not require additional pumps to be connected to the microscope, the medium must be trapped between two windows, which can decrease the spatial resolution and reduce the quality of EELS and EDX data due to increased scattering off the windows. Windows are typically made of $\mathrm{SiN_x}$ for gas and $\mathrm{SiN_x}$ or graphene for liquid. 451,452 A variety of other TEM holders are commercially available, which can control reaction conditions, such as illumination, heating, cooling, and electrical biasing holders; and more-advanced holders often combine multiple capabilities at once.

Light is introduced to the sample by either one of the aforementioned specialized sample holders or modifications to the microscope column. While a holder is more versatile and readily swapped between instruments, it generally precludes coupling of gas or liquid into the system through the same holder, thus requiring a differentially pumped system, although new custom holders are being developed, which can combine both illumination and fluid flow. 453 In their ETEM photocatalyst experiments, Hansen and co-workers used both a fibercoupled holder that can couple to any external light source and a lensbased holder with built-in internal optics to illuminate photocatalytic Cu₂O nanocubes and Pt on GaN:ZnO nanoparticles with 405-nm Dionne and co-workers also used a fiber-coupled holder to illuminate their plasmonic antenna-reactor gold-palladium catalysts with an external tunable laser and induce plasmon-mediated dehydrogenation reactions. 111,112 Alternatively, optics can be inserted directly into the column, but this requires modifications of the microscope that are not always feasible. For their previously mentioned ETEM

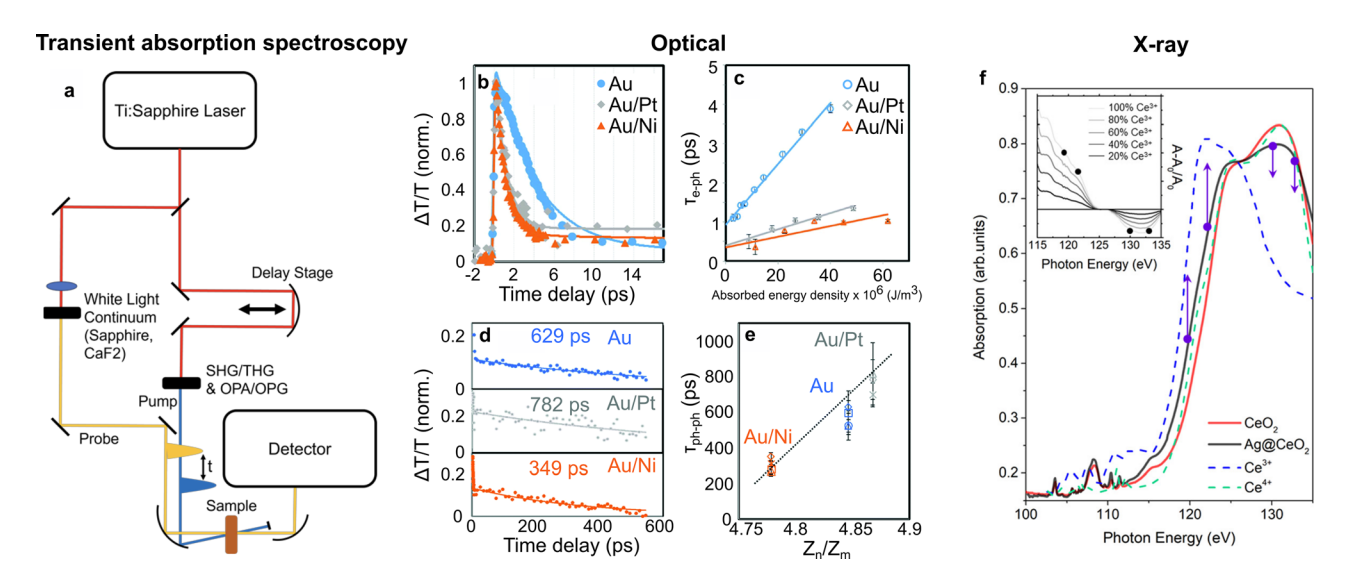


FIG. 6. Ultrafast absorption spectroscopies. (a) Schematic of a common ultrafast TA spectroscopy setup design. (b) Transient absorption traces of gold, gold–platinum, and gold–nickel nanoparticles, showing a dependence of the transient decay on the particle composition. The solid lines correspond to exponential fit functions. (c) Electron–phonon coupling times of the sample in (b) as a function of the absorbed energy density and linear fit functions (solid lines). (d) Transient absorption traces from (b) over long time delays. (e) Phonon–phonon coupling times of the different nanoparticle samples, extracted from the traces in (d), plotted against the ratio of the acoustic impedances Z of the metals in each sample. (f) Time-resolved XAS of cerium in Ag@CeO₂. Solid lines are experimental measurements, and dashed lines are reference values. The purple vectors indicate energies measured in TRXAS, corresponding to the highlighted points on literature spectra in the inset, as Ce⁴⁺ is reduced to Ce³⁺. (b)–(e) Adapted with permission from Sim *et al.*, Nanoscale 12, 10284–10291 (2020). 464 Copyright 2020 Royal Society of Chemistry. (f) Adapted with permission from Pelli Cresi *et al.*, Nano Lett. 21, 1729–1734 (2021). 466 Copyright 2021 Author(s), licensed under a Creative Commons Attribution.

photocatalyst study, Zhang *et al.* inserted a separate optical fiber into the microscope aimed at the sample holder tip and used a broadband white light to illuminate ${\rm TiO_2}$ nanocrystals, observing surface layer amorphization. ⁴⁴⁶ Other methods for introducing light include using a microelectromechanical chip outfitted with a light-emitting component at the holder tip. ^{454,455} Numerous papers discuss the construction of illumination holders, ^{434,446–448,456,457} and several recent reviews cover the topic of sample illumination in a TEM in greater detail. ^{453,456}

With developments in TEM such as spherical aberration correctors and monochromators, which improve spatial and energy resolution, respectively, quantitative information from in situ experiments is increasingly accessible. Despite the many advancements, there are still essential limitations of in situ TEM methods. One outstanding challenge is to minimize electron beam effects and to distinguish such effects from those caused by optical excitation. 458 The electron beam can cause knock-on damage of the sample and radiolysis of gaseous and liquid environments, which forms reactive radical species. 447 effects make extensive control experiments necessary and limit the researchers' ability to draw quantifiable conclusions from the data. One recent advance that reduces these effects is direct electron detectors, which allow researchers to produce atomic-resolution data with lower electron doses. Despite these limitations, TEM stands as an incredibly powerful technique for characterizing plasmonic photocatalysts at the nanoscale, especially when many or all of the above subtechniques are combined.

VI. HIGH TEMPORAL RESOLUTION TECHNIQUES

Relevant hot carrier relaxation processes happen on the order of hundreds of fs to tens of ps. ³⁴ While the above-mentioned *in situ*

techniques offer spatial resolutions down to picometers, they perform steady-state measurements and do not provide the temporal resolution to directly study these ultrafast carrier dynamics. ⁴⁵⁹ However, a mechanistic understanding of charge carrier lifetimes is crucial to optimize plasmonic materials for applications, which generally benefit from long-lived carriers to, e.g., create electric currents or drive chemical reactions. ⁴⁶⁰

We will describe in Secs. VI A and VI B the use of ultrafast methods when exciting plasmons using a pulsed pump beam at UV/VIS/near-infrared (NIR) wavelengths, then performing time-resolved measurements with a pulsed probe beam at either optical or x-ray wavelengths, depending on the desired spectroscopy.

A. Ultrafast transient absorption spectroscopy

All-optical, ultrafast pump-probe transient absorption (TA) spectroscopy captures ultrafast carrier dynamics with temporal resolution down to hundreds of femtoseconds by exciting and subsequently interrogating a sample using two time-delayed femtosecond light pulses. A typical setup is pictured in [Fig. 6(a)]. A Ti:Sapphire laser provides laser pulses, and the laser light is split into pump and probe pulses. To achieve time delay between pump and probe pulses, a delay stage is employed in either the pump or the probe path. Harmonic generation or optical parametric amplification is used to generate the desired pump wavelength. In the probe path, a white light continuum is achieved by focusing the light into nonlinear crystal plates. Both beams are directed onto the sample, and, after removal of the pump, the probe is collected by a detector to acquire images or spectra. A first pulse, the pump pulse, excites carriers in the plasmonic material that rapidly thermalize to create a Fermi–Dirac distribution. The resulting

changes in the absorption cross section affect the interaction of the plasmonic material with the second pulse, the probe pulse. Depending on the measurement geometry, the pump-induced changes are then measured in the transmitted or reflected intensity of the probe. By varying the pump-probe time delay, it is possible to monitor the temporal evolution and lifetimes of plasmonic carriers with only the pulse lengths limiting the temporal resolution. Note that pump-probe experiments are limited to reversible processes due to the need for repeated measurements at various delay times. The robust experimental setup of TA spectroscopy allows for *in situ* measurements of plasmonic materials in various environments.

Using femtosecond light pulses in the VIS and NIR, TA spectroscopy has been applied to study the dynamics of charge carriers in plasmonic materials ranging from metallic nanoparticles to organic, nonmetallic, and semiconductor hybrid structures. 91,92,233,462-465 example, Sim et al. utilized an ultrafast TA spectroscopy setup comparable to Fig. 6(a) to study the ultrafast dynamics of pure nanoparticles and bimetallic gold particles with the catalytic metals Pt and Ni. 464 The authors found that the electron-phonon coupling times decreased for the bimetallic particles, indicating that the coupling of hot carriers to the lattice accelerates with the addition of catalytic elements to gold nanoparticles, thus decreasing the hot carrier lifetimes [Figs. 6(b) and 6(c)]. They also showed that the addition of Pt and Ni led to either increased or decreased phonon-phonon coupling times, respectively, indicating that the radiation of heat into the environment can be modified by varying the nanoparticle composition [Figs. 6(d) and 6(e)]. These results proved that the addition of catalytic materials to nanoparticles importantly changes the charge carrier dynamics, showcasing the importance of ultrafast TA spectroscopic measurements. Zhang et al. used ultrafast in situ diffuse reflectance infrared Fourier transform spectroscopy to show that plasmonic Au@AuRu nanoparticles on g-C₃N₄ efficiently hydrogenated CO₂ to methane.⁹¹ The temporal information from ultrafast spectroscopy revealed here that the combination of the metal and semiconductor materials extended the time window of hot electrons to participate in the reaction. Similarly, Pelli Cresi et al. used ultrafast TA spectroscopy to probe the dynamics of charge transfer between silver nanoparticles and CeO₂, observing that long-lived hot electrons are injected into the ceria likely via both indirect charge transfer and PIICT mechanisms based on the observed efficiencies.²³³ Zhang et al. studied W₁₈O₄₉ nanowires on TiO₂ nanofibers and found enhanced catalytic generation of H2 from ammonium borane compared to the case without nanofibers. 92 The high temporal resolution of their measurement allowed them to determine that the W₁₈O₄₉ nanowires passed hot electrons to the nanofibers within 200 fs, leading to large rate constants up to $5.5 \times 10^{12} \text{ s}^{-1}$.

B. Ultrafast x-ray probes

With wavelengths of less than ~ 10 nm, x rays, unlike visible light, are energetic enough to interact with the core electrons of atoms and be diffracted by atomic lattices, giving information about a material's electronic states and crystal structure, respectively. The probability of absorbing an x ray is approximately proportional to the x ray's wavelength cubed, and hence x rays become more penetrating as their energy increases. Low-energy x rays with wavelengths greater than 0.1 nm ($\sim 10 \, \text{keV}$) are considered "soft" and typically used for absorption spectroscopy, while x rays with higher energies are considered "hard" and typically used for imaging (see Sec. VII B) or

scattering. 240,467,468 X-ray techniques are widely used in catalysis studies to determine properties like the spatially resolved elemental composition of elements in alloys, 469–472 the shape and size distributions of nanoparticles in ensemble measurements, 243,473 elemental oxidation state, 474,475 and band structure of semiconductors. 476,477

Due to the recent advent of x-ray free-electron lasers (XFELs), which produce extremely bright and fast pulsed x rays of durations in the femtosecond regime, 478 the same pump-probe methods described in Sec. VI A using UV/VIS/NIR light can be performed with x rays with similar ultrafast temporal resolution. With a pulsed optical pump and subsequent pulsed x-ray probe, ultrafast x-ray methods can acquire material information available from conventional x-ray techniques at the pico- to femtosecond timescale to uncover plasmonic mechanisms. 466,479

While studies on plasmonic photocatalysts are still emerging, ultrafast x-ray methods have been used to track and differentiate between plasmonic energy transfer pathways by observing the time-resolved response of the plasmonic catalyst's material and electronic structures to photoexcitation. These preliminary studies indicate that ultrafast x-ray techniques can be another valuable tool to quantify charge carrier dynamics within material systems such as plasmonic nanoparticle photocatalysts or between materials such as plasmonic particle–semiconductor interfaces.

Before we discuss each ultrafast x-ray technique, we will briefly introduce their conventional forms without temporal resolution. Several other reviews discuss these base methods in greater detail, including how they have been applied to nanoparticles and heterogeneous catalysis. ^{236,237,467,480,481}

1. X-ray absorption

X-ray absorption spectroscopy (XAS) provides information about the electronic structure of atoms and the local atomic environment of a sample. 237 The absorption of x rays by an atom excites core electrons at characteristic energies, enabling elemental identification analogous to EDX and core-loss EELS (Sec. V D 2). 236 Finer details of the spectrum past the absorption edge provide most of the electronic and structural information. The x-ray absorption near-edge structure (XANES), from the edge energy to 30–40 eV above it, gives information about the atom's chemical states, including its oxidation state and orbital hybridizations with neighboring atoms. $^{237-239}$ The extended x-ray absorption fine structure (EXAFS), at energies $\gtrapprox 40~{\rm eV}$ from the edge, provides short-range structural information about the species, number, and disorder of the neighboring atoms, as well as the distance to them. $^{237-239}$

After an x-ray absorption event ejects a core electron, the relaxation of a valence electron into the core hole can emit another x-ray characteristic of the occupied valence band, measured using x-ray emission spectroscopy or x-ray fluorescence. Combining conduction band measurements from XAS and valence band measurements from x-ray emission spectroscopy (or another method like STM, Sec. VB1), the bandgap of a material can be calculated. The ference between the incident and emitted x-ray energies can be measured as resonant inelastic x-ray scattering, analogous to Raman scattering but in the x-ray regime, which can give information about lower energy excited states normally inaccessible by total absorption of x-ray energies. ANNES and variations thereof can be used to monitor the surface coverage of adsorbates on nanoparticles and oxidation

states of the catalyst. 482,483 EXAFS has been used to determine changes in binding between surface atoms and adsorbates. 484 Performing conventional XAS experiments still requires particle accelerators to provide sufficiently high x-ray intensities and a continuous energy spectrum. 238

Ultrafast, time-resolved XAS (TRXAS) promises all of the above information from conventional XAS with pico- to femtosecond resolution. 485 For photocatalysts, TRXAS has been used to track the dynamics of excited charge carriers through different atomic species, since the presence of excited charge carriers alters the materials' electronic states. 485 This technique has recently been used to directly probe charge carrier dynamics in semiconductor oxide materials such as TiO₂ and Fe₂O₃. ^{479,486,487} Ismail et al. used TRXAS and time-resolved resonant inelastic x-ray scattering to observe charge carrier dynamics in a semiconductor oxide material. Hematite (Fe₂O₃) was photoexcited with 400 nm light; then, changes in the Fe L₃ x-ray absorption edge were used to track electron transfer from the hematite occupied 2p to unoccupied 3d bands. After this initial excitation, the ultrafast time resolution of 180 fs allowed the authors to observe a hot carrier relaxation process with a time constant of 0.2 ps and a subsequent carrier recombination process with a time constant of 6 ps, in addition to longerlived photoexcited states suggesting trapped excited electrons.

As a first demonstration in using the technique to elucidate plasmonic mechanisms in a photocatalyst, TRXAS has similarly been used to probe electron transfer dynamics in a hybrid plasmonic-semiconductor system. 466 Pelli Cresi et al. used TRXAS with a time resolution on the order of \sim 200 fs to monitor changes in the cerium oxidation state of a CeO₂ film induced by plasmonic photoexcitation of embedded silver nanoparticles, the same system they earlier investigated with optical TA spectroscopy (Sec. VIA). Upon illumination of the silver nanoparticles' LSPR using a 430-nm pump pulse, a 119–133 eV x-ray probe pulse was used to detect the reduction of cerium from Ce⁴⁺ to Ce³⁺ within a few hundred femtoseconds, based on changes in the cerium XAS signal at the probe energies, indicated by the purple vectors in Fig. 6(f). This observed reduction confirmed the mechanism of photoexcited energy transfer in this hybrid plasmonic-semiconductor material after decay of the silver LSPR as an electron-transfer process from silver to cerium rather than a photothermal effect. The lifetime of these transferred electrons was measured as up to 1 ps, indicating the lack of rapid recombination. 40 Quantification of the TRXAS signal additionally suggested that only the first interfacial monolayer of cerium surrounding the silver nanoparticles was excited. TRXAS has yet to be widely applied to plasmonic photocatalysis, but this technique shows promise for more direct and quantitative measurements of charge transfer processes compared to other time-resolved spectroscopies thanks to its greater chemical specificity and sensitivity to changes in electronic states, as demonstrated in Pelli Cresi et al.'s two studies on the same photocatalyst.²

2. X-ray scattering

X-ray scattering methods obtain structural information about a material system in reciprocal space by measuring the angle at which x rays elastically scatter off the electrons.²⁴⁰ In x-ray diffraction (XRD), the scattered x rays that constructively interfere are used to calculate the periodic structure of a sample, obtaining crystallographic information, including atomic lattice spacings and crystal phase.²⁴¹ For ordered materials such as nanoparticle catalysts, scattering and

diffraction are often used synonymously.²⁴² Atomic-scale spatial resolution can be achieved by collecting angles scattered by more than 10.^{243,244} X rays at lower scattering angles are indicative of longerrange structure, obtaining overall size and shape statistics of large systems of nanoparticles, complementary to TEM.²⁴³

Ultrafast, time-resolved x-ray scattering can probe a catalyst's structural changes immediately after photoexcitation. Plech and coworkers used this technique to quantify the plasmonic heating of gold nanoparticles, as measurements of lattice dynamics can be correlated with thermal expansion as a form of nanocalorimetry. 488-490 They were able to observe ps-timescale shifts in the x-ray scattering of gold spheres and nanorods after laser excitation and used the data to determine the nanoparticles' lattice expansion. They then used this structural information to calculate the temperature change in the particles over the same time frame, tracking the magnitude and rate of photothermal heating and subsequent cooling. In addition, they observed further structural changes in the nanoparticles resulting from this heating and compared the heating efficiency of interband vs plasmonresonance illumination. 488-490 We predict for other plasmonic photocatalytic systems, ultrafast x-ray scattering can be similarly used to monitor time-resolved temperature changes in the catalyst material and thus differentiate between photothermal and non-thermal mechanisms. Additionally, x-ray scattering can detect morphological changes in the catalyst that could correlate with changes in reactivity, potentially informing photocatalyst stability studies.

3. In situ x-ray methods

Since pump-probe methods are characterizing transient processes induced by the pump beam, we define all the above ultrafast x-ray techniques as *in situ*, especially in the context of plasmonic photocatalysis, as by default they take snapshots of photoexcited catalysts evolving in real time with ultrafast temporal resolution. Ultrafast x-ray measurements require XFELs at linear accelerators for adequately intense brightness and short pulse durations, so accelerator x-ray sources typically have built-in support for optical elements to manipulate light as needed among the x-ray source, an additional pump laser, the sample, and detector(s), including time synchronization between the XFEL and pump laser. ⁴⁹¹

For more complex in situ conditions, just like in optical microscopy (Sec. VA5), SPM (Sec. VB3), and TEM (Sec. VD2), tailored reaction cells have been designed for x-ray experiments with various specifications for a host of environments and applied conditions, including, but not limited to, containment and flow of gas⁴⁹² or liquid, 488 transparency to other wavelengths of light, 482 control of temperature, ^{492,493} application of electrical bias, ⁴⁹⁴ measurement of reaction products, 482 and any combination of these in a robust manner, all while maintaining sufficient x-ray signal and resolution. Doronkin et al. have outlined a detailed list of considerations when designing an in situ cell for x-ray experiments, both in general 495 and for catalytic reactions. 469 Since hard x rays are highly penetrating and can be used with most materials and chemical environments, ⁴⁹⁵ while lower-energy soft x rays are more likely to be absorbed, experiments using hard x rays have less-restrictive in situ setups, 496 while experiments using soft x rays can require more specialized sample chambers, often operating in the presence of high vacuum.²²

In the ultrafast plasmon studies discussed earlier, the experimental setup varied greatly based on the applied conditions. In Pelli Cresi

et al.'s study of Ag@CeO2, they only required a visible pump beam in addition to the XAS probe, so their sample was in an ambient environment, while they set up two separate optical paths for the pump 430 nm laser and the probe XFEL, which were synchronized jitter-free by using the same pulse generator to initiate both sources. 466 In Ziefuss et al.'s study of gold nanosphere fragmentation after plasmonic heating, they used a thin commercially available quartz capillary (0.35 mm diameter) as a liquid reaction cell that was illuminated at the same spot by both a pump 532 nm laser and a probe synchrotron x-ray beam. They flowed an aqueous suspension of nanoparticles to introduce fresh sample to the illumination spot for every pulse. 48 Ultimately, many in situ setups for ultrafast x-ray experiments may need to be custom-built depending on the reaction needs, which can be a significant experimental consideration and hurdle, though generalized commercial reaction cells are still being actively developed.

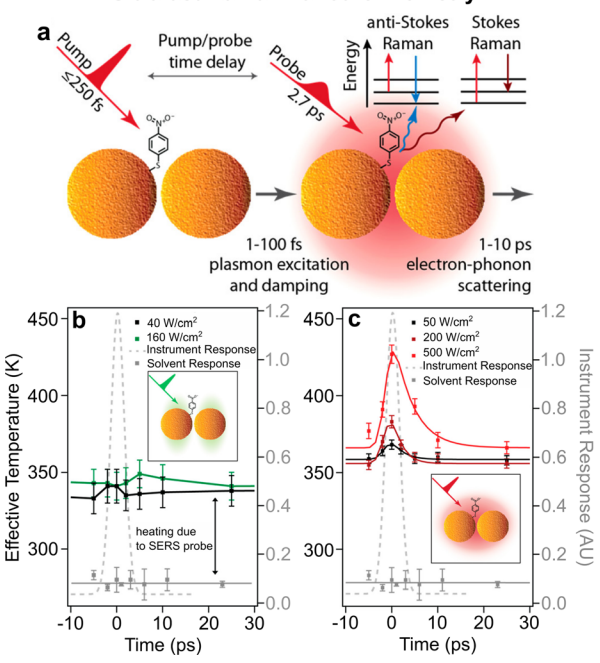
VII. HIGH SPATIOTEMPORAL RESOLUTION **TECHNIQUES**

While the high spatial resolution methods discussed previously have helped develop an improved understanding of the structurefunction relationship in plasmonic photocatalysis, they do not provide information at the timescales necessary to probe electronic transitions. Meanwhile, high temporal resolution methods tell us about electronic properties, but cannot generally be correlated with atomic-resolution structural properties. The spatial resolution in ultrafast pump-probe microscopy is generally limited by the spot size of the probe laser beam and thus the diffraction limit of light.²³¹ These challenges limit the conclusions that can be drawn about how catalysts and adsorbates are interacting. In order to further our understanding of photocatalyst materials, methods that achieve both high spatial and temporal resolution are needed. While many of these methods are not as developed and thus have not been demonstrated in situ, the same considerations as discussed above apply. Additionally, demonstrations of these emerging methods on plasmonic photocatalytic systems are sparse, but we describe use cases on various photoexcited systems as examples of how these may be applied to plasmonic photocatalysis in the future.

A. Ultrafast optical microscopy

Several of the optical methods discussed in Sec. V A can be made ultrafast by replacing continuous wave (CW) illumination with a pump-probe method. For example, ultrafast photoluminescence microscopy has very recently been demonstrated to probe the lifetimes of hot holes in gold nanoparticles. 499 Stroboscopic scattering microscopy has been used to map changes in polarizability arising from the motion of carriers in a material, a method that is poised to greatly contribute to our understanding of charge transfer in plasmonic catalysts. 500 Below, we more extensively highlight some of the methods which are most pertinent to studying plasmonic catalysts.





Ultrafast electron microscopy

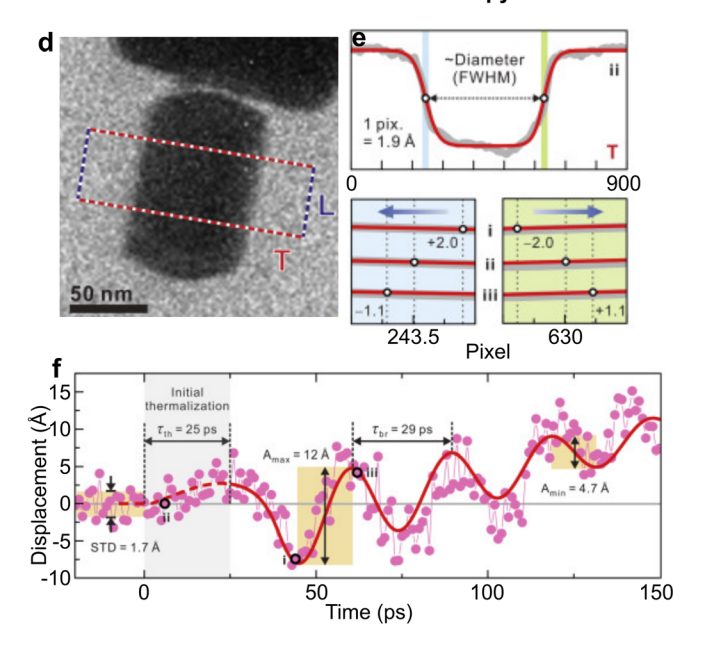


FIG. 7. High spatiotemporal characterization. (a) Schematic for ultrafast Raman nanothermometry. The pump pulse excites the nanoparticles and, after a variable delay, Stokes and anti-Stokes surface-enhanced Raman spectra of the adsorbed molecules are acquired using a probe pulse. (b) When the transverse mode of the dimer was excited by a 518-nm pump, polarized transverse to the long axis, essentially no change in temperature was observed. (c) When the coupled mode of the dimer was excited using a 1039nm pump polarized along the long axis, the temperature increased by less than 100 K. (d) TEM image of a gold nanorod and (e) its cross-sectional intensity profile, fit to a sum of two sigmoidal functions shown in red, taken along T and integrated along L as indicated in (d). The shift in the diameter (FWHM) at various points in (f) is shown in the lower panels of (e). (f) The displacement in the FWHM as a function of time, showing acoustic vibrations. (a)-(c) adapted with permission from Keller and Frontiera, ACS Nano 12, 5848-5855 (2018). 497 Copyright 2018 American Chemical Society. (d)-(f) Adapted with permission from Kim et al., Matter 1, 481-495 (2019). 498 Copyright 2019 Elsevier B.V.

1. Transient absorption microscopy

The lifetimes of plasmonic carriers strongly depend on the physical properties of the plasmonic material, for instance, defects, oxide layers, particle shapes, and sizes. Similarly, defects and interfaces affect the spatial diffusion of excited carriers. In order to obtain a mechanistic understanding of plasmonic catalysis and optimize promising catalytic processes, it is crucial to consider the inherent heterogeneity and physical structure of any plasmonic material, while retaining the detailed temporal information of ultrafast pump-probe spectroscopy. For this reason, researchers have employed ultrafast pump-probe transient absorption microscopy, which combines conventional TA spectroscopy setups with optical microscopes to focus pump and probe beams down to the diffraction limit.²³¹ Hence, ultrafast pump-probe transient absorption microscopy couples the temporal resolution of TA spectroscopy with diffraction-limited spatial resolution. Even though focusing the laser beams to the minimum spot sizes through optical objectives complicates the experimental setup, this method still allows the investigation of materials in various environments and is suitable for in situ studies.^{231,501} In addition to previous reports based on spectroscopy, microscopic studies were able to image carrier diffusion in semiconducting and plasmonic materials, illustrating the significance of interfaces, defects, and oxide layers as potential carrier traps and obstacles for carrier dynamics. 231,50

2. Ultrafast Raman microscopy

a. SERS. Ultrafast Raman spectroscopy allows the detection of bond changes on the timescale in which they take place. 180,507 Ultrafast SERS has been used to probe the transfer of hot carriers. 246 Brandt et al. used ultrafast SERS to investigate the plasmon-induced dimerization of 4-nitrobenzenethiol to p.p'-dimercaptoazobenzene on aggregates of silver particles ($\sim 100 \, \mathrm{nm}$). 292 In addition to the typical information regarding molecular changes derived from the change in the SERS spectrum, changes in surface electron density can also be inferred from transient interference lineshapes. An increase in the p.p'-dimercaptoazobenzene signal after plasmon excitation was correlated with an increase in photoluminescence resulting from a buildup in surface electrons, indicative of dimerization driven by indirect charge transfer.

In a method known as Raman thermometry, the effective temperatures of molecules in a system are determined by measuring the population of excited vibrational states using the relative intensity of the Stokes and anti-Stokes signals. 180 Monitoring the temperature of the molecules separately from the metal nanoparticles helps distinguish between photochemical and photothermal reaction pathways. Keller and Frontiera used this method to measure the transient effective temperature evolution of analytes on gold nanoparticles. The probe was polarized along the long axis of the dimer to measure the SERS signal of molecules in the inter-particle gap and revealed a relatively modest increase in temperature (~100 K) and fast dissipation, indicating photoexcitation of the system was unlikely to contribute to a thermal reaction pathway [Figs. 7(a)-7(c)]. 497 More work is needed to apply this ultrafast method to studying reactive molecules as a reaction progresses. 180 While CW illumination could result in cumulative effects, another study by the same group demonstrated that CW illumination of various viologens chemisorbed to gold film-over-nanosphere substrates similarly resulted in temperature changes below 100 K.⁵⁰

Comparisons between steady-state and ultrafast SERS help distinguish between the unique effects arising from pulsed vs CW illumination (see Sec. IX A). ¹⁸⁰ Methods such as surface-enhanced femtosecond stimulated Raman spectroscopy have the potential for achieving sufficient simultaneous time and spectral resolution to correlate early LSPR dephasing with molecular changes, which could contribute to our understanding of direct charge transfer. ¹⁸⁰ A much more detailed discussion of Raman spectroscopy methods across time scales is found in the review by Warkentin *et al.* ¹⁸⁰

b. TERS and CARS. Beyond SERS, other Raman methods have been implemented in ultrafast configurations with high spatial resolution. While studies are still limited, ultrafast TERS has been performed. 509-511 Klingsporn et al. used an optical parametric oscillator for picosecond pulsed excitation of a silver tip in an ambient STM to measure the Raman signal from two dyes, although the measurements suffered from a signal decay on the order of 10 s, which was not observed with CW illumination.⁵¹⁰ Decay of the TERS signal was reduced when measurements were performed at UHV.511 Luo et al. extended ultrafast TERS to 500 fs temporal resolution (limited to maintain sufficient spectral resolution) in a low-temperature UHV STM and found the signal to be stable for more than 270 s.⁵⁰⁹ Raman methods relying on higher-order nonlinear optical responses to enhance the signal can improve the spatial resolution, such as coherent anti-Stokes Raman scattering (CARS), which has been demonstrated in the imaging of semiconducting carbon nanotubes.⁵¹² Further development will be needed to make such measurements viable in varied environmental conditions.

B. Ultrafast x-ray microscopy

Many x-ray techniques can provide nanoscale-order information, for example, measuring atomic lattice spacings or local atomic environments, obtaining down to sub-angstrom resolution in terms of differentiating between distances. However, this spatial information is in reciprocal space, and therefore, it is an ensemble-averaged measurement across the portion of the sample being probed in real space. The spot size is often hundreds of micrometers or more and thus may contain a multitude of heterogeneities. If one instead considers spatial resolution in real space only, for example, to probe sub-particle optical modes within a photocatalyst, then x rays cannot yet achieve a comparable resolution to electron microscopy. However, their ultrafast spectroscopic capabilities and ability to penetrate through bulk materials still make x-ray microscopy (XRM), a valuable technique for the characterization of plasmonic photocatalysts, and the spatial resolution is actively being improved. ⁵¹³

In theory, the diffraction limit would allow x rays to be focused down to a spot size just below their wavelength, but because x rays are too energetic to refract in most materials and are also uncharged, manipulating the beam path of x rays is difficult, further limiting the spatial resolution achievable from many sources. 514 Developing specialized optics to improve this resolution is an active area of research. The current record lies just below 10 nm for transmission x-ray microscopes and below 5 nm using x-ray ptychography. $^{515-517}$ The advances toward more coherent x-ray sources such as XFELs and other developments promise lowering the spatial resolution to $<\!1$ nm in the near future. 516

Realized ultrafast XRM setups have not yet reached the combined limits of 10-nm spatial and fs temporal resolutions, but recent progress has gradually approached it. In 2016, Zhu et al. directed synchrotron 10 keV hard x-rays with a pulse duration of 100 ps through a Fresnel zone plate and additional apertures to achieve 350-nm spatial resolution. They photoexcited a VO2 thin film using an ultrafast (60 fs) Ti: Sapphire laser, thus limiting the temporal resolution to the 100 ps of the x-ray pulse, and monitored the phase change of the film via ultrafast XRD. 518 In 2021 at the same beamline, Frazer et al. focused the same 100-ps pulsed x-ray probe using another Fresnel zone plate to achieve 270-nm spatial resolution. They again used the probe to perform ultrafast XRD, measuring the time-resolved structural photoresponse of BiFeO₃ and FeRh thin films to UV excitation. ⁵¹⁹ In 2023, Gerlinger et al. demonstrated a vastly improved spatial resolution of 30 nm using a scanning transmission XRM directly installed at a synchrotron which provided 50-ps x-ray pulses. 520 With this resolution, the authors were able to observe ultrafast magnetization switching in GdFe induced by an IR pump laser, occurring non-homogeneously across a micrometer-sized region.

Dedicated XRMs have started to be used at XFELs, which have pushed the temporal resolution to match typical ultrafast x-ray experiments. A recent example outside of photocatalysis that demonstrates the capabilities enabled by combined XRMs and XFELs is the use of dark-field XRM by Dresselhaus-Marais *et al.* to image crystallographic distortions at 30- to 150-nm real-space resolution and 100-fs temporal resolution. We expect a similar setup combined with excitation optics will enable simultaneous sub-particle and femtosecond resolution in the near future. For plasmonic photocatalysis, this can be used to probe plasmon-induced charge transfer dynamics with site selectivity, differentiating sub-particle regions in nanoparticle catalysts.

C. Ultrafast STM

In a typical STM, collecting an image will take tens of seconds. The temporal resolution is improved to 1–100 frames per second in video-rate STM by integrating various fast electronics. ⁵²¹ When a full image is not required, atom-tracking can be achieved using the feedback loop to fix the probe to a single atom and track its motion in real time. ⁵²² None of these methods achieve temporal resolution down to the femtosecond to picosecond time scales over which plasmon dephasing and hot electron relaxation occur. For this, pump–probe methods must be incorporated. ⁵²³

Most ultrafast methods involve an optical pump and/or probe, although all-electronic STM methods using a microwave pulse generator have achieved temporal resolution down to the nanosecond range. ⁵²⁴ Photoconductive gates have been used in a combined electrical and optical approach. ⁵²⁵ While such methods could be helpful for measuring fast dynamics without relying on an optical pulse, it is also possible to measure optically induced phenomena with an optical pump and probe. An optical pump can induce a surface voltage ⁵²⁶ (as measured in KPFM, Sec. VB2), which gives rise to a tunneling current. While the tunneling current cannot be readout quickly, the time-averaged current signal is recorded as a function of the delay time between the pump and probe pulses to provide dynamical insight. ⁵²³

In addition to the fundamental limitation of only being able to probe phenomena induced by a pulsed laser and not those induced by CW illumination with optical pump–probe STM, there are other complicating factors in these methods. The laser pulses will often induce

transient thermal expansion in the tip, convoluting the results. Additionally, the results are based on the correlation between the two pulses, and thus, complicated nonlinear effects are induced, which make data interpretation difficult. One alternative method to overcome some of these limitations is terahertz-STM, in which the STM tip couples a THz pulse to the tunnel junction. This coupling results in a sub-picosecond transient voltage, which modulates the electron tunneling, and the time-averaged change in the current is measured. The particular advantage of this method is that THz pulses do not result in any substantial thermal expansion of the tip. This method has been used to measure sub-picosecond dynamics with a spatial resolution of 2 nm. S27

As with many scanning probe methods, much of the foundational work that must be extended to the current field comes out of the surface science community from the 1990s and 2000s. Work by Bartels et al. combined STM with femtosecond laser pulses to probe the motion of CO molecules on a Cu(110) surface. 528 In order to avoid laser-induced thermal expansion of the tip, the tip was moved away from the surface during irradiation and STM images from before and after irradiation were compared. Terada et al. developed a method using a pulse-picker to modulate the delay time between the optical pump and probe pulses, and the time-averaged current was measured as a function of delay time. 526 By measuring the time-averaged current and the signal as a function of set-point current at various surface sites, the hole capture rate through the semiconductor gap-state produced by a cobalt nanoparticle on GaAs was measured. 526 Taninaka et al. also studied the effect of molecular conformations and bonding states on the conduction properties of a gold electrode. 529 Future efforts may include adapting these early experiments to current plasmonic systems of interest.

D. Ultrafast electron microscopy

In ultrafast electron microscopy, transitions are excited by a pump light pulse and monitored using a probe electron pulse. The time resolution of a traditional TEM is typically limited to the frame rate of a CCD camera, on the order of several milliseconds per frame, 530 while that of an SEM is lower, limited by the scanning speed of the SEM. Direct electron detectors in TEM have much higher frame rates, surpassing 3000 frames per second. 531 Slowing the kinetics of a reaction by modifying the temperature and pressure conditions and using a direct electron detector makes many reactions accessible for real-time observation. However, the formation of clusters on the surface and other restructuring events may still occur too quickly to be observed by a traditional TEM, let alone electron dynamics. Femtosecond optical and electron pulses can be used in a pump-probe configuration inside an SEM or TEM to excite the plasmon resonance and detect resulting structural transformations, and adsorbate-induced changes in bond lengths and local electric fields can be monitored.

1. Ultrafast SEM

Ultrafast environmental SEM has been employed for investigating molecular dynamics on a surface. A sample is excited by an optical pump, after which an electron pulse probes the sample, and secondary and backscattered electrons are detected for imaging and diffraction, respectively. As in other pump-probe experiments, the delay between the pump and probe determines the temporal resolution

of the measurement. Yang *et al.* used differences in SEM images obtained at varying pump–probe delays to elucidate the surface restructuring on CdSe exposed to vacuum, ambient air, and water vapor.⁵³³ Ultrafast SEM has been used to probe the dynamics of photoexcited charge carriers in semiconductors and insulators.^{535,536}

2. Dynamic TEM

In dynamic TEM (DTEM), the system operates in a single-shot mode; a single electron pulse with sufficient intensity to collect a measurable signal interacts with the sample after it is excited with a laser pulse. 537 The maximum achievable temporal resolution with this mode is around 1 ns, allowing observations of fast catalytic processes. 538 The DTEM at Lawrence Livermore National Laboratory collects 16 frames with interframe spacing below 100 ns in movie mode.⁵³⁹ The temporal region between nanoseconds and milliseconds continues to be largely inaccessible, but the development of methods in this time range would make even more catalytic processes observable in the TEM. 540 Incorporation of a liquid cell with DTEM has allowed for imaging of laser-induced cavitation of water bubbles with a temporal resolution of tens of nanoseconds, although the spatial resolution was limited to over 100 nm, in part due to the liquid thickness.⁵⁴¹ In situ experiments involving the heating of samples by laser irradiation have been performed.⁵⁴² EELS has also been incorporated into DTEM, opening new opportunities for observing chemical reactions at their characteristic timescales.⁵⁴³ More advanced methods have enabled the probing of electron clouds produced by irradiating a metal substrate.544 DTEM is particularly useful for studying fast and irreversible processes; however, it is not sufficiently fast for studying electron dynamics.

3. Ultrafast TEM

Ultrafast TEM (UEM), pioneered by Zewail and co-workers, offers improved temporal resolution compared to DTEM by operating in a stroboscopic mode in which a large number (\sim 108) of pulse cycles each containing a small number of electrons are used accumulate signal. ⁵³⁰ This approach minimizes Coulomb repulsion inside the pulse and allows a temporal resolution on the femtosecond timescale, ⁵⁴⁵ although the stroboscopic mode limits its application to processes that can be driven repeatedly in the same sample. Laser-free methods of stroboscopic TEM using a fast beam blocker are also possible, with the potential to reach a temporal resolution on the order of 100 fs. ⁵⁴⁶

Zewail and co-workers demonstrated photon-induced near-field microscopy in the UEM to determine near-field plasmonic properties. The evanescent near-field induced by the photoexcitation of a metal nanoparticle was probed by an electron pulse, which inelastically scatters off the electric field. This scattering results in a quantized gain in the energy of the electrons, which was measured similar to electron energy loss, although the source of the energy change is different. Energy-filtered imaging was used to isolate those electrons that had gained energy and thus image the polarization-dependent evanescent near-field in triangular and spherical silver nanoparticles. This method has also been used to image the near-field of entangled silver nanoparticles, carbon nanotubes and silver wires, surface plasmon polaritons launched along a buried silver and silicon nitride interface, and the plasmonic coupling between individual gold

nanocapsules and graphene step edges.⁵⁵¹ Yurtsever *et al.* used ultrafast spectrum imaging, wherein an energy gain/loss spectrum is collected for each position in a STEM image, to map the electric field distribution and spatiotemporal dielectric response of optically excited silver nanotriangles and the decay length and evolution of a plasmonic field along a copper-vacuum interface.⁵⁵² While methods such as dual-color coherent anti-Stokes Raman scattering, SNOM, and time-resolved nonlinear photoemission electron microscopy have been used to study near-field plasmonic properties, including at buried interfaces, they are still only sensitive to fields external to the sample.⁵⁵⁰ As photon-induced near-field microscopy is a transmission method, it can probe fields within the material.

Beyond plasmonic properties, UEM has been used to probe structural dynamics in a number of systems. Valley et al. imaged photoinduced acoustic phonon modes in gold nanorods.⁵⁵³ Diffraction contrast in bright-field images was used to identify changes in strain and crystal orientation. Difference images from these ultrafast diffraction-contrast bright-field images revealed oscillations arising from vibrational modes, both within isolated gold nanorods and across small clusters. 553 A similar study was performed by Kim et al., revealing additional details about the acoustic vibrational modes in gold nanorods. 498 In addition to the diffraction-contrast imaging performed by Flannigan and co-workers, the use of a direct electron detector allowed the authors to further reduce the number of electrons per pulse, increasing resolution and enabling direct observation of angstrom-scale displacements in the particle [Figs. 7(d)–7(f)]. 498 Van der Veen et al. used selected area diffraction to collect single-particle diffraction patterns of Fe(pyrazine)Pt(CN)4 MOFs.⁵⁵⁴ A single-spin crossover transition was induced by heating due to optical excitation, and both dark-field images and diffraction patterns were analyzed to visualize the phase transition.⁵⁵⁴ Yoo et al. have also visualized the transient structural changes of a titanium active center in a (nonplasmonic) photocatalyst using electron diffraction.⁵⁵⁵ The change in intensity of diffraction spots was correlated with the motion of atoms in the unit cell, indicating the transformation of the titanium and oxygen bond upon charge transfer from the oxygen to titanium. Ultrafast EELS, in conjunction with molecular dynamics simulations, has been used to study thermally induced changes in bond lengths.⁵⁵⁶ This method was combined with ultrafast energy-filtered electron microscopy to study temporal changes in the valence state of iron in an iron oxide (non-plasmonic) photocatalyst. 55

Ultrafast electron diffraction provides atomic resolution in reciprocal space. 558,559 Single-particle studies often require frequent switching between electron imaging and diffraction. 553 Ultrafast electron diffraction performed at energies much higher than typically found in UEM (\sim 3 MeV) was used to investigate the thermal relaxation in gold nanocrystals with varying size and surface ligands and structural dynamics in 2D perovskites. 506,560 Ultrafast electron microscopy methods represent an exciting new frontier in the field. The unprecedented combination of sub-nanometer spatial resolution, femtosecond temporal resolution, and energy resolution in the area of a few meV will enable new insight into previously unreachable phenomena. While ultrafast TEM has numerous applications in plasmonic photocatalysis and stands to contribute majorly to the field in the next several years, more work will be required to combine ultrafast TEM with environmental TEM, which will further expand the relevance of the method.45

VIII. COMPUTATIONAL METHODS

The experimental techniques discussed in this review provide information about the plasmon resonance, lattice structure, electronic structure, and adsorbate configurations that emerge from a nonequilibrium plasmonic catalyst system. Each is limited in spatial and temporal resolution, observable quantities, and signal-to-noise. Similarly, an array of theoretical approaches can provide estimates of these quantities as well as more fundamental quantities, which are challenging or presently impossible to observe empirically. Each offers a trade-off between accuracy, computational cost, and computable quantities. Taken together, combined experimental-theoretical approaches should address critical questions in plasmonic photocatalysis, including: (1) What is the mechanism (Fig. 1) that drives photocatalysis for a given system? (2) What are the fundamental microscopic limits in photocatalysis? (3) How can material selection, nanoparticle shape, and environment be co-optimized for a given reaction? (4) Are there general, robust design rules that are applicable to a large class of reactions?

Sections VIII A and VIII B briefly review several popular theoretical frameworks (Sec. VIII A) and relevant theoretical findings (Sec. VIII B) for plasmonic catalytic systems. In particular, we emphasize the growing importance of *ab initio* methods as experimental characterization techniques advance toward higher spatial and temporal resolution.

A. Theoretical approaches

Nearly, all methods for computing material properties make some approximation to the electronic interactions involved in the system of interest (e.g., Born-Oppenheimer, mean-field, etc.), often describing the truly interacting electronic system in terms of a fictitious system with weakly interacting particles, such as within Kohn-Sham DFT. The advantages and limitations of each approach may be understood by examining the ways in which its fictitious system approximates the true interacting many-body system. Ab initio approaches take only the atomic-scale structure and fundamental constants as input, while empirical and semi-empirical models require additional assumptions and parameters from experiments or ab initio models. Ab initio theories have assumed a central role in the study of many material classes, 562-566 enabled by supercomputing resources and massively parallel electronic structure codes. Quantities such as the electronic density in real space, electronic state occupations, electronic density of states (DOS) and projected DOS, electron-electron and electronphonon scattering rates, plasmon dephasing, optical absorption spectra, and PESs for chemical reactions are frequently computed and used to support and rule out possible explanations for experimental observations. Understanding the inherent approximations in each theoretical method is essential to avoid drawing unwarranted conclusions. In particular, the prediction of optically driven excited-state properties relevant to plasmonic catalysis such as absorption, hot carrier transport, and excited-state PESs require more complex approaches than ground-state properties.

The Kohn–Sham DFT for computing ground-state properties is the most widely applied *ab initio* method due to its ability to qualitatively describe the electronic properties of materials within a reasonable computational effort. Here, an interacting many-electron system is approximated by a fictitious system of Kohn–Sham electrons, in which each electron interacts only indirectly with others through an

effective potential that depends on the electronic charge density. 567,568 The $3N_e$ -dimensional many-electron wavefunction, where N_e is the number of electrons in the system, is replaced with the electronic density as the central quantity to compute. Common implementations rely on pseudopotentials to remove the core electrons and deal only with the problems of valence electrons, which contribute predominantly to the physics and chemistry discussed here. DFT can in principle obtain the exact total ground-state energy for a system of interacting electrons, but it requires a universal exchange-correlation (XC) functional of the charge density, which must be approximated for any practical calculations. Many forms of XC potentials beyond those based on the local density approximation (LDA) and generalized gradient approximation (GGA) have been recently proposed and applied to complex chemical systems. These include, for instance, hybrid and range-separated hybrid functionals, 569,570 which include a fraction of the nonlocal Fock exchange, and meta-GGA functionals,⁵ which typically include the kinetic energy of each Kohn-Sham orbital. These approximations make the many-electron problem tractable while including atomistic structural detail, scaling as O(N³) or better, where N is proportional to the system size.

Despite these attractive features, however, the direct application of DFT calculations to plasmonic photocatalysis has shortcomings since it is rigorously a ground-state formalism. In addition, common approximations of XC functionals fail to capture nonlocal dielectric screening relevant to describe image-charge effects and electronic correlation for molecules close to metallic surfaces, which arise in many chemical reactions.^{572–574} Recently developed hybrid XC potentials can address this issue to some extent at an increased computational cost. 575,576 Still, the fictitious one-electron orbitals and energy levels of Kohn-Sham DFT do not rigorously correspond to physical observables, such as quasiparticle wavefunctions and quasiparticle excitation energies,⁵⁷⁷ and cannot be used to explain excited-state phenomena with the exception of the energy of the highest-occupied orbital, corresponding to the ionization energy. 578-580 An accurate prediction of excited-state properties requires dynamic interaction and physics beyond the level of static mean-field theories such as DFT.

Rigorous excited-state properties of nanoparticles, as well as dynamic interactions arising from the photogenerated excitations, can be in principle captured in time-dependent DFT (TDDFT)⁵⁸¹—an extension of DFT in which the time-dependent Schrödinger-like equations are solved as a function of time in response to a perturbation, such as an external light pulse. In principle, TDDFT can yield exact excited-state properties of materials, but requires a time-dependent approximation to the exchange-correlation functional. Practical approximations, such as the adiabatic LDA, can capture plasmons and, hence, have been popular in describing the optical and catalytic properties of nanoparticles. TDDFT can also approximate the dynamics of hot electrons, though the eventual thermalization of the system is not captured in standard TDDFT approaches, such as those based on Ehrenfest dynamics. 582 Additionally, adiabatic LDA cannot capture bound excitons, which may be important in describing the optical properties of small metallic nanoparticles, 583,584 and also have the same aforementioned limitations in capturing nonlocal dielectric screening and image-charge responses.

The many-body perturbation theory (MBPT), such as the GW approach ^{585–588} to describe electronic excitations and the GW plus Bethe–Salpeter equation approach ^{589–594} for optical excitations, and

wavefunction-based quantum chemistry techniques, such as based on coupled clusters,59 5-599 are higher-level ab initio theories that account for the dynamical and nonlocal electronic interaction and correlation systematically, without the need for yet-to-be-determined approximations to XC functionals. These incur a higher computational cost than DFT and TDDFT calculations [O(N3) to O(N7) in most common implementations] but provide a theoretically rigorous and quantitatively accurate description of excited-state properties for weakly to moderately correlated electron systems. In particular, such formalisms capture either explicitly or implicitly the dynamic nature of electronic screening in such materials and the formation of correlated e-h pairs (or excitons) upon photoexcitation. The latter effect significantly impacts the excited-state properties of low-dimensional materials like monolayer transition metal dichalcogenides, 600-60 molecules, 604-606 and small nanoparticles. 584 MBPT-based approaches have traditionally been used to describe charged and neutral (e.g., optical) excitations on both extended, confined, and nanostructured materials with success, including 2D materials.⁶⁰ While calculations of realistic plasmonic systems are challenging due to the number of atoms in the simulation cell, recent advances in algorithms and code performance,607-619 which can handle several thousands of atoms, are expected to make MBPT calculations routinely accessible to predicting plasmonic photocatalysis, i.e., describing both the plasmonic properties and ground- and excited-state

For instance, while quantum chemistry methods were previously limited to small molecules, ⁶²⁰ Aikens and co-workers have used quantum chemistry configuration interaction methods to shed light on the fundamental nature of plasmonic excitations in atomic silver nanowires. ^{621,622} Wavefunction-embedding approaches have also recently become popular in the plasmonic catalysis community. ^{17,59,60} These include exact exchange and correlation only for important sub-regions of a system, e.g., an adsorbed molecule and cluster of nearest metal nanoparticle atoms. ⁶²³

For the implementation of each *ab initio* technique mentioned above, the formally infinite-dimensional effective Hamiltonian must be expressed in a finite basis. Many code implementations utilize a reciprocal-space (plane wave) basis, which is natural for solid-state periodic systems and often more straightforward to converge than real-space bases. ⁶²⁴ However, plane wave-based calculations require a unit cell with periodic boundary conditions. For systems that are not periodic in all dimensions (e.g., a surface, thin film, or nanoparticle), the use of a plane wave code requires unit cells with many atoms and large dimensions in the non-periodic directions, in order to suppress unphysical interactions between periodic images. ⁶²⁴ This requirement increases the number of basis functions, making calculations expensive in terms of both memory and computational time.

For this reason, large nanoparticles have long been treated by classical continuum models wherein the atomistic structure is approximated by a structure of continuously varying properties. Then, Maxwell's equations are solved analytically or numerically with the frequency-dependent macroscopic dielectric response function of the nanoparticle as an input. Mie theory, 625,626 finite element methods, 627 boundary element methods, 628-630 finite-difference time-domain methods, 631,632 and the discrete dipole approximation are popular examples of continuum models of this kind, largely inherited from the nanophotonics community. Within this

approach, the macroscopic bulk dielectric function for a nanoparticle is typically taken from empirical measurements, ⁶³⁴ the classical Drude theory, ⁶⁶ or more recently from TDDFT calculations of bulk metals, ¹¹⁸ capturing some effects of interband e–h pairs. More recently, calculations employing localized bases have been used to describe plasmons and hot-electron generation in complex nanoparticles ⁶³⁵ containing up to millions of atoms when utilizing less transferable, tight-binding bases. ^{636,637}

B. Illustrative theoretical results

1. Bulk, surfaces, and thin films

Many experimental and theoretical studies use bulk, surface, and thin-film geometries to probe plasmon excitation, decay, and catalytic activity. Theoretically, such systems are often easier to treat from *ab initio* calculations than confined nanoparticles due to smaller required unit cells.

A qualitative understanding of many material-dependent effects on hot carrier production and transport has been built through DFT calculations. Atwater and co-workers found that the electronic structure of different plasmonic metals (e.g., d-band position, band velocities) gives rise to interband hot carriers with different energy distributions and anisotropic initial momentum distributions [Figs. 8(a) and 8(b)]. 314,315 In contrast, the distribution of phonon-assisted intraband e-h pairs was found to be relatively flat and material-independent. 315 By a simple assessment of the DOS at a bulk interface between gold and p- or n-type GaAs, the group concluded that interband electrons excited just above the Fermi level are unlikely to overcome the Schottky barrier and transfer to GaAs without tunneling or thermal energy, while hot d-band holes, with energies well below the Fermi level, may transfer freely.³¹⁴ This result was later experimentally corroborated in 7- to 15-nm-diameter nanoparticles. 638 The analysis of the DFT DOS for a gold thin film has also been used to explain the observation of enhanced reaction rates over 10-30 nm SiO₂-supported nanoparticles compared to TiO₂ support. 639,640 At the DFT level of theory, interband hot electrons in gold have sufficient energy to transfer to an adsorbed 4-nitrophenol molecule but also to overcome the Schottky barrier to transfer to TiO₂ in a competing pathway.⁶

Another recent application in this field has been to aid in the interpretation of electron and scanning probe microscopy experiments. For example, DFT calculations along with electron-electron and electron-phonon scattering rates produced a hot carrier flux at the surface of plasmonic silver bowties in qualitative agreement with the spatially resolved relative reactivity estimated by SEM for the hot carrier-induced transformation of 4-NTP to 4-ATP [Figs. 8(c) and 5(a)]. Similarly, a DFT-parametrized tight-binding model led to an estimated hot carrier distribution in a gold film with energies in the range of those extracted by SPM single-molecule transport measurements.³¹⁶ The qualitative effect of surface scattering was also observed both theoretically and experimentally, with a larger hot carrier rate for a thinner film. In mechanistic studies by Kazuma et al. on silver surfaces, the analysis of the DFT DOS and projected DOS was used to support an indirect charge transfer mechanism for O₂ dissociation ¹⁸⁴ and PIRET mechanism for dimethyl sulfide dissociation³¹³ by STM and

Recently, Carter and co-workers have developed a quantum chemistry embedding approach to qualitatively explain ensemble kinetics for a number of reactions over plasmonic nanoparticles 5–10 nm in diameter. ^{17,59,60,641–643} In their approach, a semi-infinite metal surface is treated at the DFT level, and a subsystem of adsorbed molecule plus a small number of surface atoms is treated with correlated quantum chemistry methods. The higher-level theory allows the computation and comparison of ground- and excited-state PESs. In some cases, however, the quantitative accuracy of the theoretical energy barriers is limited by the idealized surface assumption, which neglects the contributions of plasmonic hot-spots and surface reconstruction. ⁶⁰

2. Large nanoparticles

While atomistic studies are inaccessible for large nanoparticles (>5 nm), numerous experimental studies apply continuum models to predict the absorption spectra and near-field enhancement of plasmonic structures at a relatively small computational cost. ^{177,181,213,247,273,278,644–646}

Models of electronic phenomena such as hot carrier generation have also been obtained from continuum models, with input from quantum theories. For example, Govorov and co-workers have related surface-assisted hot carrier production rates to local field strengths by generalizing from analytical solutions to the Schrödinger equation for non-interacting electrons confined to infinite-well potentials. These estimates shed light on the amplified hot carrier creation in plasmonic hot-spots 647,649 and the heavy skewing of non-thermal carrier populations toward low-energy intraband Drude e–h pairs. 66,650

The latter finding is further validated by calculations within the free electron gas⁶⁵¹ and jellium models, ⁶⁵² which are non-atomistic quantum toy models. From an electronic "sea" of uniform density confined to a specific geometry, these models qualitatively capture many collective electronic phenomena (e.g., plasmons) of conduction electrons in bulk metals and intraband surface-assisted e–h generation in nanoparticles. ^{653–656} Unlike atomistic *ab initio* theories, free electron gas and jellium models have been extended to nanoparticles up to 40 nm in diameter, revealing that surface-assisted hot carrier production dominates for nanoparticles below 10 nm and is less important for larger nanoparticles. ³¹⁵

However, like continuum models, free electron gas/jellium models lack the material-dependent details, which give rise to electronic band structure and determine the contributions of interband and phonon-assisted intraband e-h pair generation. In Sec. VIII B 3, we will consider the application of *ab initio* theories to smaller nanoparticles to study these and other effects.

3. Small nanoparticles

For nanoparticles smaller than 5 nm in diameter, continuum and bulk models cannot be applied; the effects of microscopically varying electric fields, spill-out of the electronic wavefunctions, quantum many-body physics, confinement-induced discretization of energy levels, surface scattering, and the reduced screening compared to bulk become non-negligible. Ab initio methods can capture these effects and make it possible to compare across structures of varying

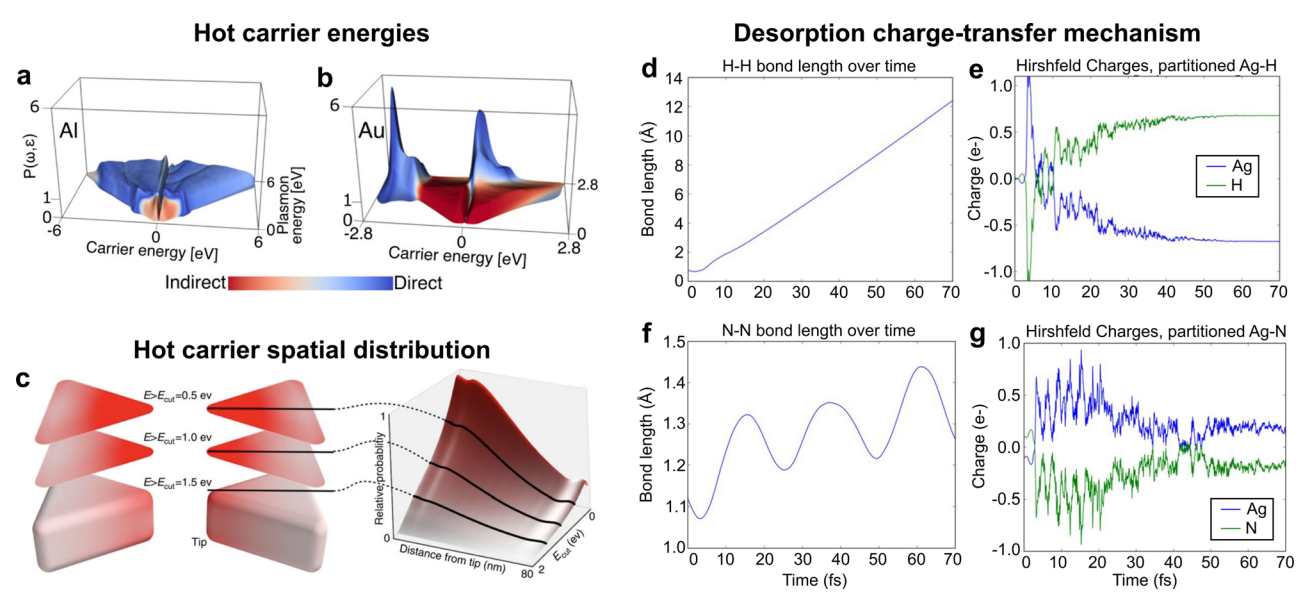


FIG. 8. Computational methods for understanding mechanisms in plasmonic photocatalysis. *Ab initio* prediction of hot carrier populations [*P*(ωε)] as a function of plasmon energy, carrier energy, and transition type for (a) Al, which has a relatively flat carrier distribution, and (b) gold, which has a sharply peaked carrier distribution with a high population of d-band holes. (c) *Ab initio* prediction of hot carrier flux at the surface of plasmonic nanoparticles in a bowtie geometry, showing the highest flux at the tips in qualitative agreement with reaction rates observed by SEM [Fig. 5(a)]. (d) H–H bond length in real time as computed by TDDFT with a hybrid XC potential, with rapid dissociation apparent. (e) Charge on silver and H₂ subsystems in real time, showing a correspondingly large, rapid peak in charge transfer of 1.22e⁻ at 3.4 fs. (f) N–N bond length in real time. Oscillations are visible, but no dissociation was observed within the simulation time. (g) Charge on silver and N₂ subsystems in real time, characterized by oscillations and a slower, smaller peak in charge transfer of 0.94e⁻ at 15.3 fs. (a) and (b) Adapted with permission from Brown *et al.*, ACS Nano 10, 957–966 (2016). Copyright 2015 American Chemical Society. (c) Reprinted with permission from Cortés *et al.*, Nat. Commun. 8, 14880 (2017). Topyright 2017 Springer Nature Limited. (d)–(g) Adapted with permission from Hull and Aikens, J. Phys. Chem. A 127, 2228–2241 (2023). American Chemical Society.

microscopic composition (i.e., doping, defects, adsorbate configuration) and to visualize the microscopic charge density oscillations comprising the LSPR.

The character of the LSPR is one fundamental focus of small nanoparticle studies. STEM-EELS studies can resolve the LSPR energy for individual nanoparticles. 206,658-661 However, the size dependence of the LSPR energy results from an interplay of the effects mentioned at the beginning of this section and is also affected by the dielectric screening of the substrate and environment, making its estimation challenging. Simple non-atomistic quantum and semiclassical theoretical models can lead to differing predicted trends for the LSPR and qualitatively different spectra. 205 Ab initio TDDFT calculations are in better qualitative agreement with each other, but vary slightly depending on the exact geometry, basis set, and XC potential.⁶ Jellium models have shown that for nanoparticles 1–3 nm in diameter, the LSPR couples strongly to individual e-h excitations. 671-674 TDDFT can capture this coupling as well, including the additional damping effects of d-band states^{665,675} and uncover a cyclical energy transfer between the LSPR and single e-h pairs. 664 Relatively small concentrations of dopants have been found to dampen the LSPR, with the effect more pronounced for dopant atoms near the surface where the LSPR

Mechanistic insights can also be obtained from *ab initio* theory. Due to the discrete electronic energy levels, *ab initio* estimates of e-h generation in small nanoparticles have shown that phonon-assisted intraband transitions contribute little⁶⁶⁴ and rates of interband and low-energy intraband e-h pair generation deviate significantly⁶⁷⁸ compared to bulk systems. TDDFT studies of small silver nanoparticles have shown that hot electrons are more likely found on lower-coordinated surface sites, while hot holes are distributed more homogeneously.⁶³⁵ Other such studies include adjacent carrier acceptors, enabling the investigation of chemical interface damping, which is difficult to separate experimentally from indirect charge transfer (Fig. 1).⁸⁶ For example, the relative contributions of direct electron and hole transfer have been quantified and found to vary with external mechanical strain⁸⁶ and adsorbate orientation.⁶⁷⁹

To our knowledge, the largest metallic clusters treated by TDDFT are 1415 atoms corresponding to a 3.8-nm-diameter nanoparticle. 680.681 *Ab initio* theories beyond DFT/TDDFT with semi-local XC potentials have so far been limited to even smaller plasmonic systems due to computational cost, but offer extraordinary fundamental insight into these small systems. Thorough TDDFT studies on silver atomic wires with hybrid XC potentials by Hull *et al.* have directly revealed the plasmon-mediated dissociation mechanisms of H₂ and N₂ with transient negative ion intermediates, which are sensitive to molecular orientation and the exciting electric field strength [Figs. 8(d)–8(g)]. 561.682 Another recent study applying correlated quantum chemistry wavefunction methods to small jellium nanoclusters suggests that excitonic and plasmonic excitations may both be present and even hybridize for small nanoparticles, 584 representing a qualitative change to the current picture of their catalytic activity.

IX. CONCLUSIONS AND OUTLOOK

Plasmon-induced catalysis is promising for driving chemical reactions using light, but an understanding of the underlying fundamental chemical and physical processes is required to take full advantage of the opportunities in the field. Chemical reactions happen at nanometer and sub-nanometer length scales and femto- and

picosecond time scales, thus requiring high spatial and temporal resolution techniques. In this review, we discussed *in situ* optical, scanning tip-based, and electron techniques that can achieve high spatial and temporal resolution. We have emphasized methods that are able to be performed *in situ* and highlighted experiments that have already provided insight into several mechanistic uncertainties. We also highlighted relevant theoretical methods, especially powerful *ab initio* methods, which have been used to further explain mechanisms in plasmonic catalysis.

A. Challenges

Despite the enormous progress described here, several challenges remain. ¹² More improvements to resolution are needed on a pertechnique basis. While we have focused on the improved spatial and temporal resolution here to characterize material properties and plasmonic behavior, improved spectral resolution and lower limits of detection for chemical species will also be necessary for *in situ* experiments and quantification of correlated catalytic activity. Many of the methods described here suffer from instabilities caused by reaction conditions; realistic gas pressures and liquid environments limit the signal-to-noise and coherence of optical and electron probes, reducing the maximum achievable spatial and spectral resolutions. Realistic flow conditions introduce additional instabilities, particularly in methods that depend on a precisely positioned probe.

In some methods, even achieving the requisite resolution does not guarantee accurate characterization. The known methods for probing ultrafast phenomena might be fundamentally unable to provide mechanistic insights in some cases. Much of the field is motivated by using direct solar energy or CW, low-power LEDs to drive reactions. Exciting a system with a pulsed laser can result in nonlinear effects, which are not achievable under CW illumination and thus may never accurately reflect the mechanism of a reaction driven by CW illumination. Similarly, CW illumination could cause plasmonic effects to accumulate, resulting in phenomena that do not occur in time-resolved studies given the delay between pump/probe cycles. While these challenges remain outstanding for many methods and reactions, direct comparisons between steady-state and ultrafast measurements have helped address this issue. 180

There are also practical limitations to our ability to investigate the behavior of plasmonic catalysts at the highest spatial and temporal resolution. Many of the methods described in this review require hard-to-access and/or extremely expensive and difficult-to-operate equipment, whereas many ensemble methods are more readily available to a larger number of researchers. Building lower-cost equipment is an active and critical area of research, for this field and many others. Beyond the necessary developments in characterization methods, challenges such as implementing more sustainable catalyst materials and translating our nanoscale mechanistic insights into ensemble-scale improvements must be addressed to drive reactions on an industrially relevant scale.

Finally, to tackle the challenge of rigorously and systematically determining the mechanism (Fig. 1) behind plasmonic photocatalysis, one must have computationally tractable theoretical methods that can accurately describe the excited states, electronic correlation, electron–phonon interactions, and phonon thermalization in realistic materials. Such methods are still not available, and different domain techniques are often optimized to capture either larger nanoparticles

(continuum models), electronic correlation (quantum chemistry/ MBPT), or dynamics (TDDFT) individually.

B. Opportunities

Many of the methods highlighted in this review have been applied primarily to non-plasmonic photocatalytic systems, and thus, there is plenty of opportunity in using these methods more in future experiments to answer the open mechanistic questions on how plasmon excitation leads to directed chemistry. We have not covered an exhaustive list of methods, and others that have yet to be used for ultrafast or ultrasmall measurements may be used in the future.

There is a fundamental limit to the simultaneously achievable spatial, spectral, and temporal resolution, making it infeasible to fully optimize a characterization method on all fronts. Thought must be given to choosing the method which is most well-suited for answering a given question or finding correlative approaches that allow several methods to be used. Correlative methods are already well established, enabling the use of various techniques for the tasks to which they are best suited and we expect these will play an important role in not only correlating various temporally and spatially resolved results but also for correlating single-particle to ensemble-scale properties. Many studies have correlated optical microscopy and spectroscopy (high energy resolution) and electron microscopy (high spatial resolution). ^{263,306,683–687} Any number of other methods can be correlated, such as optical microscopy with SPM, ⁵⁶⁰ electron microscopy with x-ray studies, ⁵¹⁷ and ultrafast optical spectroscopy with ultrafast electron diffraction. ⁵⁰⁶

Many opportunities exist at the intersection of machine learning and plasmonic catalysis and will help advance the field toward the rational design of catalysts for a given reaction. Machine learning has been used to determine the dimensions of gold nanorods from their optical spectra, a task that would otherwise require electron microscopy.²⁷⁷ Improvements in synthesis using more sustainable (easily sourced and plentiful) metals such as aluminum and magnesium will enhance the applicability of plasmonic catalysis to solving ongoing environmental problems. ^{102,103,688–691} There are many opportunities in applying this platform to address global needs beyond traditional heterogeneous catalysis, such as in water purification. ⁶⁹² Plasmonic photocatalysis sits at the intersection of two distinct and well-established fields. Methods and findings from the early surface science community should continue to be integrated. New interdisciplinary possibilities also exist, such as using strong coupling or picocavities for selective bond activation. ⁶⁹³

Finally, new algorithms, including those based on machine learning, may play a central role in combining different theoretical techniques and capturing electronic correlation and coupling electron/ion dynamics on the same footing. For instance, one may expect future TDDFT calculations to employ exchange-correlation functionals fit to MBPT or quantum chemistry calculations to describe both ion and correlated electron dynamics on the same footing.

C. Outlook

Future advancements in the field of plasmonic photocatalysis depend on developing a greater understanding of underlying mechanisms in order to design more active, selective, and stable catalysts. The methods described herein are state-of-the-art for the

characterization of these catalysts at high spatial and temporal resolution. Unfortunately, there is no single method that allows for the characterization of all relevant time and length scales. Similarly, there is no universal theory that will explain every reaction, as each is unique and the mechanism can vary widely depending on the specifics of a given reaction. Methods to conclusively distinguish between excitation mechanisms and isolate reaction pathways from one another remain elusive. Advancements in our ability to observe fast electron transfer processes and chemical intermediates on their native time scales will be crucial, with methods such as ultrafast electron microscopy pointing the way forward.

ACKNOWLEDGMENTS

This work was funded by the NSF, Center for Adopting Flaws as Features (NSF CHE-2124983); the Office of Basic Energy Sciences, Division of Materials Sciences and Engineering, Department of Energy Award No. DE-AC02-76SF00515; and the Keck Foundation (Grant No. 994816). S.L. thanks the Robert A. Welch Foundation for support through the Charles W. Duncan, Jr.-Welch Chair in Chemistry (C-0002). C.F.L. acknowledges funding from the Robert A. Welch Foundation (C-1787) and support through the Kenneth S. Pitzer-Schlumberger Chair in Chemistry.

AUTHOR DECLARATIONS Conflict of Interest

The authors have no conflicts to disclose.

Author Contributions

Claire C. Carlin and Alan X. Dai contributed equally to this work.

Claire C. Carlin: Conceptualization (equal); Project administration (equal); Writing - original draft (lead); Writing - review & editing (lead). Alan X. Dai: Conceptualization (equal); Project administration (equal); Writing original draft (lead); Writing - review & editing (lead). Alexander Al-Zubeidi: Conceptualization (equal); Writing - original draft (equal); Writing - review & editing (lead). Emma M. Simmerman: Conceptualization (equal); Writing - original draft (equal); Writing - review & editing (equal). Hyuncheol Oh: Writing - original draft (equal); Writing - review & editing (supporting). Niklas Gross: Writing - original draft (equal); Writing review & editing (supporting). Stephen Lee: Writing - review & editing (equal). Stephan Link: Funding acquisition (equal); Supervision (equal); Writing - review & editing (equal). Christy Landes: Funding acquisition (equal); Supervision (equal); Writing - review & editing (equal). Felipe da Jornada: Funding acquisition (equal); Supervision (equal); Writing review & editing (equal). Jennifer A. Dionne: Conceptualization (equal); Funding acquisition (equal); Project administration (equal); Supervision (equal); Writing - review & editing (equal).

DATA AVAILABILITY

Data sharing is not applicable to this article as no new data were created or analyzed in this study.

REFERENCES

¹E. A. Wrigley, "Energy and the English industrial revolution," Philos. Trans. R. Soc., A 371, 20110568 (2013).

- ²IEA, Tracking Clean Energy Progress 2017 (IEA, 2017).
- ³C. M. Matthews, C. Eaton, and B. Faucon, "Behind the energy crisis: Fossil fuel investment drops, and renewables aren't ready," https://www.wsj.com/articles/energy-crisis-fossil-fuel-investment-renewables-gas-oil-prices-coal-wind-solar-hydro-power-grid-11634497531 (2021).
- ⁴Basic Energy Sciences Roundtable, "Report of the basic energy sciences roundtable on liquid solar fuels," Technical Report, OSTI No. 1615599 (DOESC Office of Basic Energy Sciences, 2019).
- 5U.S. Department of Transportation Press Release, Biden-Harris Administration Releases First-Ever Blueprint to Decarbonize America's Transportation Sector (U.S. Department of Transportation Press Release, 2023).
- ⁶European Parliament, "Fit for 55: Zero CO₂ emissions for new cars and vans in 2035" (2023).
- ⁷European Environment Agency, *Decarbonising Heating and Cooling—A Climate Imperative* (European Environment Agency, 2023).
- ⁸J. Rissman, C. Bataille, E. Masanet, N. Aden, W. R. Morrow, N. Zhou, N. Elliott, R. Dell, N. Heeren, B. Huckestein, J. Cresko, S. A. Miller, J. Roy, P. Fennell, B. Cremmins, T. Koch Blank, D. Hone, E. D. Williams, S. de la Rue du Can, B. Sisson, M. Williams, J. Katzenberger, D. Burtraw, G. Sethi, H. Ping, D. Danielson, H. Lu, T. Lorber, J. Dinkel, and J. Helseth, "Technologies and policies to decarbonize global industry: Review and assessment of mitigation drivers through 2070," Appl. Energy 266, 114848 (2020).
- ⁹Y. Bicer, I. Dincer, G. Vezina, and F. Raso, "Impact assessment and environmental evaluation of various ammonia production processes," Environ. Manage. 59, 842–855 (2017).
- ¹⁰ A. G. Olabi and M. A. Abdelkareem, "Renewable energy and climate change," Renewable Sustainable Energy Rev. 158, 112111 (2022).
- ¹¹Y. Li, D. Hui, Y. Sun, Y. Wang, Z. Wu, C. Wang, and J. Zhao, "Boosting thermo-photocatalytic CO₂ conversion activity by using photosynthesis-inspired electron-proton-transfer mediators," Nat. Commun. 12, 123 (2021).
- ¹²E. Cortés, L. V. Besteiro, A. Alabastri, A. Baldi, G. Tagliabue, A. Demetriadou, and P. Narang, "Challenges in plasmonic catalysis," ACS Nano 14, 16202–16219 (2020).
- ¹³H. Sayre, H. H. Ripberger, E. Odella, A. Zieleniewska, D. A. Heredia, G. Rumbles, G. D. Scholes, T. A. Moore, A. L. Moore, and R. R. Knowles, "PCET-based ligand limits charge recombination with an Ir(III) photoredox catalyst," J. Am. Chem. Soc. 143, 13034–13043 (2021).
- ¹⁴A. M. Lifschitz, R. M. Young, J. Mendez-Arroyo, C. L. Stern, C. M. McGuirk, M. R. Wasielewski, and C. A. Mirkin, "An allosteric photoredox catalyst inspired by photosynthetic machinery," Nat. Commun. 6, 6541 (2015).
- ¹⁵E.-R. Newmeyer, J. D. North, and D. F. Swearer, "Hot carrier photochemistry on metal nanoparticles," J. Appl. Phys. **132**, 230901 (2022).
- 16J. Kou, C. Lu, J. Wang, Y. Chen, Z. Xu, and R. S. Varma, "Selectivity enhancement in heterogeneous photocatalytic transformations," Chem. Rev. 117, 1445–1514 (2017).
- 17 L. Zhou, J. M. P. Martirez, J. Finzel, C. Zhang, D. F. Swearer, S. Tian, H. Robatjazi, M. Lou, L. Dong, L. Henderson, P. Christopher, E. A. Carter, P. Nordlander, and N. J. Halas, "Light-driven methane dry reforming with single atomic site antennareactor plasmonic photocatalysts," Nat. Energy 5, 61–70 (2020).
- ¹⁸K. Wang, K. Yoshiiri, L. Rosa, Z. Wei, S. Juodkazis, B. Ohtani, and E. Kowalska, "TiO₂/Au/TiO₂ plasmonic photocatalyst with enhanced photocatalytic activity and stability under visible-light irradiation," Catal. Today 397–399, 257–264 (2022).
- ¹⁹W.-S. Wang, H. Du, R.-X. Wang, T. Wen, and A.-W. Xu, "Heterostructured Ag₃PO₄/AgBr/Ag plasmonic photocatalyst with enhanced photocatalytic activity and stability under visible light," Nanoscale 5, 3315–3321 (2013).
- ²⁰L. Zhou, D. F. Swearer, C. Zhang, H. Robatjazi, H. Zhao, L. Henderson, L. Dong, P. Christopher, E. A. Carter, P. Nordlander, and N. J. Halas, "Quantifying hot carrier and thermal contributions in plasmonic photocatalysis," Science 362, 69–72 (2018).
- ²¹M. Bonn, S. Funk, C. Hess, D. N. Denzler, C. Stampfl, M. Scheffler, M. Wolf, and G. Ertl, "Phonon-versus electron-mediated desorption and oxidation of CO on Ru(0001)," Science 285, 1042–1045 (1999).
- ²²G. A. Tritsaris, D. Vinichenko, G. Kolesov, C. M. Friend, and E. Kaxiras, "Dynamics of the photogenerated hole at the rutile TiO₂(110)/water interface: A nonadiabatic simulation study," J. Phys. Chem. C 118, 27393–27401 (2014).

- ²³K. Maeda and K. Domen, "Photocatalytic water splitting: Recent progress and future challenges," J. Phys. Chem. Lett. 1, 2655–2661 (2010).
- ²⁴S. Cho and W. Choi, "Solid-phase photocatalytic degradation of PVC-TiO₂ polymer composites," J. Photochem. Photobiol., A **143**, 221–228 (2001).
- 25 S. Zhang, Y. Zhao, R. Shi, G. I. N. Waterhouse, and T. Zhang, "Photocatalytic ammonia synthesis: Recent progress and future," EnergyChem 1, 100013 (2019).
- ²⁶Q. Han, H. Jiao, L. Xiong, and J. Tang, "Progress and challenges in photocatalytic ammonia synthesis," Mater. Adv. 2, 564–581 (2021).
- ²⁷X. Xiong, C. Mao, Z. Yang, Q. Zhang, G. I. N. Waterhouse, L. Gu, and T. Zhang, "Photocatalytic CO₂ reduction to CO over Ni single atoms supported on defect-rich zirconia," Adv. Energy Mater. 10, 2002928 (2020).
- ²⁸H. Wang, H. Rong, D. Wang, X. Li, E. Zhang, X. Wan, B. Bai, M. Xu, J. Liu, J. Liu, W. Chen, and J. Zhang, "Highly selective photoreduction of CO with suppressing H evolution by plasmonic Au/CdSe-Cu O hierarchical nanostructures under visible light," Small 16, e2000426 (2020).
- 29T. Oshikiri, K. Ueno, and H. Misawa, "Plasmon-induced ammonia synthesis through nitrogen photofixation with visible light irradiation," Angew. Chem. 126, 9960–9963 (2014).
- ³⁰S. Mubeen, J. Lee, N. Singh, S. Krämer, G. D. Stucky, and M. Moskovits, "An autonomous photosynthetic device in which all charge carriers derive from surface plasmons," Nat. Nanotechnol. 8, 247–251 (2013).
- ³¹B. Seemala, A. J. Therrien, M. Lou, K. Li, J. P. Finzel, J. Qi, P. Nordlander, and P. Christopher, "Plasmon-mediated catalytic O₂ dissociation on Ag nanostructures: Hot electrons or near fields?," ACS Energy Lett. 4, 1803–1809 (2019).
- 32T. G. U. Ghobadi, A. Ghobadi, E. Ozbay, and F. Karadas, "Strategies for plasmonic hot-electron-driven photoelectrochemical water splitting," ChemPhotoChem 2, 161–182 (2018).
- ³³E. Cortés, F. J. Wendisch, L. Sortino, A. Mancini, S. Ezendam, S. Saris, L. de S Menezes, A. Tittl, H. Ren, and S. A. Maier, "Optical metasurfaces for energy conversion," Chem. Rev. 122, 15082–15176 (2022).
- ³⁴M. L. Brongersma, N. J. Halas, and P. Nordlander, "Plasmon-induced hot carrier science and technology," Nat. Nanotechnol. 10, 25–34 (2015).
- 35G. V. Hartland, "Optical studies of dynamics in noble metal nanostructures," Chem. Rev. 111, 3858–3887 (2011).
- ³⁶D. Rioux and M. Meunier, "Seeded growth synthesis of composition and size-controlled gold-silver alloy nanoparticles," J. Phys. Chem. C 119, 13160–13168 (2015).
- ³⁷S. M. Rehn and E. Ringe, "Controllably hollow AgAu nanoparticles via non-aqueous, reduction agent-assisted galvanic replacement," Part. Part. Syst. Charact. 35, 1700381 (2018).
- ³⁸Q. N. Nguyen, C. Wang, Y. Shang, A. Janssen, and Y. Xia, "Colloidal synthesis of metal nanocrystals: From asymmetrical growth to symmetry breaking," Chem. Rev. 123(7), 3693–3760 (2022).
- 39 A. L. González, C. Noguez, J. Beránek, and A. S. Barnard, "Size, shape, stability, and color of plasmonic silver nanoparticles," J. Phys. Chem. C 118, 9128–9136 (2014).
- ⁴⁰Z. Liu, W. Hou, P. Pavaskar, M. Aykol, and S. B. Cronin, "Plasmon resonant enhancement of photocatalytic water splitting under visible illumination," Nano Lett. 11, 1111–1116 (2011).
- ⁴¹A. Tanaka, K. Teramura, S. Hosokawa, H. Kominami, and T. Tanaka, "Visible light-induced water splitting in an aqueous suspension of a plasmonic Au/TiO photocatalyst with metal co-catalysts," Chem. Sci. 8, 2574–2580 (2017).
- ⁴²L. Mascaretti, A. Dutta, Š. Kment, V. M. Shalaev, A. Boltasseva, R. Zbořil, and A. Naldoni, "Plasmon-enhanced photoelectrochemical water splitting for efficient renewable energy storage," Adv. Mater. 31, 1805513 (2019).
- ⁴³D. Mittal, M. Ahlawat, and V. Govind Rao, "Recent progress and challenges in plasmon-mediated reduction of CO₂ to chemicals and fuels," Adv. Mater. Interfaces 9, 2102383 (2022).
- ⁴⁴H. Zhang, T. Wang, J. Wang, H. Liu, T. D. Dao, M. Li, G. Liu, X. Meng, K. Chang, L. Shi, T. Nagao, and J. Ye, "Surface-plasmon-enhanced photodriven CO₂ reduction catalyzed by metal-organic-framework-derived iron nanoparticles encapsulated by ultrathin carbon layers," Adv. Mater. 28, 3703–3710 (2016).
- ⁴⁵H. Robatjazi, H. Zhao, D. F. Swearer, N. J. Hogan, L. Zhou, A. Alabastri, M. J. McClain, P. Nordlander, and N. J. Halas, "Plasmon-induced selective carbon dioxide conversion on earth-abundant aluminum-cuprous oxide antennareactor nanoparticles," Nat. Commun. 8, 27 (2017).

- ⁴⁶W. Hou, W. H. Hung, P. Pavaskar, A. Goeppert, M. Aykol, and S. B. Cronin, "Photocatalytic conversion of CO₂ to hydrocarbon fuels via plasmonenhanced absorption and metallic interband transitions," ACS Catal. 1, 929–936 (2011).
- ⁴⁷I. Thomann, B. A. Pinaud, Z. Chen, B. M. Clemens, T. F. Jaramillo, and M. L. Brongersma, "Plasmon enhanced solar-to-fuel energy conversion," Nano Lett. 11, 3440–3446 (2011).
- ⁴⁸B. Puértolas, M. Comesaña-Hermo, L. V. Besteiro, M. Vázquez-González, and M. A. Correa-Duarte, "Challenges and opportunities for renewable ammonia production via plasmon-assisted photocatalysis," Adv. Energy Mater. 12, 2103909 (2022).
- ⁴⁹X. Li, X. Zhang, H. O. Everitt, and J. Liu, "Light-induced thermal gradients in ruthenium catalysts significantly enhance ammonia production," Nano Lett. 19, 1706–1711 (2019).
- ⁵⁰ A. Marimuthu, J. Zhang, and S. Linic, "Tuning selectivity in propylene epoxidation by plasmon mediated photo-switching of Cu oxidation state," Science 339, 1590–1593 (2013).
- ⁵¹Inamuddin, M. I. Ahamed, A. M. Asiri, and E. Lichtfouse, Nanophotocatalysis and Environmental Applications: Energy Conversion and Chemical Transformations (Springer, 2019).
- ⁵²C. Wang and D. Astruc, "Nanogold plasmonic photocatalysis for organic synthesis and clean energy conversion," Chem. Soc. Rev. 43, 7188–7216 (2014).
- 53S. Swaminathan, V. G. Rao, J. K. Bera, and M. Chandra, "The pivotal role of hot carriers in plasmonic catalysis of C-N bond forming reaction of amines," Angew. Chem., Int. Ed. Engl. 60, 12532–12538 (2021).
- While the use of "in situ" varies throughout the literature, here it indicates methods where the catalyst is exposed to conditions analogous to the intended reaction conditions. These conditions can include the chemical environment, thermodynamic properties, and/or externally applied stimuli. There is no further term to distinguish whether the catalyst is under partial or full reaction conditions, and so the extent of in situ conditions varies broadly. We use in operando to refer to in situ characterization with simultaneous measurements of reaction products. 694
- 555J. Hagen, Industrial Catalysis: A Practical Approach (John Wiley & Sons, 2015).
- 56 L. Liu and A. Corma, "Metal catalysts for heterogeneous catalysis: From single atoms to nanoclusters and nanoparticles," Chem. Rev. 118, 4981–5079 (2018).
- ⁵⁷R. J. White, R. Luque, V. L. Budarin, J. H. Clark, and D. J. Macquarrie, "Supported metal nanoparticles on porous materials. Methods and applications," Chem. Soc. Rev. 38, 481–494 (2009).
- ⁵⁸J. K. Nurskov, F. Studt, F. Abild-Pedersen, and T. Bligaard, Fundamental Concepts in Heterogeneous Catalysis (John Wiley & Sons, New Jersey, 2014).
- ⁵⁹L. Zhou, M. Lou, J. L. Bao, C. Zhang, J. G. Liu, J. M. P. Martirez, S. Tian, L. Yuan, D. F. Swearer, H. Robatjazi et al., "Hot carrier multiplication in plasmonic photocatalysis," Proc. Natl. Acad. Sci. U. S. A. 118, e2022109118 (2021).
- 60 M. Lou, J. L. Bao, L. Zhou, G. N. Naidu, H. Robatjazi, A. I. Bayles, H. O. Everitt, P. Nordlander, E. A. Carter, and N. J. Halas, "Direct H₂S decomposition by plasmonic photocatalysis: Efficient remediation plus sustainable hydrogen production," ACS Energy Lett. 7, 3666–3674 (2022).
- ⁶¹N. A. K. Aramouni, J. G. Touma, B. A. Tarboush, J. Zeaiter, and M. N. Ahmad, "Catalyst design for dry reforming of methane: Analysis review," Renewable Sustainable Energy Rev. 82, 2570–2585 (2018).
- ⁶²J. Humphreys, R. Lan, and S. Tao, "Development and recent progress on ammonia synthesis catalysts for Haber-Bosch process," Adv. Energy Sustainability Res. 2, 2000043 (2021).
- ⁶³L. Mascaretti and A. Naldoni, "Hot electron and thermal effects in plasmonic photocatalysis," J. Appl. Phys. **128**, 041101 (2020).
- ⁶⁴S. A. Maier, *Plasmonics: Fundamentals and Applications* (Springer Science & Business Media, New York, 2007).
- ⁶⁵J. B. Khurgin, "How to deal with the loss in plasmonics and metamaterials," Nat. Nanotechnol. 10, 2–6 (2015).
- ⁶⁶G. V. Hartland, L. V. Besteiro, P. Johns, and A. O. Govorov, "What's so hot about electrons in metal nanoparticles?," ACS Energy Lett. 2, 1641–1653 (2017).

- ⁶⁷M. W. Knight, H. Sobhani, P. Nordlander, and N. J. Halas, "Photodetection with active optical antennas," Science 332, 702–704 (2011).
- 68S. Mubeen, G. Hernandez-Sosa, D. Moses, J. Lee, and M. Moskovits, "Plasmonic photosensitization of a wide band gap semiconductor: Converting plasmons to charge carriers," Nano Lett. 11, 5548–5552 (2011).
- ⁶⁹M. Bernardi, J. Mustafa, J. B. Neaton, and S. G. Louie, "Theory and computation of hot carriers generated by surface plasmon polaritons in noble metals," Nat. Commun. 6, 7044 (2015).
- ⁷⁰K. Wu, J. Chen, J. R. McBride, and T. Lian, "Efficient hot-electron transfer by a plasmon-induced interfacial charge-transfer transition," Science 349, 632-635 (2015).
- ⁷¹B. Foerster, V. A. Spata, E. A. Carter, C. Sönnichsen, and S. Link, "Plasmon damping depends on the chemical nature of the nanoparticle interface," Sci. Adv. 5, eaav0704 (2019).
- ⁷²B. Foerster, A. Joplin, K. Kaefer, S. Celiksoy, S. Link, and C. Sönnichsen, "Chemical interface damping depends on electrons reaching the surface," ACS Nano 11, 2886–2893 (2017).
- ⁷³C. Boerigter, U. Aslam, and S. Linic, "Mechanism of charge transfer from plasmonic nanostructures to chemically attached materials," ACS Nano 10, 6108–6115 (2016).
- 74S. K. Cushing, J. Li, J. Bright, B. T. Yost, P. Zheng, A. D. Bristow, and N. Wu, "Controlling plasmon-induced resonance energy transfer and hot electron injection processes in metal@TiO₂ core-shell nanoparticles," J. Phys. Chem. C 119, 16239–16244 (2015).
- 75T. Tatsuma, H. Nishi, and T. Ishida, "Plasmon-induced charge separation: Chemistry and wide applications," Chem. Sci. 8, 3325–3337 (2017).
- 76Y. Negrín-Montecelo, X.-T. Kong, L. V. Besteiro, E. Carbó-Argibay, Z. M. Wang, M. Pérez-Lorenzo, A. O. Govorov, M. Comesaña-Hermo, and M. A. Correa-Duarte, "Synergistic combination of charge carriers and energy-transfer processes in plasmonic photocatalysis," ACS Appl. Mater. Interfaces 14, 35734–35744 (2022).
- 77 A. Sousa-Castillo, M. Comesaña-Hermo, B. Rodríguez-González, M. Pérez-Lorenzo, Z. Wang, X.-T. Kong, A. O. Govorov, and M. A. Correa-Duarte, "Boosting hot electron-driven photocatalysis through anisotropic plasmonic nanoparticles with hot spots in Au–TiO₂ nanoarchitectures," J. Phys. Chem. C 120, 11690–11699 (2016).
- ⁷⁸S. S. E. Collins, E. K. Searles, L. J. Tauzin, M. Lou, L. Bursi, Y. Liu, J. Song, C. Flatebo, R. Baiyasi, Y.-Y. Cai, B. Foerster, T. Lian, P. Nordlander, S. Link, and C. F. Landes, "Plasmon energy transfer in hybrid nanoantennas," ACS Nano 15, 9522–9530 (2021).
- ⁷⁹X. Zhang, X. Li, M. E. Reish, D. Zhang, N. Q. Su, Y. Gutiérrez, F. Moreno, W. Yang, H. O. Everitt, and J. Liu, "Plasmon-enhanced catalysis: Distinguishing thermal and nonthermal effects," Nano Lett. 18, 1714–1723 (2018).
- 80 G. Baffou, I. Bordacchini, A. Baldi, and R. Quidant, "Simple experimental procedures to distinguish photothermal from hot-carrier processes in plasmonics," Light 9, 108 (2020).
- 81 A. V. Uskov, I. E. Protsenko, R. S. Ikhsanov, V. E. Babicheva, S. V. Zhukovsky, A. V. Lavrinenko, E. P. O'Reilly, and H. Xu, "Internal photoemission from plasmonic nanoparticles: Comparison between surface and volume photoelectric effects," Nanoscale 6, 4716–4727 (2014).
- 82 R. Jiang, B. Li, C. Fang, and J. Wang, "Metal/semiconductor hybrid nanostructures for plasmon-enhanced applications," Adv. Mater. 26, 5274–5309 (2014).
- 83X. Jiang, J. Huang, Z. Bi, W. Ni, G. Gurzadyan, Y. Zhu, and Z. Zhang, "Plasmonic active 'hot spots'-confined photocatalytic CO₂ reduction with high selectivity for CH₄ production," Adv. Mater. 34, 2109330 (2022).
- ⁸⁴D. F. Swearer, H. Zhao, L. Zhou, C. Zhang, H. Robatjazi, J. M. P. Martirez, C. M. Krauter, S. Yazdi, M. J. McClain, E. Ringe, E. A. Carter, P. Nordlander, and N. J. Halas, "Heterometallic antenna-reactor complexes for photocatalysis," Proc. Natl. Acad. Sci. U. S. A. 113, 8916–8920 (2016).
- 85 U. Aslam, V. G. Rao, S. Chavez, and S. Linic, "Catalytic conversion of solar to chemical energy on plasmonic metal nanostructures," Nat. Catal. 1, 656–665 (2018).
- 86P. V. Kumar, T. P. Rossi, D. Marti-Dafcik, D. Reichmuth, M. Kuisma, P. Erhart, M. J. Puska, and D. J. Norris, "Plasmon-induced direct hot-carrier transfer at metal–acceptor interfaces," ACS Nano 13, 3188–3195 (2019).
- 87 F. A. Shuklin, I. V. Smetanin, I. E. Protsenko, J. B. Khurgin, N. V. Nikonorov, and A. V. Uskov, "Hot electron photoemission in metal-semiconductor structures aided by resonance tunneling," Appl. Phys. Lett. 118, 181104 (2021).

- 88G. Kumari, R. Kamarudheen, E. Zoethout, and A. Baldi, "Photocatalytic surface restructuring in individual silver nanoparticles," ACS Catal. 11, 3478–3486 (2021).
- 89C. Engelbrekt, K. T. Crampton, D. A. Fishman, M. Law, and V. A. Apkarian, "Efficient plasmon-mediated energy funneling to the surface of Au@ Pt coreshell nanocrystals," ACS Nano 14, 5061–5074 (2020).
- ⁹⁰S. Tan, A. Árgondizzo, J. Ren, L. Liu, J. Zhao, and H. Petek, "Plasmonic coupling at a metal/semiconductor interface," Nat. Photonics 11, 806–812 (2017).
- ⁹¹ X. Zhang, H. Liu, Y. Wang, S. Yang, Q. Chen, Z. Zhao, Y. Yang, Q. Kuang, and Z. Xie, "Hot-electron-induced CO₂ hydrogenation on Au@AuRu/g-C₃N₄ plasmonic bimetal-semiconductor heterostructure," Chem. Eng. J. 443, 136482 (2022).
- ⁹²Z. Zhang, X. Jiang, B. Liu, L. Guo, N. Lu, L. Wang, J. Huang, K. Liu, and B. Dong, "IR-Driven ultrafast transfer of plasmonic hot electrons in nonmetallic branched heterostructures for enhanced H₂ generation," Adv. Mater. 30, 1705221 (2018).
- ⁹³L. Yuan, J. Zhou, M. Zhang, X. Wen, J. M. P. Martirez, H. Robatjazi, L. Zhou, E. A. Carter, P. Nordlander, and N. J. Halas, "Plasmonic photocatalysis with chemically and spatially specific antenna–dual reactor complexes," ACS Nano 16, 17365–17375 (2022).
- 94S. Kim, S. Lee, and S. Yoon, "Effect of nanoparticle size on plasmon-driven reaction efficiency," ACS Appl. Mater. Interfaces 14, 4163–4169 (2022).
- ⁹⁵K. Qian, B. C. Sweeny, A. C. Johnston-Peck, W. Niu, J. O. Graham, J. S. DuChene, J. Qiu, Y.-C. Wang, M. H. Engelhard, D. Su, E. A. Stach, and W. D. Wei, "Surface plasmon-driven water reduction: Gold nanoparticle size matters," J. Am. Chem. Soc. 136, 9842–9845 (2014).
- 96 D. Devasia, A. J. Wilson, J. Heo, V. Mohan, and P. K. Jain, "A rich catalog of C-C bonded species formed in CO₂ reduction on a plasmonic photocatalyst," Nat Commun 12, 2612 (2021).
- ⁹⁷M. Jin, G. He, H. Zhang, J. Zeng, Z. Xie, and Y. Xia, "Shape-controlled synthesis of copper nanocrystals in an aqueous solution with glucose as a reducing agent and hexadecylamine as a capping agent," Angew. Chem., Int. Ed. Engl. 50, 10560–10564 (2011).
- 98X. Ye, C. Zheng, J. Chen, Y. Gao, and C. B. Murray, "Using binary surfactant mixtures to simultaneously improve the dimensional tunability and monodispersity in the seeded growth of gold nanorods," Nano Lett. 13, 765–771 (2013).
- ⁹⁹N. G. Bastús, F. Merkoçi, J. Piella, and V. Puntes, "Synthesis of highly monodisperse citrate-stabilized silver nanoparticles of up to 200 nm: Kinetic control and catalytic properties," Chem. Mater. 26, 2836–2846 (2014).
- 100 B. Hammer and J. K. Nùrskov, "Electronic factors determining the reactivity of metal surfaces," Surf. Sci. 343, 211–220 (1995).
- ¹⁰¹E. R. Hopper, C. Boukouvala, J. Asselin, J. S. Biggins, and E. Ringe, "Opportunities and challenges for alternative nanoplasmonic metals: Magnesium and beyond," J. Phys. Chem. C 126, 10630–10643 (2022).
- 102C. R. Jacobson, D. Solti, D. Renard, L. Yuan, M. Lou, and N. J. Halas, "Shining light on aluminum nanoparticle synthesis," Acc. Chem. Res. 53, 2020–2030 (2020).
- 103 E. Ringe, "Shapes, plasmonic properties, and reactivity of magnesium nanoparticles," J. Phys. Chem. C 124, 15665–15679 (2020).
- 104T. T. Trinh, R. Sato, M. Sakamoto, Y. Fujiyoshi, M. Haruta, H. Kurata, and T. Teranishi, "Visible to near-infrared plasmon-enhanced catalytic activity of Pd hexagonal nanoplates for the Suzuki coupling reaction," Nanoscale 7, 12435–12444 (2015).
- ¹⁰⁵L. Zhou, C. Zhang, M. J. McClain, A. Manjavacas, C. M. Krauter, S. Tian, F. Berg, H. O. Everitt, E. A. Carter, P. Nordlander, and N. J. Halas, "Aluminum nanocrystals as a plasmonic photocatalyst for hydrogen dissociation," Nano Lett. 16, 1478–1484 (2016).
- ¹⁰⁶V. Lomonosov, T. M. R. Wayman, E. R. Hopper, Y. P. Ivanov, G. Divitini, and E. Ringe, "Plasmonic magnesium nanoparticles decorated with palladium catalyze thermal and light-driven hydrogenation of acetylene," Nanoscale 15, 7420–7429 (2023).
- 107S. Linic, P. Christopher, and D. B. Ingram, "Plasmonic-metal nanostructures for efficient conversion of solar to chemical energy," Nat. Mater. 10, 911–921 (2011).
- 108P.-C. Chen, G. Liu, Y. Zhou, K. A. Brown, N. Chernyak, J. L. Hedrick, S. He, Z. Xie, Q.-Y. Lin, V. P. Dravid, S. A. O'Neill-Slawecki, and C. A. Mirkin,

- "Tip-directed synthesis of multimetallic nanoparticles," J. Am. Chem. Soc. 137, 9167–9173 (2015).
- 109K. Sytwu, M. Vadai, and J. A. Dionne, "Bimetallic nanostructures: Combining plasmonic and catalytic metals for photocatalysis," Adv. Phys. 4, 1619480 (2019).
- ¹¹⁰M. Valenti, A. Venugopal, D. Tordera, M. P. Jonsson, G. Biskos, A. Schmidt-Ott, and W. A. Smith, "Hot carrier generation and extraction of plasmonic alloy nanoparticles," ACS Photonics 4, 1146–1152 (2017).
- ^{III}K. Sytwu, M. Vadai, F. Hayee, D. K. Angell, A. Dai, J. Dixon, and J. A. Dionne, "Driving energetically unfavorable dehydrogenation dynamics with plasmonics," Science 371, 280–283 (2021).
- ¹¹²M. Vadai, D. K. Angell, F. Hayee, K. Sytwu, and J. A. Dionne, "In-situ observation of plasmon-controlled photocatalytic dehydrogenation of individual palladium nanoparticles," Nat. Commun. 9, 4658 (2018).
- ¹¹³P. Peljo, J. A. Manzanares, and H. H. Girault, "Contact potentials, Fermi level equilibration, and surface charging," Langmuir 32, 5765–5775 (2016).
- ¹¹⁴S. Lee, H. Hwang, W. Lee, D. Schebarchov, Y. Wy, J. Grand, B. Auguié, D. H. Wi, E. Cortés, and S. W. Han, "Core-shell bimetallic nanoparticle trimers for efficient light-to-chemical energy conversion," ACS Energy Lett. 5, 3881–3890 (2020).
- ¹¹⁵K. Loza, M. Heggen, and M. Epple, "Synthesis, structure, properties, and applications of bimetallic nanoparticles of noble metals," Adv. Funct. Mater. 30, 1909260 (2020).
- ¹¹⁶C. Gao, Y. Hu, M. Wang, M. Chi, and Y. Yin, "Fully alloyed Ag/Au nanospheres: Combining the plasmonic property of Ag with the stability of Au," J. Am. Chem. Soc. 136, 7474–7479 (2014).
- ¹¹⁷M. Hu, J. Chen, Z.-Y. Li, L. Au, G. V. Hartland, X. Li, M. Marquez, and Y. Xia, "Gold nanostructures: Engineering their plasmonic properties for biomedical applications," Chem. Soc. Rev. 35, 1084–1094 (2006).
- ¹¹⁸J. M. Rahm, C. Tiburski, T. P. Rossi, F. A. A. Nugroho, S. Nilsson, C. Langhammer, and P. Erhart, "A library of late transition metal alloy dielectric functions for nanophotonic applications," Adv. Funct. Mater. 30, 2002122 (2020).
- ¹¹⁹S. Linic, S. Chavez, and R. Elias, "Flow and extraction of energy and charge carriers in hybrid plasmonic nanostructures," Nat. Mater. 20, 916–924 (2021).
- 120 L. Collado, A. Reynal, F. Fresno, M. Barawi, C. Escudero, V. Perez-Dieste, J. M. Coronado, D. P. Serrano, J. R. Durrant, and V. A. de la Peña O'Shea, "Unravelling the effect of charge dynamics at the plasmonic metal/semiconductor interface for CO photoreduction," Nat. Commun. 9, 4986 (2018).
- ¹²¹L. van Turnhout, Y. Hattori, J. Meng, K. Zheng, and J. Sá, "Direct observation of a plasmon-induced hot electron flow in a multimetallic nanostructure," Nano Lett. 20, 8220–8228 (2020).
- 122 J. Liu, J. Feng, J. Gui, T. Chen, M. Xu, H. Wang, H. Dong, H. Chen, X. Li, L. Wang, Z. Chen, Z. Yang, J. Liu, W. Hao, Y. Yao, L. Gu, Y. Weng, Y. Huang, X. Duan, J. Zhang, and Y. Li, "Metal@semiconductor core-shell nanocrystals with atomically organized interfaces for efficient hot electron-mediated photocatalysis," Nano Energy 48, 44–52 (2018).
- 123Z. Zhang, Y. Huang, K. Liu, L. Guo, Q. Yuan, and B. Dong, "Multichannel-improved charge-carrier dynamics in well-designed hetero-nanostructural plasmonic photocatalysts toward highly efficient solar-to-fuels conversion," Adv. Mater. 27, 5906–5914 (2015).
- 124P. Christopher, H. Xin, A. Marimuthu, and S. Linic, "Singular characteristics and unique chemical bond activation mechanisms of photocatalytic reactions on plasmonic nanostructures," Nat. Mater. 11, 1044–1050 (2012).
- ¹²⁵A. Wang, S. Wu, J. Dong, R. Wang, J. Wang, J. Zhang, S. Zhong, and S. Bai, "Interfacial facet engineering on the Schottky barrier between plasmonic Au and TiO₂ in boosting the photocatalytic CO₂ reduction under ultraviolet and visible light irradiation," Chem. Eng. J. 404, 127145 (2021).
- 126K. Wang, J. Lu, Y. Lu, C. H. Lau, Y. Zheng, and X. Fan, "Unravelling the CC coupling in CO₂ photocatalytic reduction with H₂O on Au/TiO_{2-x}: Combination of plasmonic excitation and oxygen vacancy," Appl. Catal., B 292, 120147 (2021).
- 127 P. Reñones, L. Collado, A. Iglesias-Juez, F. E. Oropeza, F. Fresno, and V. A. de la Peña O'Shea, "Silver-gold bimetal-loaded TiO₂ photocatalysts for CO₂ reduction," Ind. Eng. Chem. Res. 59, 9440–9450 (2020).
- ¹²⁸Q. Chen, X. Chen, M. Fang, J. Chen, Y. Li, Z. Xie, Q. Kuang, and L. Zheng, "Photo-induced Au-Pd alloying at TiO₂ 101 facets enables robust CO₂

- photocatalytic reduction into hydrocarbon fuels," J. Mater. Chem. A 7, 1334–1340 (2019).
- ¹²⁹L. Qin, G. Wang, and Y. Tan, "Plasmonic pt nanoparticles-TiO hierarchical nano-architecture as a visible light photocatalyst for water splitting," Sci. Rep. 8, 16198 (2018).
- Y. Negrín-Montecelo, M. Comesaña-Hermo, L. K. Khorashad, A. Sousa-Castillo, Z. Wang, M. Pérez-Lorenzo, T. Liedl, A. O. Govorov, and M. A. Correa-Duarte, "Photophysical effects behind the efficiency of hot electron injection in plasmon-assisted catalysis: The joint role of morphology and composition," ACS Energy Lett. 5, 395–402 (2020).
- ¹³¹M. Zhao, H. Xu, S. Ouyang, H. Tong, H. Chen, Y. Li, L. Song, and J. Ye, "Fabricating a Au@TiO₂ plasmonic system to elucidate alkali-induced enhancement of photocatalytic H₂ evolution: Surface potential shift or methanol oxidation acceleration?," ACS Catal. 8, 4266–4277 (2018).
- ¹³²S. J. P. Varapragasam, S. Mia, C. Wieting, C. Balasanthiran, M. Y. Hossan, A. Baride, R. M. Rioux, and J. D. Hoefelmeyer, "Ag-TiO₂ hybrid nanocrystal photocatalyst: Hydrogen evolution under UV irradiation but not under visible-light irradiation," ACS Appl. Energy Mater. 2, 8274–8282 (2019).
- ¹³³M. Zhu, Y. Wang, Y.-H. Deng, X. Peng, X. Wang, H. Yuan, Z.-J. Yang, Y. Wang, and H. Wang, "Strategic modulation of energy transfer in Au-TiO-Pt nanodumbbells: Plasmon-enhanced hydrogen evolution reaction," Nanoscale 12, 7035–7044 (2020).
- 134 J.-L. Yang, Y.-L. He, H. Ren, H.-L. Zhong, J.-S. Lin, W.-M. Yang, M.-D. Li, Z.-L. Yang, H. Zhang, Z.-Q. Tian, and J.-F. Li, "Boosting photocatalytic hydrogen evolution reaction using dual plasmonic antennas," ACS Catal. 11, 5047–5053 (2021).
- ¹³⁵H. Ren, J.-L. Yang, W.-M. Yang, H.-L. Zhong, J.-S. Lin, P. M. Radjenovic, L. Sun, H. Zhang, J. Xu, Z.-Q. Tian, and J.-F. Li, "Core–shell–satellite plasmonic photocatalyst for broad-spectrum photocatalytic water splitting," ACS Mater. Lett. 3, 69–76 (2021).
- 136S.-I. Naya, T. Kume, R. Akashi, M. Fujishima, and H. Tada, "Red-light-driven water splitting by Au(core)-CdS(shell) half-cut nanoegg with heteroepitaxial junction," J. Am. Chem. Soc. 140, 1251–1254 (2018).
- ¹³⁷L. Ma, K. Chen, F. Nan, J.-H. Wang, D.-J. Yang, L. Zhou, and Q.-Q. Wang, "Improved hydrogen production of Au-Pt-CdS hetero-nanostructures by efficient plasmon-induced multipathway electron transfer," Adv. Funct. Mater. 26, 6076–6083 (2016).
- ¹³⁸S. Javaid, X. Li, F. Wang, W. Chen, Y. Pang, S. Wang, G. Jia, and F. Jones, "Synthesis of magnetically separable Fe₃O₄-Au-CdS kinked heterotrimers incorporating plasmonic and semiconducting functionalities," J. Mater. Chem. C 7, 14517–14524 (2019).
- F. Pang, R. Zhang, D. Lan, and J. Ge, "Synthesis of magnetite-semiconductor-metal trimer nanoparticles through functional modular assembly: A magnetically separable photocatalyst with photothermic enhancement for water reduction," ACS Appl. Mater. Interfaces 10, 4929–4936 (2018).
- ¹⁴⁰L. Guo, C. Zhong, J. Cao, Y. Hao, M. Lei, K. Bi, Q. Sun, and Z. L. Wang, "Enhanced photocatalytic H₂ evolution by plasmonic and piezotronic effects based on periodic Al/BaTiO₃ heterostructures," Nano Energy 62, 513–520 (2019).
- 141S. Ezendam, M. Herran, L. Nan, C. Gruber, Y. Kang, F. Gröbmeyer, R. Lin, J. Gargiulo, A. Sousa-Castillo, and E. Cortés, "Hybrid plasmonic nanomaterials for hydrogen generation and carbon dioxide reduction," ACS Energy Lett. 7, 778, 815 (2022)
- 142S. Li, J. Zhao, G. Liu, L. Xu, Y. Tian, A. Jiao, and M. Chen, "Graphene oxide-grafted plasmonic Au@Ag nanoalloys with improved synergistic effects for promoting hot carrier-driven photocatalysis under visible light irradiation," Nanotechnology 32, 125401 (2021).
- ¹⁴³B. Tudu, N. Nalajala, K. P. Reddy, P. Saikia, and C. S. Gopinath, "Electronic integration and thin film aspects of Au–Pd/rGO/TiO₂ for improved solar hydrogen generation," ACS Appl. Mater. Interfaces 11, 32869–32878 (2019).
- 144Z. Lou, M. Fujitsuka, and T. Majima, "Two-dimensional Au-nanoprism/ reduced graphene oxide/Pt-nanoframe as plasmonic photocatalysts with multiplasmon modes boosting hot electron transfer for hydrogen generation," J. Phys. Chem. Lett. 8, 844–849 (2017).
- 145 T. Kashyap, S. Biswasi, A. R. Pal, and B. Choudhury, "Unraveling the catalytic and plasmonic roles of g-C₃N₄ supported Ag and Au nanoparticles under

- selective photoexcitation," ACS Sustainable Chem. Eng. 7, 19295–19302 (2019).
- 146 N. Xiao, Y. Li, S. Li, X. Li, Y. Gao, L. Ge, and G. Lu, "In-situ synthesis of PdAg/g-C₃N₄ composite photocatalyst for highly efficient photocatalytic H₂ generation under visible light irradiation," Int. J. Hydrogen Energy 44, 19929–19941 (2019).
- 147Q. Zhang, S. Yang, S.-N. Yin, and H. Xue, "Over two-orders of magnitude enhancement of the photocatalytic hydrogen evolution activity of carbon nitride via mediator-free decoration with gold-organic microspheres," Chem. Commun. 53, 11814–11817 (2017).
- 148C. Han, Y. Gao, S. Liu, L. Ge, N. Xiao, D. Dai, B. Xu, and C. Chen, "Facile synthesis of AuPd/g-C₃N₄ nanocomposite: An effective strategy to enhance photocatalytic hydrogen evolution activity," Int. J. Hydrogen Energy 42, 22765–22775 (2017).
- ¹⁴⁹Z. Xu, M. G. Kibria, B. AlOtaibi, P. N. Duchesne, L. V. Besteiro, Y. Gao, Q. Zhang, Z. Mi, P. Zhang, A. O. Govorov, L. Mai, M. Chaker, and D. Ma, "Towards enhancing photocatalytic hydrogen generation: Which is more important, alloy synergistic effect or plasmonic effect?," Appl. Catal., B 221, 77–85 (2018).
- 150 A. Naldoni, F. Riboni, U. Guler, A. Boltasseva, V. M. Shalaev, and A. V. Kildishev, "Solar-powered plasmon-enhanced heterogeneous catalysis," Nanophotonics 5, 112–133 (2016).
- 151 J. Becerra, D.-T. Nguyen, V.-N. Gopalakrishnan, and T.-O. Do, "Plasmonic Au nanoparticles incorporated in the zeolitic imidazolate framework (ZIF-67) for the efficient sunlight-driven photoreduction of CO₂," ACS Appl. Energy Mater. 3, 7659–7665 (2020).
- 152 L. Chen, Y. Peng, H. Wang, Z. Gu, and C. Duan, "Synthesis of Au@ZIF-8 single- or multi-core-shell structures for photocatalysis," Chem. Commun. 50, 8651–8654 (2014).
- 153S. De Marchi, L. Vázquez-Iglesias, G. Bodelón, I. Pérez-Juste, L. Á. Fernández, J. Pérez-Juste, and I. Pastoriza-Santos, "Programmable modular assembly of functional proteins on Raman-encoded zeolitic imidazolate framework-8 (ZIF-8) nanoparticles as SERS tags," Chem. Mater. 32, 5739–5749 (2020).
- ¹⁵⁴ C. S. L. Koh, H. Y. F. Sim, S. X. Leong, S. K. Boong, C. Chong, and X. Y. Ling, "Plasmonic nanoparticle-metal-organic framework (NP-MOF) nanohybrid platforms for emerging plasmonic applications," ACS Mater. Lett. 3, 557–573 (2021).
- 155].-D. Xiao, L. Han, J. Luo, S.-H. Yu, and H.-L. Jiang, "Integration of plasmonic effects and Schottky junctions into metal-organic framework composites: Steering charge flow for enhanced visible-light photocatalysis," Angew. Chem., Int. Ed. Engl. 57, 1103–1107 (2018).
- 156M. Wen, K. Mori, Y. Kuwahara, and H. Yamashita, "Plasmonic Au@Pd nanoparticles supported on a basic metal-organic framework: Synergic boosting of H₂ production from formic acid," ACS Energy Lett. 2, 1-7 (2017).
- 157Y. Wang, Y. Zhang, Z. Jiang, G. Jiang, Z. Zhao, Q. Wu, Y. Liu, Q. Xu, A. Duan, and C. Xu, "Controlled fabrication and enhanced visible-light photocatalytic hydrogen production of Au@CdS/MIL-101 heterostructure," Appl. Catal., B 185, 307–314 (2016).
- ¹⁵⁸L. Liu, C. He, S. P. Morgan, R. Correia, and S. Korposh, "A fiber-optic localized surface plasmon resonance (LSPR) sensor anchored with metal organic framework (HKUST-1) film for acetone sensing," Proc. SPIE 11199, 111990Z (2019).
- 159 W. Cheng, H. Su, F. Tang, W. Che, Y. Huang, X. Zheng, T. Yao, J. Liu, F. Hu, Y. Jiang, Q. Liu, and S. Wei, "Synergetic enhancement of plasmonic hot-electron injection in Au cluster-nanoparticle/C₃N₄ for photocatalytic hydrogen evolution," J. Mater. Chem. A 5, 19649–19655 (2017).
- ¹⁶⁰A. Naldoni, U. Guler, Z. Wang, M. Marelli, F. Malara, X. Meng, L. V. Besteiro, A. O. Govorov, A. V. Kildishev, A. Boltasseva, and V. M. Shalaev, "Broadband hot-electron collection for solar water splitting with plasmonic titanium nitride," Adv. Opt. Mater. 5, 1601031 (2017).
- ¹⁶¹K. Rasool, R. P. Pandey, P. A. Rasheed, S. Buczek, Y. Gogotsi, and K. A. Mahmoud, "Water treatment and environmental remediation applications of two-dimensional metal carbides (MXenes)," Mater. Today 30, 80–102 (2019).
- ¹⁶²J. Shen, Z. Wu, C. Li, C. Zhang, A. Genest, G. Rupprechter, and L. He, "Emerging applications of mxene materials in CO₂ photocatalysis," FlatChem 28, 100252 (2021).

- 163Y. Gogotsi and B. Anasori, "The rise of mxenes," ACS Nano 13, 8491–8494 (2019).
- 164 X. Wu, J. Wang, Z. Wang, F. Sun, Y. Liu, K. Wu, X. Meng, and J. Qiu, "Boosting the electrocatalysis of MXenes by plasmon-induced thermalization and hot-electron injection," Angew. Chem., Int. Ed. 60, 9416–9420 (2021).
- ¹⁶⁵H. Lin, X. Wang, L. Yu, Y. Chen, and J. Shi, "Two-dimensional ultrathin MXene ceramic nanosheets for photothermal conversion," Nano Lett. 17, 384–391 (2017).
- 166X. Wan, J. Liu, and J. Zhang, "Construction of plasmonic metal@semiconductor core-shell photocatalysts: From epitaxial to nonepitaxial strategies," Small Struct. 3, 2200045 (2022).
- 167 H. Shi, J. A. Lercher, and X.-Y. Yu, "Sailing into uncharted waters: Recent advances in the *in situ* monitoring of catalytic processes in aqueous environments," Catal. Sci. Technol. 5, 3035–3060 (2015).
- 168 J. Lu, J. Bravosuarez, A. Takahashi, M. Haruta, and S. Oyama, "In situ UV-vis studies of the effect of particle size on the epoxidation of ethylene and propylene on supported silver catalysts with molecular oxygen," J. Catal. 232, 85–95 (2005).
- 169Y. Yuan, L. Zhou, H. Robatjazi, J. L. Bao, J. Zhou, A. Bayles, L. Yuan, M. Lou, M. Lou, S. Khatiwada, E. A. Carter, P. Nordlander, and N. J. Halas, "Earthabundant photocatalyst for H₂ generation from NH₃ with light-emitting diode illumination," Science 378, 889–893 (2022).
- 170 P. Christopher, H. Xin, and S. Linic, "Visible-light-enhanced catalytic oxidation reactions on plasmonic silver nanostructures," Nat. Chem. 3, 467–472 (2011).
- ¹⁷⁷P. H. C. Camargo and E. Cortés, *Plasmonic Catalysis: From Fundamentals to Applications* (John Wiley & Sons, 2021).
- 172R. G. Hobbs, W. P. Putnam, A. Fallahi, Y. Yang, F. X. Kärtner, and K. K. Berggren, "Mapping photoemission and hot-electron emission from plasmonic nanoantennas," Nano Lett. 17, 6069–6076 (2017).
- 173 E. Cortés, W. Xie, J. Cambiasso, A. S. Jermyn, R. Sundararaman, P. Narang, S. Schlücker, and S. A. Maier, "Plasmonic hot electron transport drives nanolocalized chemistry," Nat. Commun. 8, 14880 (2017).
- 1774 A. Al-Zubeidi, L. A. McCarthy, A. Rafiei-Miandashti, T. S. Heiderscheit, and S. Link, "Single-particle scattering spectroscopy: Fundamentals and applications," Nanophotonics 10, 1621–1655 (2021).
- 175S. Celiksoy, W. Ye, K. Wandner, K. Kaefer, and C. Sönnichsen, "Intensity-based single particle plasmon sensing," Nano Lett. 21, 2053–2058 (2021).
- ¹⁷⁶V. Thambi, A. Kar, P. Ghosh, and S. Khatua, "Light-controlled *in situ* bidirectional tuning and monitoring of gold nanorod plasmon via oxidative etching with FeCl₃," J. Phys. Chem. C 122, 24885–24890 (2018).
- 177 S. A. Lee, B. Ostovar, C. F. Landes, and S. Link, "Spectroscopic signatures of plasmon-induced charge transfer in gold nanorods," J. Chem. Phys. 156, 064702 (2022).
- 178G. Kumari, X. Zhang, D. Devasia, J. Heo, and P. K. Jain, "Watching visible light-driven CO reduction on a plasmonic nanoparticle catalyst," ACS Nano 12, 8330–8340 (2018).
- 179B. Akbali, M. Yagmurcukardes, F. M. Peeters, H.-Y. Lin, T.-Y. Lin, W.-H. Chen, S. Maher, T.-Y. Chen, and C.-H. Huang, "Determining the molecular orientation on the metal nanoparticle surface through surface-enhanced Raman spectroscopy and density functional theory simulations," J. Phys. Chem. C 125, 16289–16295 (2021).
- ¹⁸⁰C. L. Warkentin, Z. Yu, A. Sarkar, and R. R. Frontiera, "Decoding chemical and physical processes driving plasmonic photocatalysis using surfaceenhanced Raman spectroscopies," Acc. Chem. Res. 54, 2457–2466 (2021).
- ¹⁸¹N. Zou, G. Chen, X. Mao, H. Shen, E. Choudhary, X. Zhou, and P. Chen, "Imaging catalytic hotspots on single plasmonic nanostructures via correlated super-resolution and electron microscopy," ACS Nano 12, 5570–5579 (2018).
- 182E. A. Wertz, B. P. Isaacoff, and J. S. Siteen, "Wavelength-dependent superresolution images of dye molecules coupled to plasmonic nanotriangles," ACS Photonics 3, 1733–1740 (2016).
- ¹⁸³K. Bian, C. Gerber, A. J. Heinrich, D. J. Müller, S. Scheuring, and Y. Jiang, "Scanning probe microscopy," Nat. Rev. Methods Primers 1, 36 (2021).
- 184 E. Kazuma, M. Lee, J. Jung, M. Trenary, and Y. Kim, "Single-molecule study of a plasmon-induced reaction for a strongly chemisorbed molecule," Angew. Chem., Int. Ed Engl. 59, 7960–7966 (2020).
- 185 E. Kazuma, N. Sakai, and T. Tatsuma, "Nanoimaging of localized plasmon-induced charge separation," Chem. Commun. 47, 5777–5779 (2011).

- ¹⁸⁶I. Tanabe and T. Tatsuma, "Plasmonic manipulation of color and morphology of single silver nanospheres," Nano Lett. 12, 5418–5421 (2012).
- 187 E. Kazuma and T. Tatsuma, "In situ nanoimaging of photoinduced charge separation at the plasmonic Au nanoparticle-TiO₂ interface," Adv. Mater. Interfaces 1, 1400066 (2014).
- ¹⁸⁸E. Kazuma and Y. Kim, "Scanning probe microscopy for real-space observations of local chemical reactions induced by a localized surface plasmon," Phys. Chem. Chem. Phys. 21, 19720–19731 (2019).
- 189 S. Wang, Y. Gao, S. Miao, T. Liu, L. Mu, R. Li, F. Fan, and C. Li, "Positioning the water oxidation reaction sites in plasmonic photocatalysts," J. Am. Chem. Soc. 139, 11771–11778 (2017).
- ¹⁹⁰Y. Gao, W. Nie, Q. Zhu, X. Wang, S. Wang, F. Fan, and C. Li, "The polarization effect in surface-plasmon-induced photocatalysis on Au/TiO nanoparticles," Angew. Chem., Int. Ed. Engl. 59, 18218–18223 (2020).
- ¹⁹¹S.-H. Lee, S. W. Lee, T. Oh, S. H. Petrosko, C. A. Mirkin, and J.-W. Jang, "Direct observation of plasmon-induced interfacial charge separation in metal/ semiconductor hybrid nanostructures by measuring surface potentials," Nano Lett. 18, 109–116 (2018).
- 192J.-Z. Wang, Z.-Q. Guo, J.-P. Zhou, and Y.-X. Lei, "Plasmon-enhanced photocatalytic activity of NaMgTiO loaded with noble metals directly observed with scanning kelvin probe microscopy," Nanotechnology 29, 305709 (2018).
- ¹⁹³J. Zhu, F. Fan, R. Chen, H. An, Z. Feng, and C. Li, "Direct imaging of highly anisotropic photogenerated charge separations on different facets of a single BiVO₄ photocatalyst," Angew. Chem., Int. Ed. Engl. 54, 9111–9114 (2015).
- 194C. L. Bentley, M. Kang, and P. R. Unwin, "Nanoscale structure dynamics within electrocatalytic materials," J. Am. Chem. Soc. 139, 16813–16821 (2017).
- 195S. Dery and E. Gross, "Ir nanospectroscopy in catalysis research," in Ambient Pressure Spectroscopy in Complex Chemical Environments, ACS Symposium Series (American Chemical Society, Washington, DC, 2021), Chap. 7, pp. 147–173.
- ¹⁹⁶U. Arieli, M. Mrejen, and H. Suchowski, "Broadband coherent hyperspectral near-field imaging of plasmonic nanostructures," Opt. Express 27, 9815–9820 (2019).
- 197 J. Karst, F. Sterl, H. Linnenbank, T. Weiss, M. Hentschel, and H. Giessen, "Watching in situ the hydrogen diffusion dynamics in magnesium on the nanoscale," Sci. Adv. 6, eaaz0566 (2020).
- 198Z. Li, P. Z. El-Khoury, and D. Kurouski, "Tip-enhanced Raman imaging of photocatalytic reactions on thermally-reshaped gold and gold-palladium microplates," Chem. Commun. 57, 891–894 (2021).
- 199°C. Barroo, Z.-J. Wang, R. Schlögl, and M.-G. Willinger, "Imaging the dynamics of catalysed surface reactions by *in situ* scanning electron microscopy," Nat. Catal. 3, 30–39 (2019).
- ²⁰⁰Y. Wu, G. Li, and J. P. Camden, "Probing nanoparticle plasmons with electron energy loss spectroscopy," Chem. Rev. **118**, 2994–3031 (2018).
- ²⁰¹C. Cherqui, N. Thakkar, G. Li, J. P. Camden, and D. J. Masiello, "Characterizing localized surface plasmons using electron energy-loss spectroscopy," Annu. Rev. Phys. Chem. 67, 331–357 (2016).
- ²⁰²F.-P. Schmidt, H. Ditlbacher, U. Hohenester, A. Hohenau, F. Hofer, and J. R. Krenn, "Dark plasmonic breathing modes in silver nanodisks," Nano Lett. 12, 5780–5783 (2012).
- 203F. P. Schmidt, H. Ditlbacher, F. Hofer, J. R. Krenn, and U. Hohenester, "Morphing a plasmonic nanodisk into a nanotriangle," Nano Lett. 14, 4810–4815 (2014).
- ²⁰⁴J. Nelayah, M. Kociak, O. Stéphan, F. J. García de Abajo, M. Tencé, L. Henrard, D. Taverna, I. Pastoriza-Santos, L. M. Liz-Marzán, and C. Colliex, "Mapping surface plasmons on a single metallic nanoparticle," Nat. Phys. 3, 348–353 (2007).
- 205 A. Campos, N. Troc, E. Cottancin, M. Pellarin, H.-C. Weissker, J. Lermé, M. Kociak, and M. Hillenkamp, "Plasmonic quantum size effects in silver nanoparticles are dominated by interfaces and local environments," Nat. Phys. 15, 275–280 (2019).
- ²⁰⁶J. A. Scholl, A. L. Koh, and J. A. Dionne, "Quantum plasmon resonances of individual metallic nanoparticles," Nature 483, 421–427 (2012).
- 207A. Campos, A. Arbouet, J. Martin, D. Gérard, J. Proust, J. Plain, and M. Kociak, "Plasmonic breathing and edge modes in aluminum nanotriangles," ACS Photonics 4, 1257–1263 (2017).
- ²⁰⁸K. P. Koirala, J. Ge, R. Kalyanaraman, and G. Duscher, "Direct detection of highly localized metal-metal interface plasmons from bimetallic nanoparticles," Plasmonics 16, 957–964 (2021).

- ²⁰⁹Y. Wu, G. Li, C. Cherqui, N. W. Bigelow, N. Thakkar, D. J. Masiello, J. P. Camden, and P. D. Rack, "Electron energy loss spectroscopy study of the full plasmonic spectrum of self-assembled Au–Ag alloy nanoparticles: Unraveling size, composition, and substrate effects," ACS Photonics 3, 130–138 (2016).
- ²¹⁰V. Flauraud, G. D. Bernasconi, J. Butet, D. T. L. Alexander, O. J. F. Martin, and J. Brugger, "Mode coupling in plasmonic heterodimers probed with electron energy loss spectroscopy," ACS Nano 11, 3485–3495 (2017).
- ²¹¹E. Ringe, C. J. DeSantis, S. M. Collins, M. Duchamp, R. E. Dunin-Borkowski, S. E. Skrabalak, and P. A. Midgley, "Resonances of nanoparticles with poor plasmonic metal tips," Sci. Rep. 5, 17431 (2015).
- ²¹²S. Griffin, N. P. Montoni, G. Li, P. J. Straney, J. E. Millstone, D. J. Masiello, and J. P. Camden, "Imaging energy transfer in Pt-decorated Au nanoprisms via electron energy-loss spectroscopy," J. Phys. Chem. Lett. 7, 3825–3832 (2016).
- ²¹³G. Li, C. Cherqui, N. W. Bigelow, G. Duscher, P. J. Straney, J. E. Millstone, D. J. Masiello, and J. P. Camden, "Spatially mapping energy transfer from single plasmonic particles to semiconductor substrates via STEM/EELS," Nano Lett. 15, 3465–3471 (2015).
- 214L. Han, Q. Meng, D. Wang, Y. Zhu, J. Wang, X. Du, E. A. Stach, and H. L. Xin, "Interrogation of bimetallic particle oxidation in three dimensions at the nanoscale," Nat. Commun. 7, 13335 (2016).
- 215R. Aso, H. Hojo, Y. Takahashi, T. Akashi, Y. Midoh, F. Ichihashi, H. Nakajima, T. Tamaoka, K. Yubuta, H. Nakanishi, H. Einaga, T. Tanigaki, H. Shinada, and Y. Murakami, "Direct identification of the charge state in a single platinum nanoparticle on titanium oxide," Science 378, 202–206 (2022).
- ²¹⁶C. Ophus, "Four-dimensional scanning transmission electron microscopy (4D-STEM): From scanning nanodiffraction to ptychography and beyond," Microsc. Microanal. 25, 563–582 (2019).
- ²¹⁷H.-Y. Chao, K. Venkatraman, S. Moniri, Y. Jiang, X. Tang, S. Dai, W. Gao, J. Miao, and M. Chi, "In situ and emerging transmission electron microscopy for catalysis research," Chem. Rev. 123, 8347–8394 (2023).
- 218C. Addiego, W. Gao, H. Huyan, and X. Pan, "Probing charge density in materials with atomic resolution in real space," Nat. Rev. Phys. 5, 117–132 (2023).
- 219O. L. Krivanek, T. C. Lovejoy, N. Dellby, T. Aoki, R. W. Carpenter, P. Rez, E. Soignard, J. Zhu, P. E. Batson, M. J. Lagos, R. F. Egerton, and P. A. Crozier, "Vibrational spectroscopy in the electron microscope," Nature 514, 209–212 (2014).
- M. J. Lagos, A. Trügler, U. Hohenester, and P. E. Batson, "Mapping vibrational surface and bulk modes in a single nanocube," Nature 543, 529–532 (2017).
- P. Rez, T. Aoki, K. March, D. Gur, O. L. Krivanek, N. Dellby, T. C. Lovejoy, S. G. Wolf, and H. Cohen, "Damage-free vibrational spectroscopy of biological materials in the electron microscope," Nat. Commun. 7, 10945 (2016).
- 222C. Dwyer, T. Aoki, P. Rez, S. L. Y. Chang, T. C. Lovejoy, and O. L. Krivanek, "Electron-beam mapping of vibrational modes with nanometer spatial resolution," Phys. Rev. Lett. 117, 256101 (2016).
- 223 F. S. Hage, R. J. Nicholls, J. R. Yates, D. G. McCulloch, T. C. Lovejoy, N. Dellby, O. L. Krivanek, K. Refson, and Q. M. Ramasse, "Nanoscale momentum-resolved vibrational spectroscopy," Sci. Adv. 4, eaar7495 (2018).
- F. S. Hage, D. M. Kepaptsoglou, Q. M. Ramasse, and L. J. Allen, "Phonon expects occupy at a tomic resolution," Phys. Pays. Lett. 122, 016102 (2019)
- spectroscopy at atomic resolution," Phys. Rev. Lett. 122, 016103 (2019).

 225 T. Miyata, M. Fukuyama, A. Hibara, E. Okunishi, M. Mukai, and T. Mizoguchi, "Measurement of vibrational spectrum of liquid using monochromated scanning transmission electron microscopy-electron energy loss spectroscopy," Microscopy 63, 377–382 (2014).
- E. R. Hoglund, D.-L. Bao, A. O'Hara, T. W. Pfeifer, M. S. B. Hoque, S. Makarem, J. M. Howe, S. T. Pantelides, P. E. Hopkins, and J. A. Hachtel, "Direct visualization of localized vibrations at complex grain boundaries," Adv. Mater. 35, e2208920 (2023).
- 227 J. A. Hachtel, J. Huang, I. Popovs, S. Jansone-Popova, J. K. Keum, J. Jakowski, T. C. Lovejoy, N. Dellby, O. L. Krivanek, and J. C. Idrobo, "Identification of site-specific isotopic labels by vibrational spectroscopy in the electron microscope," Science 363, 525–528 (2019).
- 228 R. Senga, Y.-C. Lin, S. Morishita, R. Kato, T. Yamada, M. Hasegawa, and K. Suenaga, "Imaging of isotope diffusion using atomic-scale vibrational spectroscopy," Nature 603, 68–72 (2022).
- 229D. Kordahl and C. Dwyer, "Enhanced vibrational electron energy-loss spectroscopy of adsorbate molecules," Phys. Rev. B 99, 104110 (2019).

- ²³⁰L. H. G. Tizei, V. Mkhitaryan, H. Lourenço-Martins, L. Scarabelli, K. Watanabe, T. Taniguchi, M. Tencé, J.-D. Blazit, X. Li, A. Gloter, A. Zobelli, F.-P. Schmidt, L. M. Liz-Marzán, F. J. García de Abajo, O. Stéphan, and M. Kociak, "Tailored nanoscale plasmon-enhanced vibrational electron spectroscopy," Nano Lett. 20, 2973–2979 (2020).
- 231G. Beane, T. Devkota, B. S. Brown, and G. V. Hartland, "Ultrafast measurements of the dynamics of single nanostructures: A review," Rep. Prog. Phys. 82, 016401 (2019).
- ²³²N. Gross, C. T. Kuhs, B. Ostovar, W.-Y. Chiang, K. S. Wilson, T. S. Volek, Z. M. Faitz, C. C. Carlin, J. A. Dionne, M. T. Zanni, M. Gruebele, S. T. Roberts, S. Link, and C. F. Landes, "Progress and prospects in optical ultrafast microscopy in the visible spectral region: Transient absorption and two-dimensional microscopy," J. Phys. Chem. C 127, 14557–14586 (2023).
- ²³³J. S. Pelli Cresi, M. C. Spadaro, S. D'Addato, S. Valeri, S. Benedetti, A. D. Bona, D. Catone, L. D. Mario, P. O'Keeffe, A. Paladini, G. Bertoni, and P. Luches, "Highly efficient plasmon-mediated electron injection into cerium oxide from embedded silver nanoparticles," Nanoscale 11, 10282–10291 (2019).
- ²³⁴O. L. Muskens, N. Del Fatti, and F. Vallée, "Femtosecond response of a single metal nanoparticle," Nano Lett. 6, 552–556 (2006).
- ²³⁵K. Yu, J. E. Sader, P. Zijlstra, M. Hong, Q.-H. Xu, and M. Orrit, "Probing silver deposition on single gold nanorods by their acoustic vibrations," Nano Lett. 14, 915–922 (2014).
- 236S. Mourdikoudis, R. M. Pallares, and N. T. K. Thanh, "Characterization techniques for nanoparticles: Comparison and complementarity upon studying nanoparticle properties," Nanoscale 10, 12871–12934 (2018).
- 237C.-L. Dong and L. Vayssieres, "In situ/operando x-ray spectroscopies for advanced investigation of energy materials," Chemistry 24, 18356–18373 (2018).
- 238°C. S. Schnohr and M. C. Ridgway, X-Ray Absorption Spectroscopy of Semiconductors (Springer, Heidelberg, 2014).
- 239J. Kawai, "Absorption techniques in x-ray spectrometry," in *Encyclopedia of Analytical Chemistry* (John Wiley & Sons, Ltd, 2006).
- 240B. D. Cullity and S. R. Stock, Elements of X-Ray Diffraction (Prentice Hall, 2001).
- ²⁴¹H. Khan, A. S. Yerramilli, A. D'Oliveira, T. L. Alford, D. C. Boffito, and G. S. Patience, "Experimental methods in chemical engineering: X-ray diffraction spectroscopy—XRD," Can. J. Chem. Eng. 98, 1255–1266 (2020).
- 242C. Giannini, M. Ladisa, D. Altamura, D. Siliqi, T. Sibillano, and L. De Caro, "X-ray diffraction: A powerful technique for the multiple-length-scale structural analysis of nanomaterials," Crystals 6, 87 (2016).
- ²⁴³T. Li, A. J. Senesi, and B. Lee, "Small angle x-ray scattering for nanoparticle research," Chem. Rev. 116, 11128–11180 (2016).
- 244H. Schnablegger and Y. Singh, The SAXS Guide, 5th ed. (Anton Paar GmbH, Graz, Austria, 2023).
- ²⁴⁵S. A. Lee and S. Link, "Chemical interface damping of surface plasmon resonances," Acc. Chem. Res. 54, 1950–1960 (2021).
- ²⁴⁶N. L. Gruenke, M. F. Cardinal, M. O. McAnally, R. R. Frontiera, G. C. Schatz, and R. P. Van Duyne, "Ultrafast and nonlinear surface-enhanced Raman spectroscopy," Chem. Soc. Rev. 45, 2263–2290 (2016).
- ²⁴⁷S.-C. Huang, X. Wang, Q.-Q. Zhao, J.-F. Zhu, C.-W. Li, Y.-H. He, S. Hu, M. M. Sartin, S. Yan, and B. Ren, "Probing nanoscale spatial distribution of plasmonically excited hot carriers," Nat. Commun. 11, 4211 (2020).
- ²⁴⁸L. Su, H. Yuan, G. Lu, S. Rocha, M. Orrit, J. Hofkens, and H. Uji-i, "Super-resolution localization and defocused fluorescence microscopy on resonantly coupled single-molecule, single-nanorod hybrids," ACS Nano 10, 2455–2466 (2016).
- ²⁴⁹A. J. Wilson, D. Devasia, and P. K. Jain, "Nanoscale optical imaging in chemistry," Chem. Soc. Rev. 49, 6087–6112 (2020).
- 250 X. Wang, Y. Cui, and J. Irudayaraj, "Single-cell quantification of cytosine modifications by hyperspectral dark-field imaging," ACS Nano 9, 11924–11932 (2015).
- ²⁵¹A. Weigel, A. Sebesta, and P. Kukura, "Dark field microspectroscopy with single molecule fluorescence sensitivity," ACS Photonics 1, 848–856 (2014).
- 252S.-C. Yang, H. Kobori, C.-L. He, M.-H. Lin, H.-Y. Chen, C. Li, M. Kanehara, T. Teranishi, and S. Gwo, "Plasmon hybridization in individual gold nanocrystal dimers: Direct observation of bright and dark modes," Nano Lett. 10, 632–637 (2010).

- 253W. Zhang, L. Huang, C. Santschi, and O. J. F. Martin, "Trapping and sensing 10 nm metal nanoparticles using plasmonic dipole antennas," Nano Lett. 10, 1006–1011 (2010).
- 254D. J. Hill, C. W. Pinion, J. Christesen, and J. F. Cahoon, "Waveguide scattering microscopy for dark-field imaging and spectroscopy of photonic nanostructures," ACS Photonics 1, 725–731 (2014).
- 255T. S. Heiderscheit, M. J. Gallagher, R. Baiyasi, S. S. E. Collins, S. A. Hosseini Jebeli, L. Scarabelli, A. Al-Zubeidi, C. Flatebo, W.-S. Chang, C. F. Landes, and S. Link, "Nanoelectrode-emitter spectral overlap amplifies surface enhanced electrogenerated chemiluminescence," J. Chem. Phys. 151, 144712 (2019).
- 256 A. Kumar, E. Villarreal, X. Zhang, and E. Ringe, "Micro-extinction spectroscopy (MExS): A versatile optical characterization technique," Adv. Struct. Chem. Imaging 4, 8 (2018).
- 257T.-Y. Tseng, P.-J. Lai, and K.-B. Sung, "High-throughput detection of immobilized plasmonic nanoparticles by a hyperspectral imaging system based on Fourier transform spectrometry," Opt. Express 19, 1291–1300 (2011).
- 258D. Zopf, J. Jatschka, A. Dathe, N. Jahr, W. Fritzsche, and O. Stranik, "Hyperspectral imaging of plasmon resonances in metallic nanoparticles," Biosens. Bioelectron. 81, 287–293 (2016).
- 259 C. M. Sweeney, C. L. Nehl, W. Hasan, T. Liang, A. L. Eckermann, T. J. Meade, and T. W. Odom, "Three-channel spectrometer for wide-field imaging of anisotropic plasmonic nanoparticles," J. Phys. Chem. C 115, 15933–15937 (2011).
- ²⁶⁰K. Lindfors, T. Kalkbrenner, P. Stoller, and V. Sandoghdar, "Detection and spectroscopy of gold nanoparticles using supercontinuum white light confocal microscopy," Phys. Rev. Lett. 93, 037401 (2004).
- ²⁶¹K. Holanová, M. Vala, and M. Piliarik, "[INVITED] optical imaging and localization of prospective scattering labels smaller than a single protein," Opt. Laser Technol. 109, 323–327 (2019).
- ²⁶²L. Rodríguez-Lorenzo, J. M. Romo-Herrera, J. Pérez-Juste, R. A. Alvarez-Puebla, and L. M. Liz-Marzán, "Reshaping and LSPR tuning of Au nanostars in the presence of CTAB," J. Mater. Chem. 21, 11544–11549 (2011).
- ²⁶³A. Al-Zubeidi, F. Stein, C. Flatebo, C. Rehbock, S. A. Hosseini Jebeli, C. F. Landes, S. Barcikowski, and S. Link, "Single-particle hyperspectral imaging reveals kinetics of silver ion leaching from alloy nanoparticles," ACS Nano 15, 8363–8375 (2021)
- ²⁶⁴J. Zhao, S. C. Nguyen, R. Ye, B. Ye, H. Weller, G. A. Somorjai, A. Paul Alivisatos, and F. Dean Toste, "A comparison of photocatalytic activities of gold nanoparticles following plasmonic and interband excitation and a strategy for harnessing interband hot carriers for solution phase photocatalysis," ACS Central Sci. 3, 482–488 (2017).
- ²⁶⁵Z. Mao, R. Espinoza, A. Garcia, A. Enwright, H. Vang, and S. C. Nguyen, "Tuning redox potential of gold nanoparticle photocatalysts by light," ACS Nano 14, 7038–7045 (2020).
- ²⁶⁶N. Y. Molina, T. Pungsrisai, Z. J. O'Dell, B. Paranzino, and K. A. Willets, "The hidden role of the supporting electrode for creating heterogeneity in single entity electrochemistry," ChemElectroChem 9, e202200245 (2022).
- 267 R. Jin, Y. C. Cao, E. Hao, G. S. Métraux, G. C. Schatz, and C. A. Mirkin, "Controlling anisotropic nanoparticle growth through plasmon excitation," Nature 425, 487–490 (2003).
- ²⁶⁸Z. Mao, H. Vang, A. Garcia, A. Tohti, B. J. Stokes, and S. C. Nguyen, "Carrier Diffusion—The main contribution to size-dependent photocatalytic activity of colloidal gold nanoparticles," ACS Catal. 9, 4211–4217 (2019).
- ²⁶⁹D. Andrén, L. Shao, N. Odebo Länk, S. S. Aćimović, P. Johansson, and M. Käll, "Probing photothermal effects on optically trapped gold nanorods by simultaneous plasmon spectroscopy and Brownian dynamics analysis," ACS Nano 11, 10053–10061 (2017).
- ²⁷⁰M. Chirea, S. S. E. Collins, X. Wei, and P. Mulvaney, "Spectroelectrochemistry of silver deposition on single gold nanocrystals," J. Phys. Chem. Lett. 5, 4331–4335 (2014).
- ²⁷¹L. O. Herrmann and J. J. Baumberg, "Watching single nanoparticles grow in real time through supercontinuum spectroscopy," Small 9, 3743–3747 (2013).
- 272M. Elabbadi, C. Boukouvala, E. R. Hopper, J. Asselin, and E. Ringe, "Synthesis of controllable Cu shells on Au nanoparticles with electrodeposition: A systematic in situ single particle study," J. Phys. Chem. C 127(10), 5044–5053 (2023).

- ²⁷³A. Al-Zubeidi, B. S. Hoener, S. S. E. Collins, W. Wang, S. R. Kirchner, S. A. Hosseini Jebeli, A. Joplin, W.-S. Chang, S. Link, and C. F. Landes, "Hot holes assist plasmonic nanoelectrode dissolution," Nano Lett. 19, 1301–1306 (2019).
- ²⁷⁴C. Flatebo, S. S. E. Collins, B. S. Hoener, Y.-Y. Cai, S. Link, and C. F. Landes, "Electrodissolution inhibition of gold nanorods with oxoanions," J. Phys. Chem. C 123, 13983–13992 (2019).
- 275S. Hu, J. Yi, Y.-J. Zhang, K.-Q. Lin, B.-J. Liu, L. Chen, C. Zhan, Z.-C. Lei, J.-J. Sun, C. Zong, J.-F. Li, and B. Ren, "Observing atomic layer electrodeposition on single nanocrystals surface by dark field spectroscopy," Nat. Commun. 11, 2518 (2020)
- ²⁷⁶A. Al-Zubeidi, Y. Wang, J. Lin, C. Flatebo, C. F. Landes, H. Ren, and S. Link, "d-Band holes react at the tips of gold nanorods," J. Phys. Chem. Lett. 14, 5297–5304 (2023).
- ²⁷⁷K. Shiratori, L. D. C. Bishop, B. Ostovar, R. Baiyasi, Y.-Y. Cai, P. J. Rossky, C. F. Landes, and S. Link, "Machine-learned decision trees for predicting gold nanorod sizes from spectra," J. Phys. Chem. C 125, 19353–19361 (2021).
- ²⁷⁸A. Henkel, W. Ye, Y. Khalavka, A. Neiser, C. Lambertz, S. Schmachtel, R. Ahijado-Guzmán, and C. Sönnichsen, "Narrowing the plasmonic sensitivity distribution by considering the individual size of gold nanorods," J. Phys. Chem. C 122, 10133–10137 (2018).
- 279M. Wang, B. B. Rajeeva, L. Scarabelli, E. P. Perillo, A. K. Dunn, L. M. Liz-Marzán, and Y. Zheng, "Molecular-fluorescence enhancement via blue-shifted plasmon-induced resonance energy transfer," J. Phys. Chem. C 120, 14820–14827 (2016).
- ²⁸⁰A. Carattino, S. Khatua, and M. Orrit, "In situ tuning of gold nanorod plasmon through oxidative cyanide etching," Phys. Chem. Chem. Phys. 18, 15619–15624 (2016).
- ²⁸¹Y.-Y. Cai, J. G. Liu, L. J. Tauzin, D. Huang, E. Sung, H. Zhang, A. Joplin, W.-S. Chang, P. Nordlander, and S. Link, "Photoluminescence of gold nanorods: Purcell effect enhanced emission from hot carriers," ACS Nano 12, 976–985 (2018).
- ²⁸²E. K. Searles, E. Gomez, S. Lee, B. Ostovar, S. Link, and C. F. Landes, "Single-Particle photoluminescence and dark-field scattering during charge density tuning," J. Phys. Chem. Lett. 14, 318–325 (2023).
- ²⁸³D. Kurouski, A. Dazzi, R. Zenobi, and A. Centrone, "Infrared and Raman chemical imaging and spectroscopy at the nanoscale," Chem. Soc. Rev. 49, 3315–3347 (2020).
- 284 R. Esteban, J. J. Baumberg, and J. Aizpurua, "Molecular optomechanics approach to surface-enhanced Raman scattering," Acc. Chem. Res. 55, 1889–1899 (2022).
- 285Y. Zhang, R. Esteban, R. A. Boto, M. Urbieta, X. Arrieta, C. Shan, S. Li, J. J. Baumberg, and J. Aizpurua, "Addressing molecular optomechanical effects in nanocavity-enhanced Raman scattering beyond the single plasmonic mode," Nanoscale 13, 1938–1954 (2021).
- ²⁸⁶D. Kurouski, M. Mattei, and R. P. Van Duyne, "Probing redox reactions at the nanoscale with electrochemical tip-enhanced Raman spectroscopy," Nano Lett. 15, 7956–7962 (2015).
- 287D. L. Jeanmaire and R. P. Van Duyne, "Surface Raman spectroelectrochemistry: Part I. heterocyclic, aromatic, and aliphatic amines adsorbed on the anodized silver electrode," J. Electroanal. Chem. Interfacial Electrochem. 84, 1–20 (1977).
- 288S. M. Stranahan and K. A. Willets, "Super-resolution optical imaging of single-molecule SERS hot spots," Nano Lett. 10, 3777–3784 (2010).
- ²⁸⁹L. Velleman, L. Scarabelli, D. Sikdar, A. A. Kornyshev, L. M. Liz-Marzán, and J. B. Edel, "Monitoring plasmon coupling and SERS enhancement through in situ nanoparticle spacing modulation," Faraday Discuss. 205, 67–83 (2017).
- ²⁹⁰K. Chen and H. Wang, "Metal-adsorbate interactions modulate plasmonic reactivity of chemisorbed nitrophenyl derivatives," J. Phys. Chem. C 127, 4104–4114 (2023).
- ²⁹¹E. C. Le Ru, E. Blackie, M. Meyer, and P. G. Etchegoin, "Surface enhanced Raman scattering enhancement factors: A comprehensive study," J. Phys. Chem. C 111, 13794–13803 (2007).
- ²⁹²N. C. Brandt, E. L. Keller, and R. R. Frontiera, "Ultrafast surface-enhanced Raman probing of the role of hot electrons in plasmon-driven chemistry," J. Phys. Chem. Lett. 7, 3179–3185 (2016).

- ²⁹³L. Cui, X. Ren, X. Yang, P. Wang, Y. Qu, W. Liang, and M. Sun, "Plasmon-driven catalysis in aqueous solutions probed by SERS spectroscopy," J. Raman Spectrosc. 47, 877–883 (2016).
- 294X. Zhang, G. Kumari, J. Heo, and P. K. Jain, "In situ formation of catalytically active graphene in ethylene photo-epoxidation," Nat. Commun. 9, 3056 (2018)
- 295 C. Blum, T. Schmid, L. Opilik, S. Weidmann, S. R. Fagerer, and R. Zenobi, "Understanding tip-enhanced Raman spectra of biological molecules: A combined Raman, SERS and TERS study," J. Raman Spectrosc. 43, 1895–1904 (2012).
- 296 J. Langer, D. Jimenez de Aberasturi, J. Aizpurua, R. A. Alvarez-Puebla, B. Auguié, J. J. Baumberg, G. C. Bazan, S. E. J. Bell, A. Boisen, A. G. Brolo, J. Choo, D. Cialla-May, V. Deckert, L. Fabris, K. Faulds, F. J. García de Abajo, R. Goodacre, D. Graham, A. J. Haes, C. L. Haynes, C. Huck, T. Itoh, M. Käll, J. Kneipp, N. A. Kotov, H. Kuang, E. C. Le Ru, H. K. Lee, J.-F. Li, X. Y. Ling, S. A. Maier, T. Mayerhöfer, M. Moskovits, K. Murakoshi, J.-M. Nam, S. Nie, Y. Ozaki, I. Pastoriza-Santos, J. Perez-Juste, J. Popp, A. Pucci, S. Reich, B. Ren, G. C. Schatz, T. Shegai, S. Schlücker, L.-L. Tay, K. G. Thomas, Z.-Q. Tian, R. P. Van Duyne, T. Vo-Dinh, Y. Wang, K. A. Willets, C. Xu, H. Xu, Y. Xu, Y. S. Yamamoto, B. Zhao, and L. M. Liz-Marzán, "Present and future of surface-enhanced Raman scattering," ACS Nano 14, 28–117 (2020).
- ²⁹⁷A. Mahadevan-Jansen and R. R. Richards-Kortum, "Raman spectroscopy for the detection of cancers and precancers," J. Biomed. Opt. 1, 31–70 (1996).
- ²⁹⁸R. Baiyasi, S. A. H. Jebeli, Q. Zhang, L. Su, J. Hofkens, H. Uji-i, S. Link, and C. F. Landes, "PSF distortion in dye-plasmonic nanomaterial interactions: Friend or foe?," ACS Photonics 6, 699–708 (2019).
- 299H. J. Goldwyn, K. C. Smith, J. A. Busche, and D. J. Masiello, "Mislocalization in plasmon-enhanced single-molecule fluorescence microscopy as a dynamical Young's interferometer," ACS Photonics 5, 3141–3151 (2018).
- 300 D. Axelrod, "Total internal reflection fluorescence microscopy in cell biology," Traffic 2, 764–774 (2001).
- 301W. Wang, H. Shen, B. Shuang, B. S. Hoener, L. J. Tauzin, N. A. Moringo, K. F. Kelly, and C. F. Landes, "Super temporal-resolved microscopy (STReM)," J. Phys. Chem. Lett. 7, 4524–4529 (2016).
- 302S. A. Lee and J. S. Biteen, "Interplay of nanoparticle resonance frequency and array surface coverage in live-cell plasmon-enhanced single-molecule imaging," J. Phys. Chem. C 122, 5705–5709 (2018).
- 303 K. L. Blythe and K. A. Willets, "Super-resolution imaging of fluorophore-labeled DNA bound to gold nanoparticles: A single-molecule, single-particle approach," J. Phys. Chem. C 120, 803–815 (2016).
- 304S. Chatterjee, S. N. Kramer, B. Wellnitz, A. Kim, and L. Kisley, "Spatially resolving size effects on diffusivity in nanoporous extracellular matrix-like materials with fluorescence correlation spectroscopy super-resolution optical fluctuation imaging," J. Phys. Chem. B 127, 4430–4440 (2023).
- 305 M. Raab, C. Vietz, F. D. Stefani, G. P. Acuna, and P. Tinnefeld, "Shifting molecular localization by plasmonic coupling in a single-molecule mirage," Nat. Commun. 8, 13966 (2017).
- 306 A. S. De Silva Indrasekara, B. Shuang, F. Hollenhorst, B. S. Hoener, A. Hoggard, S. Chen, E. Villarreal, Y.-Y. Cai, L. Kisley, P. J. Derry, W.-S. Chang, E. R. Zubarev, E. Ringe, S. Link, and C. F. Landes, "Optimization of spectral and spatial conditions to improve super-resolution imaging of plasmonic nanoparticles," J. Phys. Chem. Lett. 8, 299–306 (2017).
- 307P. Anger, P. Bharadwaj, and L. Novotny, "Enhancement and quenching of single-molecule fluorescence," Phys. Rev. Lett. 96, 113002 (2006).
- J. Seelig, K. Leslie, A. Renn, S. Kühn, V. Jacobsen, M. van de Corput, C. Wyman, and V. Sandoghdar, "Nanoparticle-induced fluorescence lifetime modification as nanoscopic ruler: Demonstration at the single molecule level," Nano Lett. 7, 685–689 (2007).
- 309M. J. Rust, M. Bates, and X. Zhuang, "Sub-diffraction-limit imaging by stochastic optical reconstruction microscopy (STORM)," Nat. Methods 3, 793–796 (2006).
- 310S.-C. Huang, J.-Z. Ye, X.-R. Shen, Q.-Q. Zhao, Z.-C. Zeng, M.-H. Li, D.-Y. Wu, X. Wang, and B. Ren, "Electrochemical tip-enhanced Raman spectroscopy with improved sensitivity enabled by a water immersion objective," Anal. Chem. 91, 11092–11097 (2019).
- ³¹¹A. I. Pérez-Jiménez, D. Lyu, Z. Lu, G. Liu, and B. Ren, "Surface-enhanced Raman spectroscopy: Benefits, trade-offs and future developments," Chem. Sci. 11, 4563–4577 (2020).

- 312S. R. Kirchner, K. W. Smith, B. S. Hoener, S. S. E. Collins, W. Wang, Y.-Y. Cai, C. Kinnear, H. Zhang, W.-S. Chang, P. Mulvaney, C. F. Landes, and S. Link, "Snapshot hyperspectral imaging (SHI) for revealing irreversible and heterogeneous plasmonic processes," J. Phys. Chem. C 122, 6865–6875 (2018).
- ³¹³E. Kazuma, J. Jung, H. Ueba, M. Trenary, and Y. Kim, "Real-space and real-time observation of a plasmon-induced chemical reaction of a single molecule," Science 360, 521–526 (2018).
- 314 R. Sundararaman, P. Narang, A. S. Jermyn, W. A. Goddard 3rd, and H. A. Atwater, "Theoretical predictions for hot-carrier generation from surface plasmon decay," Nat. Commun. 5, 5788 (2014).
- 315 A. M. Brown, R. Sundararaman, P. Narang, W. A. Goddard 3rd, and H. A. Atwater, "Nonradiative plasmon decay and hot carrier dynamics: Effects of phonons, surfaces, and geometry," ACS Nano 10, 957–966 (2016).
- 316H. Reddy, K. Wang, Z. Kudyshev, L. Zhu, S. Yan, A. Vezzoli, S. J. Higgins, V. Gavini, A. Boltasseva, P. Reddy, V. M. Shalaev, and E. Meyhofer, "Determining plasmonic hot-carrier energy distributions via single-molecule transport measurements," Science 369, 423–426 (2020).
- 317 B. Voigtlander, Scanning Probe Microscopy: Atomic Force Microscopy and Scanning Tunneling Microscopy, Nanoscience and Technology (Springer, 2015).
- ³¹⁸V. A. Ukraintsev, "Data evaluation technique for electron-tunneling spectroscopy," Phys. Rev. B 53, 11176–11185 (1996).
- A. Piednoir, E. Perrot, S. Granjeaud, A. Humbert, C. Chapon, and C. R. Henry, "Atomic resolution on small three-dimensional metal clusters by STM," Surf. Sci. 391, 19–26 (1997).
- 320 L. Gross, N. Moll, F. Mohn, A. Curioni, G. Meyer, F. Hanke, and M. Persson, "High-resolution molecular orbital imaging using a p-wave STM tip," Phys. Rev. Lett. 107, 086101 (2011).
- ³²¹E. Kazuma, "Real-space studies of plasmon-induced dissociation reactions with an STM," Bull. Chem. Soc. Jpn. 93, 1552–1557 (2020).
- 322 A. Yu, S. Li, G. Czap, and W. Ho, "Tunneling-electron-induced light emission from single gold nanoclusters," Nano Lett. 16, 5433–5436 (2016).
- 323P. Myrach, N. Nilius, and H.-J. Freund, "Photon mapping of individual Ag particles on MgO/Mo(001)," Phys. Rev. B 83, 035416 (2011).
- ³²⁴E. Kazuma, J. Jung, H. Ueba, M. Trenary, and Y. Kim, "STM studies of photochemistry and plasmon chemistry on metal surfaces," Prog. Surf. Sci. 93, 163–176 (2018).
- 325H. Böckmann, S. Gawinkowski, J. Waluk, M. B. Raschke, M. Wolf, and T. Kumagai, "Near-field enhanced photochemistry of single molecules in a scanning tunneling microscope junction," Nano Lett. 18, 152–157 (2018).
- ³²⁶E. Pensa and T. Albrecht, "Controlling the dynamic instability of capped metal nanoparticles on metallic surfaces," J. Phys. Chem. Lett. 9, 57–62 (2018).
- 327 T. Frederiksen, M. Paulsson, and H. Ueba, "Theory of action spectroscopy for single-molecule reactions induced by vibrational excitations with STM," Phys. Rev. B 89, 035427 (2014).
- 328S. K. Khanna and J. Lambe, "Inelastic electron tunneling spectroscopy," Science 220, 1345–1351 (1983).
- 329 S. Wieghold, L. Nienhaus, F. L. Knoller, F. F. Schweinberger, J. J. Shepherd, J. W. Lyding, U. Heiz, M. Gruebele, and F. Esch, "Plasmonic support-mediated activation of 1 nm platinum clusters for catalysis," Phys. Chem. Chem. Phys. 19, 30570–30577 (2017).
- B. Hulsken, J. W. Gerritsen, and S. Speller, "Measuring the Au(111) surface state at the solid–liquid interface," Surf. Sci. 580, 95–100 (2005).
- ⁵³¹B. Hulsken, R. Van Hameren, J. W. Gerritsen, T. Khoury, P. Thordarson, M. J. Crossley, A. E. Rowan, R. J. M. Nolte, J. A. A. W. Elemans, and S. Speller, "Real-time single-molecule imaging of oxidation catalysis at a liquid-solid interface," Nat. Nanotechnol. 2, 285–289 (2007).
- ³³²T. Takami, T. Ye, B. K. Pathem, D. P. Arnold, K.-I. Sugiura, Y. Bian, J. Jiang, and P. S. Weiss, "Manipulating double-decker molecules at the liquid-solid interface," J. Am. Chem. Soc. 132, 16460–16466 (2010).
- ⁵³³L. Gross, B. Schuler, N. Pavliček, S. Fatayer, Z. Majzik, N. Moll, D. Peña, and G. Meyer, "Atomic force microscopy for molecular structure elucidation," Angew. Chem., Int. Ed. Engl. 57, 3888–3908 (2018).
- 334R. García, "Dynamic atomic force microscopy methods," Surf. Sci. Rep. 47,
- ³³⁵A. Sanders, R. W. Bowman, L. Zhang, V. Turek, D. O. Sigle, A. Lombardi, L. Weller, and J. J. Baumberg, "Understanding the plasmonics of nanostructured atomic force microscopy tips," Appl. Phys. Lett. 109, 153110 (2016).

- ³³⁶A. Giugni, B. Torre, A. Toma, M. Francardi, M. Malerba, A. Alabastri, R. Proietti Zaccaria, M. I. Stockman, and E. Di Fabrizio, "Hot-electron nanoscopy using adiabatic compression of surface plasmons," Nat. Nanotechnol. 8, 845–852 (2013).
- 337H. Lee, H. Lee, and J. Y. Park, "Direct imaging of surface plasmon-driven hot electron flux on the Au Nanoprism/TiO₂," Nano Lett. 19, 891–896 (2019).
- ³³⁸B. C. Galarreta, I. Rupar, A. Young, and F. Lagugné-Labarthet, "Mapping hot-spots in hexagonal arrays of metallic nanotriangles with azobenzene polymer thin films," J. Phys. Chem. C 115, 15318–15323 (2011).
- 339 L. Itzel Meza, M. W. Anderson, B. Slater, and J. R. Agger, "In situ atomic force microscopy of zeolite a dissolution," Phys. Chem. Chem. Phys. 10, 5066-5076 (2008).
- 340 W. Melitz, J. Shen, A. C. Kummel, and S. Lee, "Kelvin probe force microscopy and its application," Surf. Sci. Rep. 66, 1–27 (2011).
- 341R. Chen, F. Fan, T. Dittrich, and C. Li, "Imaging photogenerated charge carriers on surfaces and interfaces of photocatalysts with surface photovoltage microscopy," Chem. Soc. Rev. 47, 8238–8262 (2018).
- 342M. Bowker and P. R. Davies, Scanning Tunneling Microscopy in Surface Science, Nanoscience, and Catalysis (Wiley, 2010).
- 343M. Rößler, P. Geng, and J. Wintterlin, "A high-pressure scanning tunneling microscope for studying heterogeneous catalysis," Rev. Sci. Instrum. 76, 023705 (2005).
- 344F. Zaera, "Probing liquid/solid interfaces at the molecular level," Chem. Rev. 112, 2920–2986 (2012).
- 345M. Assig, M. Etzkorn, A. Enders, W. Stiepany, C. R. Ast, and K. Kern, "A 10 mK scanning tunneling microscope operating in ultra high vacuum and high magnetic fields," Rev. Sci. Instrum. 84, 033903 (2013).
- 346 M. S. Hoogeman, D. G. van Loon, R. W. M. Loos, H. G. Ficke, E. de Haas, J. J. van der Linden, H. Zeijlemaker, L. Kuipers, M. F. Chang, M. A. J. Klik, and J. W. M. Frenken, "Design and performance of a programmable-temperature scanning tunneling microscope," Rev. Sci. Instrum. 69, 2072–2080 (1998).
- ³⁴⁷L. L. Patera, F. Bianchini, C. Africh, C. Dri, G. Soldano, M. M. Mariscal, M. Peressi, and G. Comelli, "Real-time imaging of adatom-promoted graphene growth on nickel," Science 359, 1243–1246 (2018).
- 348S. B. Roobol, M. E. Cañas-Ventura, M. Bergman, M. A. van Spronsen, W. G. Onderwaater, P. C. van der Tuijn, R. Koehler, A. Ofitserov, G. J. C. van Baarle, and J. W. M. Frenken, "The ReactorAFM: Non-contact atomic force microscope operating under high-pressure and high-temperature catalytic conditions," Rev. Sci. Instrum. 86, 033706 (2015).
- ³⁴⁹C. T. Herbschleb, P. C. van der Tuijn, S. B. Roobol, V. Navarro, J. W. Bakker, Q. Liu, D. Stoltz, M. E. Cañas-Ventura, G. Verdoes, M. A. van Spronsen, M. Bergman, L. Crama, I. Taminiau, A. Ofitserov, G. J. C. van Baarle, and J. W. M. Frenken, "The ReactorSTM: Atomically resolved scanning tunneling microscopy under high-pressure, high-temperature catalytic reaction conditions," Rev. Sci. Instrum. 85, 083703 (2014).
- 350 M. A. van Spronsen, G. J. C. van Baarle, C. T. Herbschleb, J. W. M. Frenken, and I. M. N. Groot, "High-pressure operando STM studies giving insight in CO oxidation and NO reduction over Pt(110)," Catal. Today 244, 85–95 (2015).
- 351R. V. Mom, J. N. Louwen, J. W. M. Frenken, and I. M. N. Groot, "In situ observations of an active MoS model hydrodesulfurization catalyst," Nat. Commun. 10, 2546 (2019).
- 352M. A. van Spronsen, J. W. M. Frenken, and I. M. N. Groot, "Observing the oxidation of platinum," Nat. Commun. 8, 429 (2017).
- 353K. Manthiram, B. J. Beberwyck, and A. Paul Alivisatos, "Enhanced electro-chemical methanation of carbon dioxide with a dispersible nanoscale copper catalyst," J. Am. Chem. Soc. 136, 13319–13325 (2014).
- 354M. A. Hubert, L. A. King, and T. F. Jaramillo, "Evaluating the case for reduced precious metal catalysts in proton exchange membrane electrolyzers," ACS Energy Lett. 7, 17–23 (2022).
- 355M. Li, K.-H. Ye, W. Qiu, Y. Wang, and H. Ren, "Heterogeneity between and within single hematite nanorods as electrocatalysts for oxygen evolution reaction," J. Am. Chem. Soc. 144, 5247–5252 (2022).
- 356L. A. Baker, "Perspective and prospectus on single-entity electrochemistry," J. Am. Chem. Soc. 140, 15549–15559 (2018).

- 357Y. Yu, K. D. Wijesekara, X. Xi, and K. A. Willets, "Quantifying wavelength-dependent plasmonic hot carrier energy distributions at Metal/Semiconductor interfaces," ACS Nano 13, 3629–3637 (2019).
- 358 J. Kim, C. Renault, N. Nioradze, N. Arroyo-Currás, K. C. Leonard, and A. J. Bard, "Electrocatalytic activity of individual Pt nanoparticles studied by nanoscale scanning electrochemical microscopy," J. Am. Chem. Soc. 138, 8560–8568 (2016).
- 359S. E. Pust, W. Maier, and G. Wittstock, "Investigation of localized catalytic and electrocatalytic processes and corrosion reactions with scanning electrochemical microscopy (SECM)," Z. Phys. Chem. 222, 1463–1517 (2008).
- 360 M. Etienne, A. Schulte, and W. Schuhmann, "High resolution constant-distance mode alternating current scanning electrochemical microscopy (AC-SECM)," Electrochem. Commun. 6, 288–293 (2004).
- ³⁶¹Y. Wang, X. Shan, S. Wang, N. Tao, P.-Y. Blanchard, K. Hu, and M. V. Mirkin, "Imaging local electric field distribution by plasmonic impedance microscopy," Anal. Chem. 88, 1547–1552 (2016).
- 362D. Perry, R. Al Botros, D. Momotenko, S. L. Kinnear, and P. R. Unwin, "Simultaneous nanoscale surface charge and topographical mapping," ACS Nano 9, 7266–7276 (2015).
- ³⁶³P. Saha, J. W. Hill, J. D. Walmsley, and C. M. Hill, "Probing electrocatalysis at individual Au nanorods via correlated optical and electrochemical measurements," Anal. Chem. 90, 12832–12839 (2018).
- 364B. Blount, G. Juarez, Y. Wang, and H. Ren, "IR drop in scanning electrochemical cell microscopy," Faraday Discuss. 233, 149–162 (2022).
- 365K. Gerwert and C. Kötting, Fourier Transform Infrared (FTIR) Spectroscopy (John Wiley & Sons, Ltd, Chichester, UK, 2010).
- 366G. Delen, Z. Ristanović, L. D. B. Mandemaker, and B. M. Weckhuysen, "Mechanistic insights into growth of surface-mounted metal-organic framework films resolved by infrared (nano-) spectroscopy," Chemistry 24, 187–195 (2018).
- 367J. Chae, S. An, G. Ramer, V. Stavila, G. Holland, Y. Yoon, A. A. Talin, M. Allendorf, V. A. Aksyuk, and A. Centrone, "Nanophotonic atomic force microscope transducers enable chemical composition and thermal conductivity measurements at the nanoscale," Nano Lett. 17, 5587–5594 (2017).
- 368Y.-H. Lu, J. M. Larson, A. Baskin, X. Zhao, P. D. Ashby, D. Prendergast, H. A. Bechtel, R. Kostecki, and M. Salmeron, "Infrared nanospectroscopy at the graphene-electrolyte interface," Nano Lett. 19, 5388–5393 (2019).
- 369 Ramer, F. S. Ruggeri, A. Levin, T. P. J. Knowles, and A. Centrone, "Determination of polypeptide conformation with nanoscale resolution in water," ACS Nano 12, 6612–6619 (2018).
- ³⁷⁰M. Jin, F. Lu, and M. A. Belkin, "High-sensitivity infrared vibrational nanospectroscopy in water," Light 6, e17096 (2017).
- 371 J. Abed, F. Alexander, I. Taha, N. Rajput, C. Aubry, and M. Jouiad, "Investigation of broadband surface plasmon resonance of dewetted Au structures on TiO₂ by aperture-probe SNOM and FDTD simulations," Plasmonics 14, 205–218 (2019).
- ³⁷²L. Wang and X. G. Xu, "Scattering-type scanning near-field optical microscopy with reconstruction of vertical interaction," Nat. Commun. 6, 8973 (2015)
- 373 A. Centrone, "Infrared imaging and spectroscopy beyond the diffraction limit," Annu. Rev. Anal. Chem. 8, 101–126 (2015).
- 374 J. M. Atkin, S. Berweger, A. C. Jones, and M. B. Raschke, "Nano-optical imaging and spectroscopy of order, phases, and domains in complex solids," Adv. Phys. 61, 745–842 (2012).
- 375C.-Y. Wu, W. J. Wolf, Y. Levartovsky, H. A. Bechtel, M. C. Martin, F. D. Toste, and E. Gross, "High-spatial-resolution mapping of catalytic reactions on single particles," Nature 541, 511–515 (2017).
- 376S. Dery, S. Kim, D. Haddad, A. Cossaro, A. Verdini, L. Floreano, F. D. Toste, and E. Gross, "Identifying site-dependent reactivity in oxidation reactions on single Pt particles," Chem. Sci. 9, 6523–6531 (2018).
- 377 A. B. C. Mantilla, C.-F. Wang, Y. Gu, Z. D. Schultz, and P. Z. El-Khoury, "Multipolar Raman scattering vs interfacial nanochemistry: Case of 4mercaptopyridine on gold," J. Am. Chem. Soc. 144, 20561–20565 (2022).
- ³⁷⁸B. R. Wood, E. Bailo, M. A. Khiavi, L. Tilley, S. Deed, T. Deckert-Gaudig, D. McNaughton, and V. Deckert, "Tip-enhanced Raman scattering (TERS) from

- hemozoin crystals within a sectioned erythrocyte," Nano Lett. 11, 1868-1873 (2011).
- 379 H. Yin, J.-G. Lan, G. Goubert, Y.-H. Wang, J.-F. Li, and R. Zenobi, "Nanoscale surface redox chemistry triggered by plasmon-generated hot carriers," Small 15, 1903674 (2019).
- 380 M. Yang, M. S. Mattei, C. R. Cherqui, X. Chen, R. P. Van Duyne, and G. C. Schatz, "Tip-enhanced Raman excitation spectroscopy (TERES): Direct spectral characterization of the gap-mode plasmon," Nano Lett. 19, 7309–7316 (2019).
- ³⁸¹R. Zhang, Y. Zhang, Z. C. Dong, S. Jiang, C. Zhang, L. G. Chen, L. Zhang, Y. Liao, J. Aizpurua, Y. Luo, J. L. Yang, and J. G. Hou, "Chemical mapping of a single molecule by plasmon-enhanced Raman scattering," Nature 498, 82–86 (2013).
- 382K. Fiederling, M. Abasifard, M. Richter, V. Deckert, S. Gräfe, and S. Kupfer, "The chemical effect goes resonant—A full quantum mechanical approach on TERS," Nanoscale 12, 6346–6359 (2020).
- 383M. Sun, Z. Zhang, Z. H. Kim, H. Zheng, and H. Xu, "Plasmonic scissors for molecular design," Chemistry 19, 14958–14962 (2013).
- 384 Z. Zhang, S. Sheng, H. Zheng, H. Xu, and M. Sun, "Molecular resonant dissociation of surface-adsorbed molecules by plasmonic nanoscissors," Nanoscale 6, 4903–4908 (2014).
- 385S. Chaunchaiyakul, A. Setiadi, P. Krukowski, F. C. I. Catalan, M. Akai-Kasaya, A. Saito, N. Hayazawa, Y. Kim, H. Osuga, and Y. Kuwahara, "Nanoscale dehydrogenation observed by tip-enhanced Raman spectroscopy," J. Phys. Chem. C 121, 18162–18168 (2017).
- 386T. Schmid, B.-S. Yeo, G. Leong, J. Stadler, and R. Zenobi, "Performing tip-enhanced Raman spectroscopy in liquids," J. Raman Spectrosc. 40, 1392–1399 (2009)
- N. Martín Sabanés, L. M. A. Driessen, and K. F. Domke, "Versatile sideillumination geometry for tip-enhanced Raman spectroscopy at solid/liquid interfaces," Anal. Chem. 88, 7108–7114 (2016).
- ³⁸⁸E. M. van Schrojenstein Lantman, T. Deckert-Gaudig, A. J. G. Mank, V. Deckert, and B. M. Weckhuysen, "Catalytic processes monitored at the nanoscale with tip-enhanced Raman spectroscopy," Nat. Nanotechnol. 7, 583–586 (2012).
- 389P. Kusch, N. Morquillas Azpiazu, N. S. Mueller, S. Mastel, J. I. Pascual, and R. Hillenbrand, "Combined tip-enhanced Raman spectroscopy and scattering-type scanning near-field optical microscopy," J. Phys. Chem. C 122, 16274–16280 (2018).
- 390D. B. Williams and C. B. Carter, Transmission Electron Microscopy: A Textbook for Materials Science, 2nd ed. (Springer, New York, NY, 2009).
- ³⁹¹J. I. Goldstein, D. E. Newbury, J. R. Michael, N. W. M. Ritchie, J. H. J. Scott, and D. C. Joy, "Backscattered electrons," in *Scanning Electron Microscopy and X-Ray Microanalysis* (Springer, New York, NY, 2018), pp. 15–28.
- 392 A. M. Grumezescu and A. Ficai, Nanostructures for Cancer Therapy (Elsevier, Netherlands, 2017).
- 393R. F. Egerton, "Choice of operating voltage for a transmission electron microscope," Ultramicroscopy 145, 85–93 (2014).
- 394D. S. Su, B. Zhang, and R. Schlögl, "Electron microscopy of solid catalyst-s-transforming from a challenge to a toolbox," Chem. Rev. 115, 2818–2882 (2015).
- 395 M. J. Prieto and T. Schmidt, "LEEM and PEEM as probing tools to address questions in catalysis," Catal. Lett. 147, 2487–2497 (2017).
- 396H. Robatjazi, L. Yuan, Y. Yuan, and N. J. Halas, "Heterogeneous plasmonic photocatalysis: Light-driven chemical reactions introduce a new approach to industrially-relevant chemistry," in *Emerging Trends in Chemical Applications of Lasers*, ACS Symposium Series (American Chemical Society, Washington, DC, 2021), Chap. 16, pp. 363–387.
- 397Y. Ning, Q. Fu, Y. Li, S. Zhao, C. Wang, M. Breitschaft, S. Hagen, O. Schaff, and X. Bao, "A near ambient pressure photoemission electron microscope (NAP-PEEM)," Ultramicroscopy 200, 105–110 (2019).
- ³⁹⁸Y. Lu, W.-J. Yin, K.-L. Peng, K. Wang, Q. Hu, A. Selloni, F.-R. Chen, L.-M. Liu, and M.-L. Sui, "Self-hydrogenated shell promoting photocatalytic H₂ evolution on anatase TiO₂," Nat. Commun. 9, 2752 (2018).
- 399D. Zhu, M. Bosman, and J. K. W. Yang, "A circuit model for plasmonic resonators," Opt. Express 22, 9809–9819 (2014).

- 400G. Baffou, R. Quidant, and C. Girard, "Heat generation in plasmonic nanostructures: Influence of morphology," Appl. Phys. Lett. 94, 153109 (2009).
- 401 R. S. Weatherup, A. J. Shahani, Z.-J. Wang, K. Mingard, A. J. Pollard, M.-G. Willinger, R. Schloegl, P. W. Voorhees, and S. Hofmann, "In situ graphene growth dynamics on polycrystalline catalyst foils," Nano Lett. 16, 6196–6206 (2016).
- 402Z.-J. Wang, G. Weinberg, Q. Zhang, T. Lunkenbein, A. Klein-Hoffmann, M. Kurnatowska, M. Plodinec, Q. Li, L. Chi, R. Schloegl, and M.-G. Willinger, "Direct observation of graphene growth and associated copper substrate dynamics by in situ scanning electron microscopy," ACS Nano 9, 1506–1519 (2015).
- 403X. Huang, Z.-J. Wang, G. Weinberg, X.-M. Meng, and M.-G. Willinger, "In situ scanning electron microscopy observation of growth kinetics and catalyst splitting in vapor-liquid-solid growth of nanowires," Adv. Funct. Mater. 25, 5979–5987 (2015).
- 404K. Takahashi, K. Yamada, H. Kato, H. Hibino, and Y. Homma, "In situ scanning electron microscopy of graphene growth on polycrystalline ni substrate," Surf. Sci. 606, 728–732 (2012).
- 405 M. R. Hauwiller, J. C. Ondry, C. M. Chan, P. Khandekar, J. Yu, and A. P. Alivisatos, "Gold nanocrystal etching as a means of probing the dynamic chemical environment in graphene liquid cell electron microscopy," J. Am. Chem. Soc. 141, 4428–4437 (2019).
- 406M. Li, M. T. Curnan, M. A. Gresh-Sill, S. D. House, W. A. Saidi, and J. C. Yang, "Unusual layer-by-layer growth of epitaxial oxide islands during Cu oxidation," Nat. Commun. 12, 2781 (2021).
- 407H.-G. Liao, D. Zherebetskyy, H. Xin, C. Czarnik, P. Ercius, H. Elmlund, M. Pan, L.-W. Wang, and H. Zheng, "Nanoparticle growth. Facet development during platinum nanocube growth," Science 345, 916–919 (2014).
- 408 W. Zheng, M. R. Hauwiller, W.-I. Liang, C. Ophus, P. Ercius, E. M. Chan, Y.-H. Chu, M. Asta, X. Du, A. P. Alivisatos, and H. Zheng, "Real time imaging of two-dimensional iron oxide spherulite nanostructure formation," Nano Res. 12, 2889–2893 (2019).
- 409X. Ye, M. R. Jones, L. B. Frechette, Q. Chen, A. S. Powers, P. Ercius, G. Dunn, G. M. Rotskoff, S. C. Nguyen, V. P. Adiga, A. Zettl, E. Rabani, P. L. Geissler, and A. P. Alivisatos, "Single-particle mapping of nonequilibrium nanocrystal transformations," Science 354, 874–877 (2016).
- 410 M. R. Hauwiller, L. B. Frechette, M. R. Jones, J. C. Ondry, G. M. Rotskoff, P. Geissler, and A. P. Alivisatos, "Unraveling kinetically-driven mechanisms of gold nanocrystal shape transformations using graphene liquid cell electron microscopy," Nano Lett. 18, 5731–5737 (2018).
- ⁴¹¹T. Ghosh, J. M. Arce-Ramos, W.-Q. Li, H. Yan, S. W. Chee, A. Genest, and U. Mirsaidov, "Periodic structural changes in Pd nanoparticles during oscillatory CO oxidation reaction," Nat. Commun. 13, 6176 (2022).
- 412 A. M. Gänzler, M. Casapu, P. Vernoux, S. Loridant, F. J. Cadete Santos Aires, T. Epicier, B. Betz, R. Hoyer, and J.-D. Grunwaldt, "Tuning the structure of platinum particles on ceria *in situ* for enhancing the catalytic performance of exhaust gas catalysts." Angew. Chem. Int. Ed. Engl. 56, 13078–13082 (2017).
- exhaust gas catalysts," Angew. Chem., Int. Ed, Engl. 56, 13078–13082 (2017). 413 Y. He, J.-C. Liu, L. Luo, Y.-G. Wang, J. Zhu, Y. Du, J. Li, S. X. Mao, and C. Wang, "Size-dependent dynamic structures of supported gold nanoparticles in CO oxidation reaction condition," Proc. Natl. Acad. Sci. U. S. A. 115, 7700–7705 (2018).
- 414M. Tang, W. Yuan, Y. Ou, G. Li, R. You, S. Li, H. Yang, Z. Zhang, and Y. Wang, "Recent progresses on structural reconstruction of nanosized metal catalysts via controlled-atmosphere transmission electron microscopy: A review," ACS Catal. 10, 14419–14450 (2020).
- 415 T. W. Hansen and J. B. Wagner, "Catalysts under controlled atmospheres in the transmission electron microscope," ACS Catal. 4, 1673–1685 (2014).
- 416 B. He, Y. Zhang, X. Liu, and L. Chen, "In-situ transmission electron microscope techniques for heterogeneous catalysis," ChemCatChem 12, 1853–1872 (2020).
- 417T. C. Narayan, F. Hayee, A. Baldi, A. Leen Koh, R. Sinclair, and J. A. Dionne, "Direct visualization of hydrogen absorption dynamics in individual palladium nanoparticles," Nat. Commun. 8, 14020 (2017).
- 418D. K. Angell, B. Bourgeois, M. Vadai, and J. A. Dionne, "Lattice-resolution, dynamic imaging of hydrogen absorption into bimetallic AgPd nanoparticles," ACS Nano 16, 1781–1790 (2022).

- 419 D. F. Swearer, B. B. Bourgeois, D. K. Angell, and J. A. Dionne, "Advancing plasmon-induced selectivity in chemical transformations with optically coupled transmission electron microscopy," Acc. Chem. Res. 54, 3632–3642 (2021).
- ⁴²⁰P. Sutter, Y. Li, C. Argyropoulos, and E. Sutter, "In situ electron microscopy of plasmon-mediated nanocrystal synthesis," J. Am. Chem. Soc. 139, 6771–6776 (2017).
- 421B. Weng, Y. Jiang, H.-G. Liao, M. B. J. Roeffaers, F. Lai, H. Huang, and Z. Tang, "Visualizing light-induced dynamic structural transformations of Au clusters-based photocatalyst via in situ TEM," Nano Res. 14, 2805–2809 (2021).
- 422R. F. Egerton, Electron Energy-Loss Spectroscopy in the Electron Microscope (Springer US, Boston, MA, 2011).
- 423 R. Egerton, Physical Principles of Electron Microscopy (Springer International Publishing, Cham, 2016).
- 424°C. J. Wrasman, A. R. Riscoe, H. Lee, and M. Cargnello, "Dilute Pd/Au alloys replace Au/TiO₂ interface for selective oxidation reactions," ACS Catal. 10, 1716–1720 (2020).
- 425 K. Suenaga and M. Koshino, "Atom-by-atom spectroscopy at graphene edge," Nature 468, 1088–1090 (2010).
- ⁴²⁶M. J. Lagos, I. C. Bicket, S. S. Mousavi M, and G. A. Botton, "Advances in ultrahigh-energy resolution EELS: Phonons, infrared plasmons and strongly coupled modes," <u>Microscopy</u> 71, i174–i199 (2022).
- 427Y. Wu, Z. Hu, X.-T. Kong, J. C. Idrobo, A. G. Nixon, P. D. Rack, D. J. Masiello, and J. P. Camden, "Infrared plasmonics: STEM-EELS characterization of Fabry-Pérot resonance damping in gold nanowires," Phys. Rev. B 101, 085409 (2020).
- 428 V. Mkhitaryan, K. March, E. N. Tseng, X. Li, L. Scarabelli, L. M. Liz-Marzán, S.-Y. Chen, L. H. G. Tizei, O. Stéphan, J.-M. Song, M. Kociak, F. J. García de Abajo, and A. Gloter, "Can copper nanostructures sustain high-quality plasmons?," Nano Lett. 21, 2444–2452 (2021).
- 429 A. Baldi, T. C. Narayan, A. L. Koh, and J. A. Dionne, "In situ detection of hydrogen-induced phase transitions in individual palladium nanocrystals," Nat. Mater. 13, 1143–1148 (2014).
- ⁴³⁰J. Miao, P. Ercius, and S. J. L. Billinge, "Atomic electron tomography: 3D structures without crystals," Science 353, aaf2157 (2016).
- 431 J. Zhou, Y. Yang, Y. Yang, D. S. Kim, A. Yuan, X. Tian, C. Ophus, F. Sun, A. K. Schmid, M. Nathanson, H. Heinz, Q. An, H. Zeng, P. Ercius, and J. Miao, "Observing crystal nucleation in four dimensions using atomic electron tomography," Nature 570, 500–503 (2019).
- 432W. Albrecht and S. Bals, "Fast electron tomography for nanomaterials," J. Phys. Chem. C 124, 27276–27286 (2020).
- 433A. Suzuta, K. Yamazaki, K. Gohara, and T. Uchida, "In situ observation of the motion of platinum and gold single atoms on graphene using aberration-corrected electron microscopy," J. Phys. Chem. C 126, 12780-12789 (2022).
- 434M. Picher, S. Mazzucco, S. Blankenship, and R. Sharma, "Vibrational and optical spectroscopies integrated with environmental transmission electron microscopy," Ultramicroscopy 150, 10–15 (2015).
- 435 F. I. Allen, E. Kim, N. C. Andresen, C. P. Grigoropoulos, and A. M. Minor, "In situ TEM Raman spectroscopy and laser-based materials modification," Ultramicroscopy 178, 33–37 (2017).
- 436 A. A. E. Saleh, D. K. Angell, and J. A. Dionne, "Electron- and light-induced stimulated Raman spectroscopy for nanoscale molecular mapping," Phys. Rev. B 102, 085406 (2020).
- 437Y. Ohno, "Development of an apparatus for *in-situ* near-field photoexcitation in a transmission electron microscope," Appl. Phys. Express 5, 125204 (2012).
- 438P. Haluai, M. R. McCartney, and P. A. Crozier, "Detection of adsorbates induced changes on Pt/CeO₂ catalyst using *in situ* electron holography," Microsc. Microanal. 28, 1906–1907 (2022).
- 439J. AE. Hyllested and M. Beleggia, "Investigation of gas-electron interactions with electron holography," Ultramicroscopy 221, 113178 (2021).
- ⁴⁴⁰M. J. Zachman, V. Fung, F. Polo-Garzon, S. Cao, J. Moon, Z. Huang, D.-E. Jiang, Z. Wu, and M. Chi, "Measuring and directing charge transfer in heterogenous catalysts," Nat. Commun. 13, 3253 (2022).
- 441 M. Mavrikakis, B. Hammer, and J. K. Nùrskov, "Effect of strain on the reactivity of metal surfaces," Phys. Rev. Lett. 81, 2819–2822 (1998).

- ⁴⁴²J. R. Kitchin, J. K. Nùrskov, M. A. Barteau, and J. G. Chen, "Role of strain and ligand effects in the modification of the electronic and chemical properties of bimetallic surfaces," Phys. Rev. Lett. 93, 156801 (2004).
- 443B. K. Miller and P. A. Crozier, "Analysis of catalytic gas products using electron energy-loss spectroscopy and residual gas analysis for *operando* transmission electron microscopy," Microsc. Microanal. 20, 815–824 (2014).
- 4444S. Chenna and P. A. Crozier, "Operando transmission electron microscopy: A technique for detection of catalysis using electron energy-loss spectroscopy in the transmission electron microscope," ACS Catal. 2, 2395–2402 (2012).
- 445 FEI, Titan ETEM G2 Datasheet (FEI, 2012).
- 446 L. Zhang, B. K. Miller, and P. A. Crozier, "Atomic level in situ observation of surface amorphization in anatase nanocrystals during light irradiation in water vapor," Nano Lett. 13, 679–684 (2013).
- 447J. B. Wagner, F. Cavalca, C. D. Damsgaard, L. D. L. Duchstein, and T. W. Hansen, "Exploring the environmental transmission electron microscope," Micron 43, 1169–1175 (2012).
- ⁴⁴⁸F. Cavalca, A. B. Laursen, B. E. Kardynal, R. E. Dunin-Borkowski, S. Dahl, J. B. Wagner, and T. W. Hansen, "In situ transmission electron microscopy of light-induced photocatalytic reactions," Nanotechnology 23, 075705 (2012).
- 449W.-C. D. Yang, C. Wang, L. A. Fredin, P. A. Lin, L. Shimomoto, H. J. Lezec, and R. Sharma, "Site-selective CO disproportionation mediated by localized surface plasmon resonance excited by electron beam," Nat. Mater. 18, 614–619 (2019).
- 450S. Sharna, M. Bahri, C. Bouillet, V. Rouchon, A. Lambert, A.-S. Gay, D. Chiche, and O. Ersen, "STEM study on the morphological evolution of copper-based nanoparticles during high-temperature redox reactions," Nanoscale 13, 9747–9756 (2021).
- 451 F. Ye, M. Xu, S. Dai, P. Tieu, X. Ren, and X. Pan, "In situ TEM studies of catalysts using windowed gas cells," Catalysts 10, 779 (2020).
- 452H.-G. Liao and H. Zheng, "Liquid cell transmission electron microscopy," Annu. Rev. Phys. Chem. 67, 719–747 (2016).
- 453 A. M. Żak, "Light-induced in situ transmission electron microscopy— Development, challenges, and perspectives," Nano Lett. 22, 9219–9226 (2022).
- 454 H. Dong, F. Xu, Z. Sun, X. Wu, Q. Zhang, Y. Zhai, X. D. Tan, L. He, T. Xu, Z. Zhang, X. Duan, and L. Sun, "*In situ* interface engineering for probing the limit of quantum dot photovoltaic devices," Nat. Nanotechnol. 14, 950–956 (2019)
- 455P. Gao, Z. Z. Wang, K. H. Liu, Z. Xu, W. L. Wang, X. D. Bai, and E. G. Wang, "Photoconducting response on bending of individual ZnO nanowires," J. Mater. Chem. 19, 1002–1005 (2009).
- 456S. Kadkhodazadeh, F. C. Cavalca, B. J. Miller, L. Zhang, J. B. Wagner, P. A. Crozier, and T. W. Hansen, "In situ TEM under optical excitation for catalysis research," Top. Curr. Chem. 380, 52 (2022).
- 457J. Martis, Z. Zhang, H. Li, A. Majumdar, R. Kim, and A. Marshall, "Design and construction of an optical TEM specimen holder," Microsc. Microanal. 27, 2310–2312 (2021).
- 458 M. L. Taheri, E. A. Stach, I. Arslan, P. A. Crozier, B. C. Kabius, T. LaGrange, A. M. Minor, S. Takeda, M. Tanase, J. B. Wagner, and R. Sharma, "Current status and future directions for in situ transmission electron microscopy," Ultramicroscopy 170, 86–95 (2016).
- 459E. Ortega, D. Nicholls, N. D. Browning, and N. de Jonge, "High temporalresolution scanning transmission electron microscopy using sparse-serpentine scan pathways," Sci. Rep. 11, 22722 (2021).
- 460 Z. Zhang, C. Zhang, H. Zheng, and H. Xu, "Plasmon-driven catalysis on molecules and nanomaterials," Acc. Chem. Res. 52, 2506–2515 (2019).
- 461T. J. Miao and J. Tang, "Characterization of charge carrier behavior in photocatalysis using transient absorption spectroscopy," J. Chem. Phys. 152, 194201 (2020).
- 462Q. Ding, Y. Shi, M. Chen, H. Li, X. Yang, Y. Qu, W. Liang, and M. Sun, "Ultrafast dynamics of plasmon-exciton interaction of Ag nanowire-graphene hybrids for surface catalytic reactions," Sci. Rep. 6, 32724 (2016).
- 463G. F. Ferbonink, T. S. Rodrigues, D. P. Dos Santos, P. H. C. Camargo, R. Q. Albuquerque, and R. A. Nome, "Correlating structural dynamics and catalytic activity of AgAu nanoparticles with ultrafast spectroscopy and all-atom molecular dynamics simulations," Faraday Discuss. 208, 269–286 (2018).

- 464S. Sim, A. Beierle, P. Mantos, S. McCrory, R. P. Prasankumar, and S. Chowdhury, "Ultrafast relaxation dynamics in bimetallic plasmonic catalysts," Nanoscale 12, 10284–10291 (2020).
- 465X. Zhang, Y. Fan, E. You, Z. Li, Y. Dong, L. Chen, Y. Yang, Z. Xie, Q. Kuang, and L. Zheng, "MOF encapsulated sub-nm Pd skin/Au nanoparticles as antenna-reactor plasmonic catalyst for light driven CO₂ hydrogenation," Nano Energy 84, 105950 (2021).
- 466 J. S. Pelli Cresi, E. Principi, E. Spurio, D. Catone, P. O'Keeffe, S. Turchini, S. Benedetti, A. Vikatakavi, S. D'Addato, R. Mincigrucci, L. Foglia, G. Kurdi, I. P. Nikolov, G. De Ninno, C. Masciovecchio, S. Nannarone, J. Kopula Kesavan, F. Boscherini, and P. Luches, "Ultrafast dynamics of plasmon-mediated charge transfer in Ag@CeO studied by free electron laser time-resolved x-ray absorption spectroscopy," Nano Lett. 21, 1729–1734 (2021).
- 467 M. Lee, X-Ray Diffraction for Materials Research: From Fundamentals to Applications (Apple Academic Press, Ontario, 2017).
- 468 E. Lifshin, X-Ray Characterization of Materials (John Wiley & Sons, 2008).
- 469B. B. Sarma, F. Maurer, D. E. Doronkin, and J.-D. Grunwaldt, "Design of single-atom catalysts and tracking their fate using *operando* and advanced x-ray spectroscopic tools," Chem. Rev. 123, 379–444 (2023).
- 470°C. J. Wrasman, A. Boubnov, A. R. Riscoe, A. S. Hoffman, S. R. Bare, and M. Cargnello, "Synthesis of colloidal Pd/Au dilute alloy nanocrystals and their potential for selective catalytic oxidations," J. Am. Chem. Soc. 140, 12930–12939 (2018).
- 471 L. Wang, H. Peng, S. Lamaison, Z. Qi, D. M. Koshy, M. B. Stevens, D. Wakerley, J. A. Zamora Zeledón, L. A. King, L. Zhou, Y. Lai, M. Fontecave, J. Gregoire, F. Abild-Pedersen, T. F. Jaramillo, and C. Hahn, "Bimetallic effects on Zn-Cu electrocatalysts enhance activity and selectivity for the conversion of CO₂ to CO," Chem Catal. 1, 663–680 (2021).
- 472 Q. Wu, L. D. L. Duchstein, G. L. Chiarello, J. M. Christensen, C. D. Damsgaard, C. F. Elkjaer, J. B. Wagner, B. Temel, J.-D. Grunwaldt, and A. D. Jensen, "In situ observation of Cu-Ni alloy nanoparticle formation by x-ray diffraction, x-ray absorption spectroscopy, and transmission electron microscopy: Influence of Cu/Ni ratio," ChemCatChem 6, 301–310 (2014).
- ⁴⁷³C. Yu, S. Koh, J. E. Leisch, M. F. Toney, and P. Strasser, "Size and composition distribution dynamics of alloy nanoparticle electrocatalysts probed by anomalous small angle x-ray scattering (ASAXS)," Faraday Discuss. 140, 283–296 (2008).
- 474F. Zhang, P. Wang, J. Koberstein, S. Khalid, and S.-W. Chan, "Cerium oxidation state in ceria nanoparticles studied with x-ray photoelectron spectroscopy and absorption near edge spectroscopy," Surf. Sci. 563, 74–82 (2004).
- 475F. Zheng, S. Alayoglu, J. Guo, V. Pushkarev, Y. Li, P.-A. Glans, J.-L. Chen, and G. Somorjai, "In-situ x-ray absorption study of evolution of oxidation states and structure of cobalt in Co and CoPt bimetallic nanoparticles (4 nm) under reducing (H₂) and oxidizing (O₂) environments," Nano Lett. 11, 847–853 (2011).
- 476Y.-S. Liu, X. Feng, P.-A. Glans, and J. Guo, "In situ/operando soft x-ray spectroscopy characterization of energy and catalytic materials," Sol. Energy Mater. Sol. Cells 208, 110432 (2020).
- 477 B. Gilbert, C. Frandsen, E. R. Maxey, and D. M. Sherman, "Band-gap measurements of bulk and nanoscale hematite by soft x-ray spectroscopy," Phys. Rev. B 79, 035108 (2009).
- 478K. Asakura, K. J. Gaffney, C. Milne, and M. Yabashi, "XFELs: Cutting edge x-ray light for chemical and material sciences," Phys. Chem. Chem. Phys. 22, 2612–2614 (2020).
- 479 A. S. M. Ismail, Y. Uemura, S. H. Park, S. Kwon, M. Kim, H. Elnaggar, F. Frati, Y. Niwa, H. Wadati, Y. Hirata, Y. Zhang, K. Yamagami, S. Yamamoto, I. Matsuda, U. Halisdemir, G. Koster, B. M. Weckhuysen, and F. M. F. de Groot, "Direct observation of the electronic states of photoexcited hematite with ultrafast 2p3d x-ray absorption spectroscopy and resonant inelastic x-ray scattering," Phys. Chem. Chem. Phys. 22, 2685–2692 (2020).
- ⁴⁸⁰S. Bordiga, E. Groppo, G. Agostini, J. A. van Bokhoven, and C. Lamberti, "Reactivity of surface species in heterogeneous catalysts probed by *in situ* x-ray absorption techniques," Chem. Rev. 113, 1736–1850 (2013).
- 481A. I. Frenkel, "Applications of extended x-ray absorption fine-structure spectroscopy to studies of bimetallic nanoparticle catalysts," Chem. Soc. Rev. 41, 8163–8178 (2012).

- 482Y. Zhou, D. E. Doronkin, Z. Zhao, P. N. Plessow, J. Jelic, B. Detlefs, T. Pruessmann, F. Studt, and J.-D. Grunwaldt, "Photothermal catalysis over non-plasmonic Pt/TiO₂ studied by operando HERFD-XANES, resonant XES, and DRIFTS," ACS Catal. 8, 11398–11406 (2018).
- 483 J. B. Priebe, J. Radnik, A. J. J. Lennox, M.-M. Pohl, M. Karnahl, D. Hollmann, K. Grabow, U. Bentrup, H. Junge, M. Beller, and A. Brückner, "Solar hydrogen production by plasmonic Au–TiO₂ catalysts: Impact of synthesis protocol and TiO₂ phase on charge transfer efficiency and H₂ evolution rates," ACS Catal. 5, 2137–2148 (2015).
- 484 T. Peng, J. Miao, Z. Gao, L. Zhang, Y. Gao, C. Fan, and D. Li, "Reactivating catalytic surface: Insights into the role of hot holes in plasmonic catalysis," Small 14, e1703510 (2018).
- 485 C. S. Ponseca, Jr., P. Chábera, J. Uhlig, P. Persson, and V. Sundström, "Ultrafast electron dynamics in solar energy conversion," Chem. Rev. 117, 10940–11024 (2017).
- 486S. H. Park, A. Katoch, K. H. Chae, S. Gautam, P. Miedema, S. W. Cho, M. Kim, R.-P. Wang, M. Lazemi, F. de Groot, and S. Kwon, "Direct and real-time observation of hole transport dynamics in anatase TiO₂ using x-ray free-electron laser," Nat. Commun. 13, 2531 (2022).
- 487 Y. Obara, H. Ito, T. Ito, N. Kurahashi, S. Thürmer, H. Tanaka, T. Katayama, T. Togashi, S. Owada, Y.-I. Yamamoto, S. Karashima, J. Nishitani, M. Yabashi, T. Suzuki, and K. Misawa, "Femtosecond time-resolved x-ray absorption spectroscopy of anatase TiO₂ nanoparticles using XFEL," Struct. Dyn. 4, 044033 (2017).
- 488 A. R. Ziefuss, S. Reich, S. Reichenberger, M. Levantino, and A. Plech, "In situ structural kinetics of picosecond laser-induced heating and fragmentation of colloidal gold spheres," Phys. Chem. Chem. Phys. 22, 4993–5001 (2020).
- 489 A. Plech, S. Ibrahimkutty, S. Reich, and G. Newby, "Thermal dynamics of pulsed-laser excited gold nanorods in suspension," Nanoscale 9, 17284–17292 (2017).
- 490 A. Plech, A. R. Ziefuß, M. Levantino, R. Streubel, S. Reich, and S. Reichenberger, "Low efficiency of laser heating of gold particles at the plasmon resonance: An x-ray calorimetry study," ACS Photonics 9, 2981–2990 (2022).
- ⁴⁹¹S. H. Park, M. Kim, C.-K. Min, I. Eom, I. Nam, H.-S. Lee, H.-S. Kang, H.-D. Kim, H. Y. Jang, S. Kim, S.-M. Hwang, G.-S. Park, J. Park, T.-Y. Koo, and S. Kwon, "PAL-XFEL soft x-ray scientific instruments and x-ray optics: First commissioning results," Rev. Sci. Instrum. 89, 055105 (2018).
- 492 N. Fischer and M. Claeys, "Phase changes studied under in situ conditions—A novel cell," Catal. Today 275, 149–154 (2016).
- 493 T. Huthwelker, V. Zelenay, M. Birrer, A. Krepelova, J. Raabe, G. Tzvetkov, M. G. C. Vernooij, and M. Ammann, "An in situ cell to study phase transitions in individual aerosol particles on a substrate using scanning transmission x-ray microspectroscopy," Rev. Sci. Instrum. 81, 113706 (2010).
- 494 T. Binninger, E. Fabbri, A. Patru, M. Garganourakis, J. Han, D. F. Abbott, O. Sereda, R. Kötz, A. Menzel, M. Nachtegaal, and T. J. Schmidt, "Electrochemical flow-cell setup for in situ x-ray investigations," J. Electrochem. Soc. 163, H906 (2016).
- ⁴⁹⁵D. E. Doronkin, H. Lichtenberg, and J.-D. Grunwaldt, "Cell designs for in situ and operando studies," in XAFS Techniques for Catalysts, Nanomaterials, and Surfaces, edited by Y. Iwasawa, K. Asakura, and T. Mizuki (Springer Nature, Switzerland, 2017), Chap. 6, pp. 75–89.
- 496 J. Feng, M. Kriechbaum, and L. e Liu, "In situ capabilities of small angle x-ray scattering," Nanotechnol. Rev. 8, 352–369 (2019).
- 497E. L. Keller and R. R. Frontiera, "Ultrafast nanoscale Raman thermometry proves heating is not a primary mechanism for plasmon-driven photocatalysis," ACS Nano 12, 5848–5855 (2018).
- 498 Y.-J. Kim, H. Jung, S. W. Han, and O.-H. Kwon, "Ultrafast electron microscopy visualizes acoustic vibrations of plasmonic nanorods at the interfaces," Matter 1, 481–495 (2019).
- 499S. A. Lee, C. T. Kuhs, E. K. Searles, H. O. Everitt, C. F. Landes, and S. Link, "d-Band hole dynamics in gold nanoparticles measured with time-resolved emission upconversion microscopy," Nano Lett. 23(8), 3501–3506 (2023).
- 500 M. Delor, H. L. Weaver, Q. Yu, and N. S. Ginsberg, "Imaging material functionality through three-dimensional nanoscale tracking of energy flow," Nat. Mater. 19, 56–62 (2020).

- ⁵⁰¹K. Yu, P. Zijlstra, J. E. Sader, Q.-H. Xu, and M. Orrit, "Damping of acoustic vibrations of immobilized single gold nanorods in different environments," Nano Lett. 13, 2710–2716 (2013).
- 502G. Grancini, M. Biasiucci, R. Mastria, F. Scotognella, F. Tassone, D. Polli, G. Gigli, and G. Lanzani, "Dynamic microscopy study of ultrafast charge transfer in a hybrid P3HT/Hyperbranched CdSe nanoparticle blend for photovoltaics," J. Phys. Chem. Lett. 3, 517–523 (2012).
- 503 M.-N. Su, C. J. Ciccarino, S. Kumar, P. D. Dongare, S. A. Hosseini Jebeli, D. Renard, Y. Zhang, B. Ostovar, W.-S. Chang, P. Nordlander, N. J. Halas, R. Sundararaman, P. Narang, and S. Link, "Ultrafast electron dynamics in single aluminum nanostructures," Nano Lett. 19, 3091–3097 (2019).
- 504 J. Sung, C. Schnedermann, L. Ni, A. Sadhanala, R. Y. S. Chen, C. Cho, L. Priest, J. M. Lim, H.-K. Kim, B. Monserrat, P. Kukura, and A. Rao, "Longrange ballistic propagation of carriers in methylammonium lead iodide perovskite thin films," Nat. Phys. 16, 171–176 (2020).
- 505 E. M. Grumstrup, M. M. Gabriel, E. E. M. Cating, E. M. Van Goethem, and J. M. Papanikolas, "Pump-probe microscopy: Visualization and spectroscopy of ultrafast dynamics at the nanoscale," Chem. Phys. 458, 30–40 (2015).
- 506H. Zhang, W. Li, J. Essman, C. Quarti, I. Metcalf, W.-Y. Chiang, S. Sidhik, J. Hou, A. Fehr, A. Attar, M.-F. Lin, A. Britz, X. Shen, S. Link, X. Wang, U. Bergmann, M. G. Kanatzidis, C. Katan, J. Even, J.-C. Blancon, and A. D. Mohite, "Ultrafast relaxation of lattice distortion in two-dimensional perovskites," Nat. Phys. 19, 545–550 (2023).
- 507 D. W. McCamant, P. Kukura, and R. A. Mathies, "Femtosecond time-resolved stimulated Raman spectroscopy: Application to the ultrafast internal conversion in beta-carotene," J. Phys. Chem. A 107, 8208–8214 (2003).
- 508 J. L. Brooks, D. V. Chulhai, Z. Yu, J. D. Goodpaster, and R. R. Frontiera, "Plasmon-driven C-N bond cleavage across a series of viologen derivatives," J. Phys. Chem. C 123, 29306–29313 (2019).
- 509Y. Luo, A. Martin-Jimenez, R. Gutzler, M. Garg, and K. Kern, "Ultrashort pulse excited tip-enhanced Raman spectroscopy in molecules," Nano Lett. 22, 5100–5106 (2022).
- 510 J. M. Klingsporn, M. D. Sonntag, T. Seideman, and R. P. Van Duyne, "Tip-enhanced Raman spectroscopy with picosecond pulses," J. Phys. Chem. Lett. 5, 106–110 (2014).
- 511 E. A. Pozzi, M. D. Sonntag, N. Jiang, N. Chiang, T. Seideman, M. C. Hersam, and R. P. Van Duyne, "Ultrahigh vacuum tip-enhanced Raman spectroscopy with picosecond excitation," J. Phys. Chem. Lett. 5, 2657–2661 (2014).
- 512K. Furusawa, N. Hayazawa, F. C. Catalan, T. Okamoto, and S. Kawata, "Tipenhanced broadband CARS spectroscopy and imaging using a photonic crystal fiber based broadband light source," J. Raman Spectrosc. 43, 656-661 (2012).
- 513 L. E. Dresselhaus-Marais, B. Kozioziemski, T. S. Holstad, T. M. Raeder, M. Seaberg, D. Nam, S. Kim, S. Breckling, M. Chollet, P. K. Cook, E. Folsom, E. Galtier, L. Gavilan, A. Gonzalez, T. Gorhover, S. Guillet, K. Haldrup, M. Howard, K. Katagiri, S. Kim, S. Kim, S. Kim, H. Kim, E. B. Knudsen, S. Kuschel, H.-J. Lee, C. Lin, R. S. McWilliams, B. Nagler, N. Ozaki, D. Pal, R. P. Pedro, M. M. Nielsen, A. M. Saunders, F. Schoofs, T. Sekine, H. Simons, T. van Driel, B. Wang, W. Yang, C. Yildirim, H. F. Poulsen, and J. H. Eggert, "Simultaneous bright- and dark-field x-ray microscopy at x-ray free electron lasers," Sci. Rep. 13, 17573 (2023).
- 514 A. T. Macrander and X. Huang, "Synchrotron x-ray optics," Annu. Rev. Mater. Res. 47, 135–152 (2017).
- 515B. Rösner, F. Koch, F. Döring, V. A. Guzenko, M. Meyer, J. L. Ornelas, A. Späth, R. H. Fink, S. Stanescu, S. Swaraj, R. Belkhou, B. Watts, J. Raabe, and C. David, "7 nm spatial resolution in soft x-ray microscopy," Microsc. Microanal. 24, 272–273 (2018).
- 516H. Wen, M. J. Cherukara, and M. V. Holt, "Time-resolved x-ray microscopy for materials science," Annu. Rev. Mater. Res. 49, 389–415 (2019).
- 517S. Baier, C. D. Damsgaard, M. Scholz, F. Benzi, A. Rochet, R. Hoppe, T. Scherer, J. Shi, A. Wittstock, B. Weinhausen, J. B. Wagner, C. G. Schroer, and J.-D. Grunwaldt, "In situ ptychography of heterogeneous catalysts using hard x-rays: High resolution imaging at ambient pressure and elevated temperature," Microsc. Microanal. 22, 178–188 (2016).
- 518Y. Zhu, Z. Cai, P. Chen, Q. Zhang, M. J. Highland, I. W. Jung, D. A. Walko, E. M. Dufresne, J. Jeong, M. G. Samant, S. S. P. Parkin, J. W. Freeland, P. G. Evans, and H. Wen, "Mesoscopic structural phase progression in

- photo-excited VO_2 revealed by time-resolved x-ray diffraction microscopy," Sci. Rep. 6, 21999 (2016).
- 519 T. D. Frazer, Y. Zhu, Z. Cai, D. A. Walko, C. Adamo, D. G. Schlom, E. E. Fullerton, P. G. Evans, S. O. Hruszkewycz, Y. Cao, and H. Wen, "Optical transient grating pumped x-ray diffraction microscopy for studying mesoscale structural dynamics," Sci. Rep. 11, 19322 (2021).
- 520 K. Gerlinger, B. Pfau, M. Hennecke, L.-M. Kern, I. Will, T. Noll, M. Weigand, J. Gräfe, N. Träger, M. Schneider, C. M. Günther, D. Engel, G. Schütz, and S. Eisebitt, "Pump-probe x-ray microscopy of photo-induced magnetization dynamics at MHz repetition rates," Struct. Dyn. 10, 024301 (2023).
- 521M. J. Rost, L. Crama, P. Schakel, E. van Tol, G. B. E. M. van Velzen-Williams, C. F. Overgauw, H. ter Horst, H. Dekker, B. Okhuijsen, M. Seynen, A. Vijftigschild, P. Han, A. J. Katan, K. Schoots, R. Schumm, W. van Loo, T. H. Oosterkamp, and J. W. M. Frenken, "Scanning probe microscopes go video rate and beyond," Rev. Sci. Instrum. 76, 053710 (2005).
- 522X. R. Qin, B. S. Swartzentruber, and M. G. Lagally, "Diffusional kinetics of SiGe dimers on Si(100) using atom-tracking scanning tunneling microscopy," Phys. Rev. Lett. 85, 3660–3663 (2000).
- 523Y. E. Tian, F. Yang, C. Guo, and Y. Jiang, "Recent advances in ultrafast timeresolved scanning tunneling microscopy," Surf. Rev. Lett. 25, 1841003 (2018).
- 524S. Loth, M. Etzkorn, C. P. Lutz, D. M. Eigler, and A. J. Heinrich, "Measurement of fast electron spin relaxation times with atomic resolution," Science 329, 1628–1630 (2010).
- 525D. A. Yarotski, R. D. Averitt, N. Negre, S. A. Crooker, A. J. Taylor, G. P. Donati, A. Stintz, L. F. Lester, and K. J. Malloy, "Ultrafast carrier-relaxation dynamics in self-assembled InAs/GaAs quantum dots," J. Opt. Soc. Am. B 19, 1480 (2002)
- 526Y. Terada, S. Yoshida, O. Takeuchi, and H. Shigekawa, "Real-space imaging of transient carrier dynamics by nanoscale pump-probe microscopy," Nat. Photonics 4, 869-874 (2010).
- 527 T. L. Cocker, V. Jelic, M. Gupta, S. J. Molesky, J. A. J. Burgess, G. De Los Reyes, L. V. Titova, Y. Y. Tsui, M. R. Freeman, and F. A. Hegmann, "An ultrafast terahertz scanning tunnelling microscope," Nat. Photonics 7, 620–625 (2013).
- 528 L. Bartels, F. Wang, D. Möller, E. Knoesel, and T. F. Heinz, "Real-space observation of molecular motion induced by femtosecond laser pulses," Science 305, 648–651 (2004).
- 529 A. Taninaka, S. Yoshida, Y. Sugita, O. Takeuchi, and H. Shigekawa, "Evolution of local conductance pathways in a single-molecule junction studied using the three-dimensional dynamic probe method," Nanoscale 11, 5951–5959 (2019).
- 530 A. Arbouet, G. M. Caruso, and F. Houdellier, Ultrafast Transmission Electron Microscopy: Historical Development, Instrumentation, and Applications (Elsevier, 2018), Chap. 1, pp. 1–72.
- 531 Gatan, K3 Direct Detection Cameras Datasheet (Gatan, 2021).
- ⁵³²E. Montgomery, D. Leonhardt, and J. Roehling, "Ultrafast transmission electron microscopy: Techniques and applications," Micros. Today 29, 46–54 (2021).
- 533D.-S. Yang, O. F. Mohammed, and A. H. Zewail, "Environmental scanning ultrafast electron microscopy: Structural dynamics of solvation at interfaces," Angew. Chem., Int. Ed. Engl. 52, 2897–2901 (2013).
- 534D.-S. Yang, O. F. Mohammed, and A. H. Zewail, "Scanning ultrafast electron microscopy," Proc. Natl. Acad. Sci. U. S. A. 107, 14993–14998 (2010).
- 535B. Liao and E. Najafi, "Scanning ultrafast electron microscopy: A novel technique to probe photocarrier dynamics with high spatial and temporal resolutions," Mater. Today Phys. 2, 46–53 (2017).
- 536 M. Zani, V. Sala, G. Irde, S. M. Pietralunga, C. Manzoni, G. Cerullo, G. Lanzani, and A. Tagliaferri, "Charge dynamics in aluminum oxide thin film studied by ultrafast scanning electron microscopy," Ultramicroscopy 187, 93–97 (2018).
- 537T. LaGrange, G. H. Campbell, B. W. Reed, M. Taheri, J. B. Pesavento, J. S. Kim, and N. D. Browning, "Nanosecond time-resolved investigations using the *in situ* of dynamic transmission electron microscope (DTEM)," Ultramicroscopy 108, 1441–1449 (2008).
- ⁵³⁸D. J. Masiel, B. W. Reed, T. B. Lagrange, G. H. Campbell, T. Guo, and N. D. Browning, "Time-resolved annular dark field imaging of catalyst nanoparticles," Chemphyschem 11, 2088–2090 (2010).

- 539 T. LaGrange, B. W. Reed, and D. J. Masiel, "Movie-mode dynamic electron microscopy," MRS Bull. 40, 22–28 (2015).
- 540B. W. Reed, S. T. Park, and D. J. Masiel, "Beyond movie mode: Bridging the gap of time resolution," Microsc. Microanal. 22, 706–707 (2016).
- 541G. C. Egan, E. Y. Lau, and E. Schwegler, "Multiframe imaging of micron and nanoscale bubble dynamics," Nano Lett. 22, 1053–1058 (2022).
- 542S. K. Sinha, A. Khammari, M. Picher, F. Roulland, N. Viart, T. LaGrange, and F. Banhart, "Nanosecond electron pulses in the analytical electron microscopy of a fast irreversible chemical reaction," Nat. Commun. 10, 3648 (2019).
- 543M. Picher, S. K. Sinha, Y. Hu, T. LaGrange, and F. Banhart, "Time-resolved analytical electron microscopy with single nanosecond electron pulses," Microsc. Microanal. 28, 1790–1791 (2022).
- 544I. Madan, E. J. C. Dias, S. Gargiulo, F. Barantani, M. Yannai, G. Berruto, T. LaGrange, L. Piazza, T. T. A. Lummen, R. Dahan, I. Kaminer, G. M. Vanacore, F. J. G. de Abajo, and F. Carbone, "Charge dynamics electron microscopy: Nanoscale imaging of femtosecond plasma dynamics," arXiv:2206.02546 (2022).
- 545 V. A. Lobastov, R. Srinivasan, and A. H. Zewail, "Four-dimensional ultrafast electron microscopy," Proc. Natl. Acad. Sci. U. S. A. 102, 7069–7073 (2005).
- 546F. M. Alcorn, P. K. Jain, and R. M. van der Veen, "Time-resolved transmission electron microscopy for nanoscale chemical dynamics," Nat. Rev. Chem. 7(4), 256–272 (2023).
- 547 A. Yurtsever and A. H. Zewail, "Direct visualization of near-fields in nanoplasmonics and nanophotonics," Nano Lett. 12, 3334–3338 (2012).
- 548 A. Yurtsever, J. S. Baskin, and A. H. Zewail, "Entangled nanoparticles: Discovery by visualization in 4D electron microscopy," Nano Lett. 12, 5027–5032 (2012).
- 549B. Barwick, D. J. Flannigan, and A. H. Zewail, "Photon-induced near-field electron microscopy," Nature 462, 902–906 (2009).
- 550 T. T. A. Lummen, R. J. Lamb, G. Berruto, T. LaGrange, L. Dal Negro, F. J. García de Abajo, D. McGrouther, B. Barwick, and F. Carbone, "Imaging and controlling plasmonic interference fields at buried interfaces," Nat. Commun. 7, 13156 (2016).
- 551H. Liu, T. E. Gage, P. Singh, A. Jaiswal, R. D. Schaller, J. Tang, S. T. Park, S. K. Gray, and I. Arslan, "Visualization of plasmonic couplings using ultrafast electron microscopy," Nano Lett. 21, 5842–5849 (2021).
- 552A. Yurtsever, R. M. van der Veen, and A. H. Zewail, "Subparticle ultrafast spectrum imaging in 4D electron microscopy," Science 335, 59–64 (2012).
- ⁵⁵³D. T. Valley, V. E. Ferry, and D. J. Flannigan, "Imaging intra- and interparticle acousto-plasmonic vibrational dynamics with ultrafast electron microscopy," Nano Lett. 16, 7302–7308 (2016).
- 554R. M. van der Veen, O.-H. Kwon, A. Tissot, A. Hauser, and A. H. Zewail, "Single-nanoparticle phase transitions visualized by four-dimensional electron microscopy," Nat. Chem. 5, 395–402 (2013).
- 555B.-K. Yoo, Z. Su, J. M. Thomas, and A. H. Zewail, "On the dynamical nature of the active center in a single-site photocatalyst visualized by 4D ultrafast electron microscopy," Proc. Natl. Acad. Sci. U. S. A. 113, 503–508 (2016).
- 556 R. M. van der Veen, T. J. Penfold, and A. H. Zewail, "Ultrafast core-loss spectroscopy in four-dimensional electron microscopy," Struct. Dyn. 2, 024302 (2015)
- 557Z. Su, J. S. Baskin, W. Zhou, J. M. Thomas, and A. H. Zewail, "Ultrafast elemental and oxidation-state mapping of hematite by 4D electron microscopy," J. Am. Chem. Soc. 139, 4916–4922 (2017).
- 558A. H. Zewail, "4D ultrafast electron diffraction, crystallography, and microscopy," Annu. Rev. Phys. Chem. 57, 65–103 (2006).
- 559 S. Aseyev, E. Ryabov, B. Mironov, and A. Ischenko, "The development of ultrafast electron microscopy," Crystals 10, 452 (2020).
- 560 B. Guzelturk, J. K. Utterback, I. Coropceanu, V. Kamysbayev, E. M. Janke, M. Zajac, N. Yazdani, B. L. Cotts, S. Park, A. Sood, M.-F. Lin, A. H. Reid, M. E. Kozina, X. Shen, S. P. Weathersby, V. Wood, A. Salleo, X. Wang, D. V. Talapin, N. S. Ginsberg, and A. M. Lindenberg, "Nonequilibrium thermodynamics of colloidal gold nanocrystals monitored by ultrafast electron diffraction and optical scattering microscopy," ACS Nano 14, 4792–4804 (2020).
- 561O. A. Hull and C. M. Aikens, "Theoretical investigations on the plasmon-mediated dissociation of small molecules in the presence of silver atomic wires," J. Phys. Chem. A 127, 2228–2241 (2023).

- 562S. G. Louie, Y.-H. Chan, F. H. da Jornada, Z. Li, and D. Y. Qiu, "Discovering and understanding materials through computation," Nat. Mater. 20, 728–735 (2021).
- 563 A. Sanna, J. A. Flores-Livas, A. Davydov, G. Profeta, K. Dewhurst, S. Sharma, and E. K. U. Gross, "Ab initio eliashberg theory: Making genuine predictions of superconducting features," J. Phys. Soc. Jpn. 87, 041012 (2018).
- 564A. Dreuw and M. Head-Gordon, "Single-reference ab initio methods for the calculation of excited states of large molecules," Chem. Rev. 105, 4009–4037 (2005)
- 565N. Bérubé, V. Gosselin, J. Gaudreau, and M. Côté, "Designing polymers for photovoltaic applications using *ab initio* calculations," J. Phys. Chem. C 117, 7964–7972 (2013).
- ⁵⁶⁶A. R. Oganov and C. W. Glass, "Crystal structure prediction using *ab initio* evolutionary techniques: Principles and applications," J. Chem. Phys. **124**, 244704 (2006).
- 567P. Hohenberg and W. Kohn, "Inhomogeneous electron gas," Phys. Rev. 136, B864 (1964).
- 568W. Kohn and L. J. Sham, "Self-consistent equations including exchange and correlation effects," Phys. Rev. 140, A1133 (1965).
- 569 R. Baer and D. Neuhauser, "Density functional theory with correct long-range asymptotic behavior," Phys. Rev. Lett. 94, 043002 (2005).
- 570 S. Refaely-Abramson, R. Baer, and L. Kronik, "Fundamental and excitation gaps in molecules of relevance for organic photovoltaics from an optimally tuned range-separated hybrid functional," Phys. Rev. B 84, 075144 (2011).
- 571 J. Sun, R. C. Remsing, Y. Zhang, Z. Sun, A. Ruzsinszky, H. Peng, Z. Yang, A. Paul, U. Waghmare, X. Wu, M. L. Klein, and J. P. Perdew, "Accurate first-principles structures and energies of diversely bonded systems from an efficient density functional," Nat. Chem. 8, 831–836 (2016).
- 572 N. Schuch and F. Verstraete, "Computational complexity of interacting electrons and fundamental limitations of density functional theory," Nat. Phys. 5, 732–735 (2009).
- 573 J. P. Perdew, K. Burke, and M. Ernzerhof, "Generalized gradient approximation made simple," Phys. Rev. Lett. 77, 3865 (1996).
- 574 A. J. Cohen, P. Mori-Sánchez, and W. Yang, "Insights into current limitations of density functional theory," Science 321, 792–794 (2008).
- 575A. K. Manna, M. H. Lee, K. L. McMahon, and B. D. Dunietz, "Calculating high energy charge transfer states using optimally tuned range-separated hybrid functionals," J. Chem. Theory Comput. 11, 1110–1117 (2015).
- 576D. Mester and M. Kállay, "Charge-transfer excitations within density functional theory: How accurate are the most recommended approaches?," J. Chem. Theory Comput. 18, 1646–1662 (2022).
- 577 J.-L. Bredas, "Mind the gap!," Mater. Horiz. 1, 17–19 (2014).
- 578 J. F. Janak, "Proof that $\frac{\partial \vec{E}}{\partial n_i} = \varepsilon$ in density-functional theory," Phys. Rev. B 18, 7165 (1978).
- 579 J. P. Perdew and M. Levy, "Comment on "significance of the highest occupied Kohn-Sham eigenvalue," Phys. Rev. B 56, 16021 (1997).
- 580 M. E. Casida, "Correlated optimized effective-potential treatment of the derivative discontinuity and of the highest occupied Kohn-Sham eigenvalue: A Janak-type theorem for the optimized effective-potential model," Phys. Rev. B59, 4694 (1999).
- 581E. Runge and E. K. U. Gross, "Density-functional theory for time-dependent systems," Phys. Rev. Lett. 52, 997 (1984).
- 582 V. Rizzi, T. N. Todorov, J. J. Kohanoff, and A. A. Correa, "Electron-phonon thermalization in a scalable method for real-time quantum dynamics," Phys. Rev. B 93, 024306 (2016).
- 583G. Onida, L. Reining, and A. Rubio, "Electronic excitations: Density-functional versus many-body Green's-function approaches," Rev. Mod. Phys. 74, 601 (2002).
- ⁵⁸⁴B. T. G. Lau and T. C. Berkelbach, "Quantum plasmons and intraband excitons in doped nanoparticles: Insights from quantum chemistry," J. Chem. Phys. 152, 224704–224715 (2020).
- 585 L. Hedin, "New method for calculating the one-particle Green's function with application to the electron-gas problem," Phys. Rev. 139, A796–A823 (1965)
- 586M. S. Hybertsen and S. G. Louie, "First-principles theory of quasiparticles: Calculation of band gaps in semiconductors and insulators," Phys. Rev. Lett. 55, 1418–1421 (1985).

- 587 R. W. Godby, M. Schlüter, and L. J. Sham, "Accurate exchange-correlation potential for silicon and its discontinuity on addition of an electron," Phys. Rev. Lett. 56, 2415–2418 (1986).
- 588M. S. Hybertsen and S. G. Louie, "Electron correlation in semiconductors and insulators: Band gaps and quasiparticle energies," Phys. Rev. B 34, 5390–5413 (1986)
- 589G. Strinati, "Application of the Green's functions method to the study of the optical properties of semiconductors," Riv. Nuovo Cimento 11, 1–86 (1988).
- 590 G. Onida, L. Reining, R. W. Godby, R. Del Sole, and W. Andreoni, "Ab initio calculations of the quasiparticle and absorption spectra of clusters: The sodium tetramer," Phys. Rev. Lett. 75, 818–821 (1995).
- 591M. Rohlfing and S. G. Louie, "Electron-hole excitations in semiconductors and insulators," Phys. Rev. Lett. 81, 2312–2315 (1998).
- 592S. Albrecht, L. Reining, R. Del Sole, and G. Onida, "Ab initio calculation of excitonic effects in the optical spectra of semiconductors," Phys. Rev. Lett. 80, 4510–4513 (1998).
- ⁵⁹³L. X. Benedict, E. L. Shirley, and R. B. Bohn, "Optical absorption of insulators and the electron-hole interaction: An *ab initio* calculation," Phys. Rev. Lett. 80, 4514–4517 (1998).
- 594 M. Rohlfing and S. G. Louie, "Electron-hole excitations and optical spectra from first principles," Phys. Rev. B 62, 4927–4944 (2000).
- 595F. Coester, "Bound states of a many-particle system," Nucl. Phys. 7, 421–424 (1958).
- 596F. Coester and H. Kümmel, "Short-range correlations in nuclear wave functions," Nucl. Phys. 17, 477-485 (1960).
- 597 J. Čížek, "On the correlation problem in atomic and molecular systems. Calculation of wavefunction components in Ursell-type expansion using quantum-field theoretical methods," J. Chem. Phys. 45, 4256–4266 (1966).
- 598S. Hirata, R. Podeszwa, M. Tobita, and R. J. Bartlett, "Coupled-cluster singles and doubles for extended systems," J. Chem. Phys. 120, 2581–2592 (2004).
- 599 T. Gruber, K. Liao, T. Tsatsoulis, F. Hummel, and A. Grüneis, "Applying the coupled-cluster ansatz to solids and surfaces in the thermodynamic limit," Phys. Rev. X 8, 021043 (2018).
- 600 M. M. Ugeda, A. J. Bradley, S.-F. Shi, F. H. da Jornada, Y. Zhang, D. Y. Qiu, W. Ruan, S.-K. Mo, Z. Hussain, Z.-X. Shen, F. Wang, S. G. Louie, and M. F. Crommie, "Giant bandgap renormalization and excitonic effects in a monolayer transition metal dichalcogenide semiconductor," Nat. Mater. 13, 1091–1095 (2014).
- 601A. Ramasubramaniam, "Large excitonic effects in monolayers of molybdenum and tungsten dichalcogenides," Phys. Rev. B 86, 115409 (2012).
- 602D. Y. Qiu, F. H. da Jornada, and S. G. Louie, "Optical spectrum of MoS₂: Many-body effects and diversity of exciton states," Phys. Rev. Lett. 111, 216805 (2013).
- 603 A. Chernikov, T. C. Berkelbach, H. M. Hill, A. Rigosi, Y. Li, O. B. Aslan, D. R. Reichman, M. S. Hybertsen, and T. F. Heinz, "Exciton binding energy and nonhydrogenic Rydberg series in monolayer WS₂," Phys. Rev. Lett. 113, 076802 (2014).
- 604M. Schröter, S. D. Ivanov, J. Schulze, S. P. Polyutov, Y. Yan, T. Pullerits, and O. Kühn, "Exciton-vibrational coupling in the dynamics and spectroscopy of Frenkel excitons in molecular aggregates," Phys. Rep. 567, 1–78 (2015).
- 605 C. J. Bardeen, "The structure and dynamics of molecular excitons," Annu. Rev. Phys. Chem. 65, 127–148 (2014).
- 606A. S. Davydov, "The theory of molecular excitons," Sov. Phys. Usp. 7, 145 (1964).
- 607P. Umari, G. Stenuit, and S. Baroni, "GW quasiparticle spectra from occupied states only," Phys. Rev. B 81, 115104 (2010).
- 608F. Giustino, M. L. Cohen, and S. G. Louie, "Gw method with the self-consistent sternheimer equation," Phys. Rev. B 81, 115105 (2010).
- ⁶⁰⁹T. A. Pham, H.-V. Nguyen, D. Rocca, and G. Galli, "GW calculations using the spectral decomposition of the dielectric matrix: Verification, validation, and comparison of methods," Phys. Rev. B 87, 155148 (2013).
- ⁶¹⁰D. Neuhauser, Y. Gao, C. Arntsen, C. Karshenas, E. Rabani, and R. Baer, "Breaking the theoretical scaling limit for predicting quasiparticle energies: The stochastic gw approach," Phys. Rev. Lett. 113, 076402 (2014).
- ⁶¹¹F. Liu, L. Lin, D. Vigil-Fowler, J. Lischner, A. F. Kemper, S. Sharifzadeh, F. H. da Jornada, J. Deslippe, C. Yang, J. B. Neaton, and S. G. Louie, "Numerical

- integration for *ab initio* many-electron self energy calculations within the GW approximation," J. Comput. Phys. **286**, 1–13 (2015).
- 612M. Govoni and G. Galli, "Large scale GW calculations," J. Chem. Theory Comput. 11, 2680–2696 (2015).
- ⁶¹³M. Shao, L. Lin, C. Yang, F. Liu, F. H. da Jornada, J. Deslippe, and S. G. Louie, "Low rank approximation in G₀ W₀ calculations," Sci. China Math. 59, 1593–1612 (2016).
- ⁶¹⁴J. Wilhelm, D. Golze, L. Talirz, J. Hutter, and C. A. Pignedoli, "Toward GW calculations on thousands of atoms," J. Phys. Chem. Lett. 9, 306–312 (2018).
- ⁶¹⁵V. Vlček, W. Li, R. Baer, E. Rabani, and D. Neuhauser, "Swift GW beyond 10,000 electrons using sparse stochastic compression," Phys. Rev. B 98, 075107 (2018).
- 616M. D. Ben, F. H. da Jornada, A. Canning, N. Wichmann, K. Raman, R. Sasanka, C. Yang, S. G. Louie, and J. Deslippe, "Large-scale GW calculations on pre-exascale HPC systems," Comput. Phys. Commun. 235, 187–195 (2019).
- 617 M. Kim, G. J. Martyna, and S. Ismail-Beigi, "Complex-time shredded propagator method for large-scale GW calculations," Phys. Rev. B 101, 035139 (2020).
- ⁶¹⁸M. D. Ben, C. Yang, Z. Li, F. H. da Jornada, S. G. Louie, and J. Deslippe, "Accelerating large-scale excited-state GW calculations on leadership HPC systems," in SC20: International Conference for High Performance Computing, Networking, Storage and Analysis (IEEE, 2020).
- ⁶¹⁹V. W. Zhe Yu and M. Govoni, "GPU acceleration of large-scale full-frequency GW calculations," J. Chem. Theory Comput. 18, 4690–4707 (2022).
- 620 K. Raghavachari and A. Saha, "Accurate composite and fragment-based quantum chemical models for large molecules," Chem. Rev. 115, 5643–5677 (2015).
- 621E. B. Guidez and C. M. Aikens, "Plasmon resonance analysis with configuration interaction." Phys. Chem. Chem. Phys. 16, 15501–15509 (2014).
- ⁶²²F. Alkan and C. M. Aikens, "Understanding plasmon coupling in nanoparticle dimers using molecular orbitals and configuration interaction," Phys. Chem. Chem. Phys. 21, 23065–23075 (2019).
- 623 F. Libisch, C. Huang, and E. A. Carter, "Embedded correlated wavefunction schemes: Theory and applications," Acc. Chem. Res. 47, 2768–2775 (2014).
- 624D. Sanchez-Portal, E. Artacho, and J. M. Soler, "Projection of plane-wave calculations into atomic orbitals," Solid State Commun. 95, 685-690 (1995).
- 625 T. Wriedt, "Mie theory: A review," in *The Mie Theory: Basics and Applications*, edited by W. Hergert and T. Wriedt (Springer Berlin Heidelberg, Berlin, Heidelberg, 2012), pp. 53–71.
- ⁶²⁶G. Mie, "Beiträge zur optik trüber medien, speziell kolloidaler metallösungen," Ann. Phys. 330, 377–445 (1908).
- 627 J.-M. Jin, The Finite Element Method in Electromagnetics (John Wiley & Sons, 2015).
- 628F. M. H. Aliabadi, "Boundary element methods," in *Encyclopedia of Continuum Mechanics*, edited by H. Altenbach and A. Öchsner (Springer Berlin Heidelberg, Berlin, Heidelberg, 2020), pp. 182–193.
- 629U. Hohenester, "Simulating electron energy loss spectroscopy with the MNPBEM toolbox," Comput. Phys. Commun. 185, 1177–1187 (2014).
- 630 F. J. García de Abajo and A. Howie, "Retarded field calculation of electron energy loss in inhomogeneous dielectrics," Phys. Rev. B 65, 115418 (2002).
- 631 A. Taflove, S. C. Hagness, and M. Piket-May, "Computational electromagnetics: The finite-difference time-domain method," in *The Electrical Engineering Handbook* (Academic, 2005), pp. 629–670.
- 632 M. Futamata, Y. Maruyama, and M. Ishikawa, "Local electric field and scattering cross section of Ag nanoparticles under surface plasmon resonance by finite difference time domain method," J. Phys. Chem. B 107, 7607–7617 (2003)
- 633B. T. Draine and P. J. Flatau, "Discrete-dipole approximation for scattering calculations," J. Opt. Soc. Am. A 11, 1491 (1994).
- 634Y. Jiang, S. Pillai, and M. A. Green, "Re-evaluation of literature values of silver optical constants," Opt. Express 23, 2133–2144 (2015).
- 635 T. P. Rossi, P. Erhart, and M. Kuisma, "Hot-carrier generation in plasmonic nanoparticles: The importance of atomic structure," ACS Nano 14, 9963–9971 (2020).

- ⁶³⁶L. R. Castellanos, O. Hess, and J. Lischner, "Dielectric engineering of hotcarrier generation by quantized plasmons in embedded silver nanoparticles," J. Phys. Chem. C 125, 3081–3087 (2021).
- 637 H. Jin, J. M. Kahk, D. A. Papaconstantopoulos, A. Ferreira, and J. Lischner, "Plasmon-induced hot carriers from interband and intraband transitions in large noble metal nanoparticles," PRX Energy 1, 013006 (2022).
- ⁶³⁸G. Tagliabue, J. S. DuChene, M. Abdellah, A. Habib, D. J. Gosztola, Y. Hattori, W.-H. Cheng, K. Zheng, S. E. Canton, R. Sundararaman *et al.*, "Ultrafast hothole injection modifies hot-electron dynamics in Au/p-GaN heterostructures," Nat. Mater. 19, 1312–1318 (2020).
- 639S. Mukherjee, L. Zhou, A. M. Goodman, N. Large, C. Ayala-Orozco, Y. Zhang, P. Nordlander, and N. J. Halas, "Hot-electron-induced dissociation of H₂ on gold nanoparticles supported on SiO₂," J. Am. Chem. Soc. 136, 64–67 (2014).
- ⁶⁴⁰E. C. M. Barbosa, J. L. Fiorio, T. Mou, B. Wang, L. M. Rossi, and P. H. C. Camargo, "Reaction pathway dependence in plasmonic catalysis: Hydrogenation as a model molecular transformation," Chem.–Eur. J. 24, 12330–12339 (2018).
- 641J. M. P. Martirez and E. A. Carter, "Prediction of a low-temperature N₂ dissociation catalyst exploiting near-IR-to-visible light nanoplasmonics," Sci. Adv. 3, eaao4710 (2017).
- ⁶⁴²J. L. Bao and E. A. Carter, "Rationalizing the hot-carrier-mediated reaction mechanisms and kinetics for ammonia decomposition on ruthenium-doped copper nanoparticles," J. Am. Chem. Soc. 141, 13320–13323 (2019).
- 643S. Mukherjee, F. Libisch, N. Large, O. Neumann, L. V. Brown, J. Cheng, J. B. Lassiter, E. A. Carter, P. Nordlander, and N. J. Halas, "Hot electrons do the impossible: Plasmon-induced dissociation of H₂ on Au," Nano Lett. 13, 240–247 (2013).
- 644A. Al-Zubeidi, B. Ostovar, C. C. Carlin, B. C. Li, S. A. Lee, W.-Y. Chiang, N. Gross, S. Dutta, A. Misiura, E. K. Searles, A. Chakraborty, S. T. Roberts, J. A. Dionne, P. J. Rossky, C. F. Landes, and S. Link, "Mechanism for plasmongenerated solvated electrons," Proc. Natl. Acad. Sci. U. S. A. 120, e2217035120 (2023).
- 645°C. Boerigter, R. Campana, M. Morabito, and S. Linic, "Evidence and implications of direct charge excitation as the dominant mechanism in plasmonmediated photocatalysis," Nat. Commun. 7, 10545 (2016).
- 646R. F. Hamans, M. Parente, and A. Baldi, "Super-resolution mapping of a chemical reaction driven by plasmonic near-fields," Nano Lett. 21, 2149–2155 (2021).
- 647 X.-T. Kong, Z. Wang, and A. O. Govorov, "Plasmonic nanostars with hot spots for efficient generation of hot electrons under solar illumination," Adv. Opt. Mater. 5, 1600594 (2017).
- ⁶⁴⁸H. Zhang and A. O. Govorov, "Optical generation of hot plasmonic carriers in metal nanocrystals: The effects of shape and field enhancement," J. Phys. Chem. C 118, 7606–7614 (2014).
- 649 L. V. Besteiro and A. O. Govorov, "Amplified generation of hot electrons and quantum surface effects in nanoparticle dimers with plasmonic hot spots," J. Phys. Chem. C 120, 19329–19339 (2016).
- 650 A. O. Govorov and H. Zhang, "Kinetic density functional theory for plasmonic nanostructures: Breaking of the plasmon peak in the quantum regime and generation of hot electrons," J. Phys. Chem. C 119, 6181–6194 (2015).
- 651 A. O. Govorov, H. Zhang, and Y. K. Gun'ko, "Theory of photoinjection of hot plasmonic carriers from metal nanostructures into semiconductors and surface molecules," J. Phys. Chem. C 117, 16616–16631 (2013).
- 652 A. Manjavacas, J. G. Liu, V. Kulkarni, and P. Nordlander, "Plasmon-induced hot carriers in metallic nanoparticles," ACS Nano 8, 7630–7638 (2014).
- 653E. Prodan and P. Nordlander, "Electronic structure and polarizability of metallic nanoshells," Chem. Phys. Lett. 352, 140–146 (2002).
- 654E. Prodan, P. Nordlander, and N. J. Halas, "Electronic structure and optical properties of gold nanoshells," Nano Lett. 3, 1411–1415 (2003).
- 655E. Prodan and P. Nordlander, "Structural tunability of the plasmon resonances in metallic nanoshells," Nano Lett. 3, 543–547 (2003).
- 656J. Zuloaga, E. Prodan, and P. Nordlander, "Quantum description of the plasmon resonances of a nanoparticle dimer," Nano Lett. 9, 887–891 (2009).
- 657A. Varas, P. García-González, J. Feist, F. J. García-Vidal, and A. Rubio, "Quantum plasmonics: From jellium models to ab initio calculations," Nanophotonics 5, 409–426 (2016).

- ⁶⁵⁸D. Rossouw, M. Couillard, J. Vickery, E. Kumacheva, and G. A. Botton, "Multipolar plasmonic resonances in silver nanowire antennas imaged with a subnanometer electron probe," Nano Lett. 11, 1499–1504 (2011).
- 659B. Ögüt, N. Talebi, R. Vogelgesang, W. Sigle, and P. A. van Aken, "Toroidal plasmonic eigenmodes in oligomer nanocavities for the visible," Nano Lett. 12, 5239–5244 (2012).
- ⁶⁶⁰M. Bosman, E. Ye, S. F. Tan, C. A. Nijhuis, J. K. W. Yang, R. Marty, A. Mlayah, A. Arbouet, C. Girard, and M.-Y. Han, "Surface plasmon damping quantified with an electron nanoprobe," Sci. Rep. 3, 1312 (2013).
- ⁶⁶¹A. Hörl, G. Haberfehlner, A. Trügler, F.-P. Schmidt, U. Hohenester, and G. Kothleitner, "Tomographic imaging of the photonic environment of plasmonic nanoparticles," Nat. Commun. 8, 37 (2017).
- ⁶⁶²H. Haberland, "Looking from both sides," Nature **494**, E1–E2 (2013).
- 663H.-C. Weissker and C. Mottet, "Optical properties of pure and core-shell noble-metal nanoclusters from TDDFT: The influence of the atomic structure," Phys. Rev. B 84, 165443 (2011).
- ⁶⁶⁴J. Ma, Z. Wang, and L.-W. Wang, "Interplay between plasmon and single-particle excitations in a metal nanocluster," Nat. Commun. 6, 10107 (2015).
- 665 O. Baseggio, M. De Vetta, G. Fronzoni, M. Stener, L. Sementa, A. Fortunelli, and A. Calzolari, "Photoabsorption of icosahedral noble metal clusters: An efficient TDDFT approach to large-scale systems," J. Phys. Chem. C 120, 12773–12782 (2016).
- 666P. Koval, F. Marchesin, D. Foerster, and D. Sánchez-Portal, "Optical response of silver clusters and their hollow shells from linear-response TDDFT," J. Phys.: Condens. Matter 28, 214001 (2016).
- 667T. P. Rossi, S. Lehtola, A. Sakko, M. J. Puska, and R. M. Nieminen, "Nanoplasmonics simulations at the basis set limit through completeness-optimized, local numerical basis sets," J. Chem. Phys. 142, 094114 (2015).
- 668 G.-T. Bae and C. M. Aikens, "Time-dependent density functional theory studies of optical properties of Ag nanoparticles: Octahedra, truncated octahedra, and icosahedra," J. Phys. Chem. C 116, 10356–10367 (2012).
- 669F. Rabilloud, "Description of plasmon-like band in silver clusters: The importance of the long-range Hartree-Fock exchange in time-dependent density-functional theory simulations," J. Chem. Phys. 141, 144302 (2014).
- 670 M. Kuisma, A. Sakko, T. P. Rossi, A. H. Larsen, J. Enkovaara, L. Lehtovaara, and T. T. Rantala, "Localized surface plasmon resonance in silver nanoparticles: Atomistic first-principles time-dependent density-functional theory calculations," Phys. Rev. B 91, 115431 (2015).
- 671 W. Ekardt, "Size-dependent photoabsorption and photoemission of small metal particles," Phys. Rev. B 31, 6360-6370 (1985).
- 672C. Yannouleas, R. A. Broglia, M. Brack, and P. F. Bortignon, "Fragmentation of the photoabsorption strength in neutral and charged metal microclusters," Phys. Rev. Lett. 63, 255–258 (1989).
- ⁶⁷³Z. Penzar, W. Ekardt, and A. Rubio, "Temperature effects on the optical absorption of jellium clusters," Phys. Rev. B 42, 5040–5045 (1990).
- 674°C. Yannouleas and R. A. Broglia, "Collective and single-particle aspects in the optical response of metal microclusters," Phys. Rev. A 44, 5793–5802 (1991).
- 675 T. P. Rossi, M. Kuisma, M. J. Puska, R. M. Nieminen, and P. Erhart, "Kohn-Sham decomposition in real-time time-dependent density-functional theory: An efficient tool for analyzing plasmonic excitations," J. Chem. Theory Comput. 13, 4779–4790 (2017).
- ⁶⁷⁶G. Barcaro, L. Sementa, A. Fortunelli, and M. Stener, "Optical properties of Pt and Ag-Pt nanoclusters from TDDFT calculations: Plasmon suppression by Pt poisoning," J. Phys. Chem. C 118, 28101–28108 (2014).
- 677 K. M. Conley, N. Nayyar, T. P. Rossi, M. Kuisma, V. Turkowski, M. J. Puska, and T. S. Rahman, "Plasmon excitations in mixed metallic nanoarrays," ACS Nano 13, 5344–5355 (2019).
- ⁶⁷⁸X. Li, D. Xiao, and Z. Zhang, "Landau damping of quantum plasmons in metal nanostructures," New J. Phys. 15, 023011 (2013).
- ⁶⁷⁹P. V. Kumar, T. P. Rossi, M. Kuisma, P. Erhart, and D. J. Norris, "Direct hot-carrier transfer in plasmonic catalysis," Faraday Discuss. 214, 189–197 (2019).
- ⁶⁸⁰K. Iida, M. Noda, K. Ishimura, and K. Nobusada, "First-principles computational visualization of localized surface plasmon resonance in gold nanoclusters," J. Phys. Chem. A 118, 11317–11322 (2014).
- 681O. A. Douglas-Gallardo, M. Berdakin, T. Frauenheim, and C. G. Sánchez, "Plasmon-induced hot-carrier generation differences in gold and silver nanoclusters," Nanoscale 11, 8604–8615 (2019).

- ⁶⁸²O. A. Hull, D. B. Lingerfelt, X. Li, and C. M. Aikens, "Electronic structure and nonadiabatic dynamics of atomic silver nanowire-N₂ systems," J. Phys. Chem. C 124, 20834–20845 (2020).
- 683 J. Salido, G. Bueno, J. Ruiz-Santaquiteria, and G. Cristobal, "A review on low-cost microscopes for open science," Microsc. Res. Tech. 85, 3270–3283 (2022).
- 684Q. Zhang, T. Hernandez, K. W. Smith, S. A. Hosseini Jebeli, A. X. Dai, L. Warning, R. Baiyasi, L. A. McCarthy, H. Guo, D.-H. Chen, J. A. Dionne, C. F. Landes, and S. Link, "Unraveling the origin of chirality from plasmonic nanoparticle-protein complexes," Science 365, 1475–1478 (2019).
- ⁶⁸⁵Z. Zheng, T. Tachikawa, and T. Majima, "Single-particle study of Pt-modified Au nanorods for plasmon-enhanced hydrogen generation in visible to nearinfrared region," J. Am. Chem. Soc. 136, 6870–6873 (2014).
- ⁶⁸⁶M. Dieperink, F. Scalerandi, and W. Albrecht, "Correlating structure, morphology and properties of metal nanostructures by combining single-particle optical spectroscopy and electron microscopy," Nanoscale 14, 7460–7472 (2022).
- 687 L. DeRita, S. Dai, K. Lopez-Zepeda, N. Pham, G. W. Graham, X. Pan, and P. Christopher, "Catalyst architecture for stable single atom dispersion enables site-specific spectroscopic and reactivity measurements of CO adsorbed to Pt atoms, oxidized Pt clusters, and metallic Pt clusters on TiO," J. Am. Chem. Soc. 139, 14150–14165 (2017).

- 688J. S. Biggins, S. Yazdi, and E. Ringe, "Magnesium nanoparticle plasmonics," Nano Lett. 18, 3752–3758 (2018).
- 689 J. Asselin, C. Boukouvala, E. R. Hopper, Q. M. Ramasse, J. S. Biggins, and E. Ringe, "Tents, chairs, tacos, kites, and rods: Shapes and plasmonic properties of singly twinned magnesium nanoparticles," ACS Nano 14, 5968–5980 (2020).
- ⁶⁹⁰P. Dhindsa, D. Solti, C. R. Jacobson, A. Kuriakose, G. N. Naidu, A. Bayles, Y. Yuan, P. Nordlander, and N. J. Halas, "Facet tunability of aluminum nanocrystals," Nano Lett. 22, 10088–10094 (2022).
- 691 M. Lou, A. Bayles, H. O. Everitt, and N. J. Halas, "Selective photodetoxification of a sulfur mustard simulant using plasmonic aluminum nanoparticles," Nano Lett. 22, 7699–7705 (2022).
- ⁶⁹²E. C. Ignat, D. Lutic, G. Ababei, and G. Carja, "Novel heterostructures of noble plasmonic metals/Ga-substituted hydrotalcite for solar light driven photocatalysis toward water purification," Catalysts 12, 1351 (2022).
- 693 A. Thomas, L. Lethuillier-Karl, K. Nagarajan, R. M. A. Vergauwe, J. George, T. Chervy, A. Shalabney, E. Devaux, C. Genet, J. Moran, and T. W. Ebbesen, "Tilting a ground-state reactivity landscape by vibrational strong coupling," Science 363, 615–619 (2019).
- 694M. A. Bañares, M. O. Guerrero-Pérez, J. L. G. Fierro, and G. G. Cortez, "Raman spectroscopy during catalytic operations with on-line activity measurement (operando spectroscopy): A method for understanding the active centres of cations supported on porous materials," J. Mater. Chem. 12, 3337–3342 (2002).